SYNTHESIS OF β-CYCLODEXTRIN AND CHITOSAN-BASED COPOLYMERS FOR THE REMOVAL OF NAPHTHENIC ACIDS

A Thesis Submitted to the College of

Graduate Studies and Research

In Partial Fulfillment of the Requirements

In the Department of Chemistry

University of Saskatchewan

Saskatoon

By

Louis Poon

PERMISSION TO USE

In presenting this thesis in partial fulfilment of the requirements for a Postgraduate degree from the University of Saskatchewan, I agree that the Libraries of this University may make it freely available for inspection. I further agree that permission for copying of this thesis in any manner, in whole or in part, for scholarly purposes may be granted by the professor or professors who supervised my thesis work or, in their absence, by the Head of the Department or the Dean of the College in which my thesis work was done. It is understood that any copying or publication or use of this thesis or parts thereof for financial gain shall not be allowed without my written permission. It is also understood that due recognition shall be given to me and to the University of Saskatchewan in any scholarly use which may be made of any material in my thesis.

Requests for permission to copy or to make other use of material in this thesis in whole or part should be addressed to:

Head of the Department of Chemistry

University of Saskatchewan

Saskatoon, SK (S7N 5C9)

Canada

ABSTRACT

Naphthenic acids (NAs) are a group of carboxylic acids that are found in hydrocarbon deposits such as the oil sands bitumen. These compounds are a well-known corrosive agent and a toxic component in the oil sands process water (OSPW). Due to Alberta's zero discharge policy, OSPW cannot be released and must be stored until toxic components like NAs are remediated. One technique that has shown potential is to physically adsorb NAs onto a copolymer generated from economical biomaterials. Therefore, the project can be divided into three sections: 1) Synthesis of β-cyclodextrin (β-CD) copolymer for the sorption of *p*-nitrophenol (PNP); 2) Synthesis of chitosan-based copolymers (Chi-Glu) for the sorption of PNP; 3) Sorption of carboxylates and NAs using Chi-Glu copolymers. PNP sorption was used as a probe to understand the physicochemical properties of the copolymers.

In the first section, β-CD was reacted with sebacoyl chloride (SCl) and terephthaloyl chloride (TCl) at various mole ratios. Characterization was done using Fourier Transform Infrared Spectroscopy (FT-IR), thermogravimetric analysis (TGA), ^{1}H NMR spectroscopy (^{1}H NMR), elemental analysis (CHN), and nitrogen porosimetry. Copolymers synthesized at mole ratios of β-CD to SCl from 1:1 to 1:3 were hydrolyzed at acidic and basic conditions. Therefore, sorption studies were not done at these ratios. The same occurred for 1:1 to 1:3 TCl copolymers. Sorption studies with PNP at pH 4.6 demonstrated enhanced sorption capacity when comparing with a standard: granular activated carbon (GAC). The sorption capacity, Q_m (mmol/g), ordered from largest to smallest is 1:9 SCl>1:9 TCl>1:6 SCl> GAC> 1:6 TCl.

Chi-Glu copolymers were synthesized by cross-linking glutaraldehyde with pristine chitosan. A systematic study on the effects reaction conditions have on the sorption capacity of the materials was done. Three conditions were changed: pH, temperature, and mole ratios. Chi-Glu copolymers were synthesized at various chitosan to glutaraldehyde mole ratios (1:400, 1:700, 1:1000). Sufficient time was allowed for the aging process. Characterization was done using TGA, FT-IR, CHN, and nitrogen porosimetry. Sorption study with PNP were done at pH = 7.0 and 9.0. At pH = 7.0 sorption capacity appears to correlate to the quantity of homo-polymerized glutaraldehyde: 1:700>1:1000>1:400. While at pH = 9.0, the sorption capacity is inversely proportional to the degree of crosslinking: 1:400>1:700>1:1000. By increasing the pH at the

shrinkage phase, PNP was weakly bound onto the Chi-Glu copolymer. Varying temperature before gelation caused a decrease in the sorption capacity with PNP.

Sorption studies involving carboxylates and NAs were done at pH = 9.0 at ambient temperature using Chi-Glu copolymers (1:400, 1:700, and 1:1000) and chitosan. Three carboxylates were chosen to reflect the diverse components in NAs. Varying degrees of cyclization (Z = 0, -2, -4) and lipophilic surface area were the main criteria for carboxylates. The sorption capacity depended mainly on the lipophilic surface area (LSA) with sorption capacity highest for 2-hexyldecanoic acid (S1) which has the largest LSA and lowest for, *trans*-4-pentylcyclohexanecarboxylic acid (S2) and dicyclohexylacetic acid (S3). Unfortunately, cross-linking with glutaraldehyde does not enhance sorption as pristine chitosan retained a higher sorption capacity compared to Chi-Glu copolymers. Acros and Fluka NAs were chosen for sorption and no significant sorption was recorded for any copolymers. Problems involving the micellization process can explain the lack of sorption.

ACKNOWLEDGEMENTS

General George Patton noted he measures success not by how high one climbs but by how high one bounces when hitting rock bottom. As such, there were many times in research where I hit rock bottom and would not have rebounded were it not for the support of my supervisor Dr. Lee D. Wilson. Those were trying times and I tried his patience often but through his tireless guidance my projects have borne fruit and the bad days are now behind me. I am grateful for his mentorship as I have learned much in becoming a successful researcher and wish him the best in his future research projects.

Naphthenic acid research requires collaborations with numerous experts either for advice or access to instruments not normally accessible in a lab. For his expertise and advice on naphthenic acids I thank my co-supervisor Dr. John V. Headley. I am also grateful Dr. Headley devoted precious time to critiquing and editing my thesis. To Dr. Mohamed H. Mohamed, I could not have done my naphthenate sorption experiments smoothly without your help and our mutual enjoyment of music by Jay-Z. Lastly, I am thankful to Jon Bailey and Kerry M. Peru for their aid in mass spectrometry analysis.

I am thankful for the funding provided by University of Saskatchewan Department of Chemistry through the graduate teaching assistantship. The benefits of being a teaching assistant extended beyond research as I felt I became a better teacher in the process. To Environment Canada for supporting me through the youth horizon award which helped me as I started my master's program. Lastly, I would like to thank Valerie Mackenzie, Keith Brown, Gabrielle Schatte, Jason Maley, and Pia Wennek for their comprehensive training on various instruments.

To the committee members who acted as advisors and spared time in their busy schedule to guide my research I offer my thanks: Dr. Dale Ward (Chair, 2011), Dr. Stephen Urquhart (Chair, 2012), Dr. Robert Scott (Defense-Chair, 2013), and Dr. Stephen Foley (Committee Advisor and soon-to-be sorption expert). To Dr. Mehdi Nemati, thank you for accepting to be my external examiner and the many constructive criticisms that have improved the quality of my thesis and research.

Anybody who steps into the Wilson lab will note research is often done there to the sound of Hip-Hop music from the latest artists (American, Canadian, Kenyan, and Chinese). I am

thankful to my laboratory colleagues for intriguing discussions on research and non-stop music to work to. To Dr. Abdalla Karoyo, Dr. Rui Guo, Dr. Jae Kwon, Dr. Shaguftah Younus, and Dr. Leila Dehabadi, my wish to you is that you obtain your doctorate of philosophy. To Chen Xue, I wish you a fruitful master's program. I wish Tarek Aboumourad and Lewis Casey the best of luck in their research projects.

I would like to thank my best friends who made life in chemistry thoroughly interesting here: Myron Wilde, Concepcion Ponce, Terri Thunder, Michelle Li, Brian Wong, and Anna Woo.

Dedication

This thesis is dedicated to my family: Daniel Poon, Connie Chan, Norman Poon, and Joice Yerro.

樂 不 思 蜀

TABLE OF CONTENTS

LIST OF TABLES

LIST OF FIGURES

LIST OF SCHEMES

LIST OF ABBREVIATIONS

1: x SCl ..... Sebacoyl copolymers

1: x TCl ..... Terephthaloyl copolymers

AOS..... Athabasca Oil Sands

as (e.g. ν_{as} or δ_{as}) .....Asymmetric

BET .....Brunauer-Emmett-Teller

BJH .....Barrett-Joyner-Halenda

CD ..... Cyclodextrin

CDI.....4,4'-Dicyclohexylmethane diisocyanate

ChiECH..... Chitosan Epichlorohydrin copolymers

Chi-Glu .....Chitosan Glutaraldehyde copolymers

CHN ..... Carbon, Nitrogen, and Hydrogen Elemental Analysis

CMC..... Critical Micelle Concentration

DMA .....N,N-Dimethylacetamide

DTG ..... Differential Thermogravimmetry

EC_{50}..... Half Maximal Effective Concentration

ECH..... Epichlorohydrin

EF..... Empirical Formula

Eqn. .....Equation

ESI-MS .....Electrospray Ionization Mass Spectrometry

eV.....Electronvolt

Fig. .....Figure

FT-IR..... Fourier Transform Infrared Spectroscopy

GAC .....Granular Activated Carbon

H-bonding ..... Hydrogen bonding

HDI .....1,6-Hexamethylene diisocynate

HPLC .....High Performance Liquid Chromatography

IC_{50}.....Half Maximal Inhibitory Concentration

IR.....Infrared Spectroscopy

LC .....Liquid Chromatography

LC_{50} ..... Half Maximal Lethal Concentration

LC-MS ..... Liquid Chromatography Mass Spectrometry

LD_{50} ..... Half Maximal Lethal Dosage

m/z ..... Mass to Charge ratio

MAC ..... Monomeric Atomic Composition

MDI ..... 4,4,-Diphenylmethane diisocyanate

MHz ..... Megahertz

mM ..... Millimolar

NAs ..... Naphthenic Acids. In Chapter 7, NAs means naphthenates

ND ..... Not Determined

NDI ..... 1,5-Naphthalene diisocyanate

NMR ..... Nuclear Magnetic Resonance

NOE ..... Nuclear Overhauser Effect

OSPW ..... Oil Sands Process Water

PDI ..... 1,4-Phenylene diisocyanate

PNP ..... *para*-Nitrophenol

PNP^- ..... Deprotonated *para*-nitrophenol or anionic *para*-nitrophenol

ppm ..... parts per million (mg/L)

RMSE ..... Root Mean Square Error

rpm ..... Revolution per minute

s (e.g. ν_s or δ_s) ..... Symmetric

S1 ..... 2-Hexyldecanoic acid

S2 ..... *trans*-4-Pentylcyclohexanecarboxylic acid

S3 ..... 2,2-Dicyclohexylacetic acid

S_{BET} ..... Brunauer-Emmett-Teller Total Specific Surface Area

SCl ..... Sebacoyl Chloride

S_{EXT} ..... External Specific Surface Area

S_{MIC} ..... Micropore Specific Surface Area

SSA ..... Specific Surface Area

TCl ..... Terephthaloyl Chloride

TGA ..... Thermalgravimetric Analysis

TMS ..... Tetramethylsilane

t-plot ..... de Boer thickness plot

UV-Vis ..... Ultraviolet-Visible

v (e.g. v_{as} or v_s) ..... Bond Stretching

VDW ..... van der Waal's

β-CD ..... β-Cyclodextrin

δ (e.g. δ_{as} or δ_s) ..... Bond bending or deformation

μM ..... Micromolar

μmHg ..... Micrometer of mercury

CHAPTER 1

INTRODUCTION

1.1 Naphthenic Acids (NAs)

In 2002, the Alberta Department of Energy estimated the total oil sands bitumen in the province was 1.7-2.5 trillion barrels of oil with 300 billion barrels of oil recoverable from the bitumen through open pit and *in situ* mining (*1,2*). Using the process pioneered by Karl Clark, approximately 4 barrels of water are needed to extract 1 barrel of oil (*3,4*) from the oil sands bitumen. One consequence of the Clark Extraction Process is the transfer of naphthenic acids (NAs) as well as tailings from the oil to the water. NAs are a toxic and corrosive agent and due to Alberta's zero discharge policy, NAs are retained in the oil sands process waters (OSPW) or tailings ponds (*4,5*). In recent estimates, Suncor alone has nine tailing ponds with a total surface area of 31.8 square kilometers (*6*). Secondly, as the water is recycled, the concentration of NAs increases which results in an increase in toxicity. Therefore, remediation of NAs in OSPW becomes important as NAs are a growing environmental concern.

1.1.1 Oil Sands Extraction Process

To understand the problem posed by NAs requires some background in oil sands extraction. Bitumen in the oil sands is actually separated from the sand particles by a small layer of water (2). This layer of water prevents bitumen adsorption into the pores of the sand or clay particles which would render the oil unrecoverable (*2*). Bitumen extracted from oil sand uses a process developed by Karl Clark called "The Clark Caustic Extraction Process". This involves heating ground bitumen in caustic water between 50^{o}C to 80^{o}C (*2-6*). The heat reduces the viscosity of the oil while the base protonates NAs (*cf*. Scheme 1.1) and sulfates to enhance separation of phases between the oil and water/clay. Low molecular weight NAs and colloidal clay particles (tailings) will remain in the aqueous phase while the more hydrophobic NAs will remain in the oil (*2*). Aeration of the bitumen slurry aids in oil recovery by providing hydrophobic surfaces for adsorption of hydrocarbons. The froth that is generated is separated off and de-aerated. Any water and dissolved NAs goes to the OSPW while the bitumen is upgraded (*2*). If any NAs remain in the bitumen then corrosion caused by NAs may occur. At 220^{o}C, NAs become corrosive with 350^{o}C being the optimal temperature for NAs corrosion (5). A small

amount of NAs can be beneficial in enhancing oil recovery as NAs can reduce the oil-water interface (2), it will corrode pipelines should NAs remain in the oil during the upgrading process. Secondly, any NAs removed from the oil during de-aeration will also be transferred to the OSPW. Therefore, NAs remain in the aqueous layer.

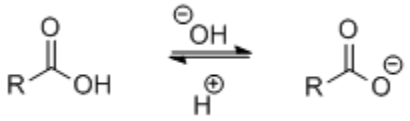

Scheme 1.1 Conversion of Naphthenic Acids into Naphthenates in aqueous solution

Originally, 15 m^3 of fresh water drawn from the Athabasca River was needed to refine 1 m^3 of bitumen (*4*). Through the process, consumption of water was reduced to ~ 4 m^3 for 1 m^3 where 80% of the water is recycled through the system (*4*). This merely delays the problem of NAs as the acid has not been removed from the system. As a consequence of the extraction process, the 4 m^3 slurry is deposited as oil sands process water (OSPW) (*8*). Cleaner crude oil is obtained but it also increases the sheer volume of water containing naphthenates. As the OSPW cannot be released to the Athabasca River due to Alberta's zero discharge policy (*4*), remediation of the water has grown in importance.

1.1.2 Physical and Chemical Properties of NAs

The presence of naphthenic acids (NAs) in oil deposits has been known for at least 130 years. The first study on identifying NAs was done in 1874 (*4*), only four years after the founding of Standard Oil. Naphthenic Acids (NAs) are a mixture of naturally occurring organic carboxylic acids found in crude petroleum reserves as well as oil sands deposits (*4, 7*). The types of carboxylic acids in NAs are classified according to the formula $C_nH_{2n+Z}O_2$ where n is the number of carbon atoms, and Z is the number of hydrogen atoms lost due to cyclization (*4*). This conventional naming system is used solely for a mixture of NAs that are aliphatic and cycloaliphatic carboxylic acids. More recently (*4,2*), the definition of NAs has expanded to include aromatic, heterocyclic, nitrogen, and sulfur containing species have been reported. Therefore, the conventional definition of NAs is limited in scope but it is adopted for use in this thesis research project.

The concentration and type of carboxylic acids that compose the complex mixture known as naphthenic acids differs according to the source of the crude oil. Secondly, even if the ore is from one source the composition of NAs can vary drastically according to the Z number, the number of heteroatoms depends on the type of extraction process. For example: Clemente et al. (*8*) found that one ore sample contained 3 times the level of NAs as compared to a previous batch. This was also held true for NAs obtained from the Athabasca Oil Sands (AOS). The average concentration of NAs found in the Alberta oil sands deposit was determined to be 2% (*4, 7*). Natural amounts of NAs found in the Athabasca River (*4*) averaged around 1 mg/L while tailing pond waters may reach levels as high as 110 mg/L where NAs contributed to the toxicity of OSPW. The relatively high levels of NAs were thought to be possible due to micelle formation caused by the saponification of NAs (CMC values of carboxylic acids in NAs vary between 35 μM to 4.5 mM (*10*)). This micelle formation coupled to high pH is considered an important factor in the toxicity of NAs (*11-13*).

1.1.3 Toxicity of NAs

Assessing the toxicity of NAs has proven to be a challenge because of the numerous carboxylic acids that contribute to the complex mixture. Studies on the heterocyclic and aromatic NAs toxicity are unknown and this review will focus on the cycloaliphatic and aliphatic NAs. NAs from OSPW contain dozens of different aliphatic and cyclic carboxylic acids and each batch of NAs from the same OSPW can result in drastically different combinations of NAs (*4*). The former limits knowledge of whether an individual component of NAs was responsible for the toxicity and the latter prevented reproducible toxicological results between batches of NAs. As a consequence, toxicological assessments carried out on NAs follow one of the two procedures: feeding of NAs mixture to organisms, or feeding of individual components of NAs to organisms. Both toxicological assessments on NAs have been made with the earliest in 1955 (*14*) where the LD_{50} for NAs in humans were approximated using rats to be 0.64-0.73g/Kg. Results from toxicity assessments were usually represented using one of the four terms: LD_{50}, LC_{50}, EC_{50}, and IC_{50}. LD_{50} is the lethal dosage of NAs per volume of solution that causes 50% mortality. LC_{50} is the concentration of NAs per weight of organism where 50% mortality occurs. EC_{50} is the concentration of NAs where a side effect occurs to 50% of the animal population; for example, the formation of lesions in rats. Lastly, IC_{50} is the concentration of NAs that reduces a

normal response to 50%; an example would be the reduction of bioluminescent intensity produced by the *Vibrio Fischeri* bacteria (*13*, *15*). For toxicological assessments, standard test organisms were used for NAs. The most common and economical test organism is the bacterial species of the *Vibrio* Genus. Other species were used such as fleas (*15-20*, *25*), rats (*12*, *14*), trout (*16*, *21-22*), and even plants (*23*). This Genus of *Vibrio* bacterium is bioluminescent which allows a quantitative spectroscopic analysis of the inhibition concentration and/or determination of the effective concentration. Through this property in the *Vibrio* family, toxicity results from NAs were measured by various research groups (*16-22*). The results demonstrate that toxicity of NAs ranged with an IC_{50} of 20-30% v/v of NAs in water. Secondly, the toxicity of NAs was highly dependent on the molecular weight of the NAs (*17*). At low molecular weight such as hexanoic acid the EC_{50} was approximately 0.700 mM. In contrast, undecanoic acid had an EC_{50} of 0.042 mM, and suggested greater acute toxicity for high molecular weight NAs. The same trend was seen for cyclic NAs containing aliphatic substituents as well as aromatic NAs. More importantly, the more substituted and bulky the substituents are on the NAs the lower the EC_{50}. This means acute toxicity seen in the OSPW derived NAs is mainly contributed by the cyclic and bicyclic carboxylic acids. Bitumen from the oil sands has an abundance of NAs that contain bicyclic carboxylic acids (*17*) which has an EC_{50} that ranges from 0.004 to 0.218 mM. This is three times smaller than the EC_{50} from aliphatic NAs. An interesting question emerges concerning toxicity. If bulky lipophilic species in NAs are the main contributor to the toxicity in OSPW then their relatively low solubility in water needs to be addressed. If the lipophilic cyclic NAs do not dissolve in water then the cyclic NAs should not be the main components of NAs in the OSPW. Two possible explanations can account for this discrepancy: pH effects, and micelle formation of NAs. Solubility is dependent on pH and the toxic properties of NAs are more pronounced at higher pH due to concomitant increases in solubility.

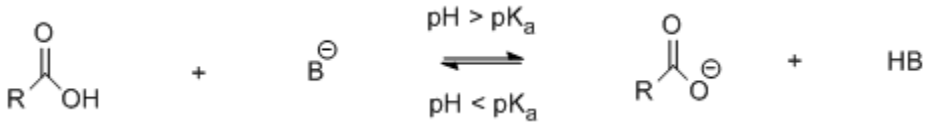

Scheme 1.2 Acid Base Equilibrium of the NAs in the presence of Base (B^-)

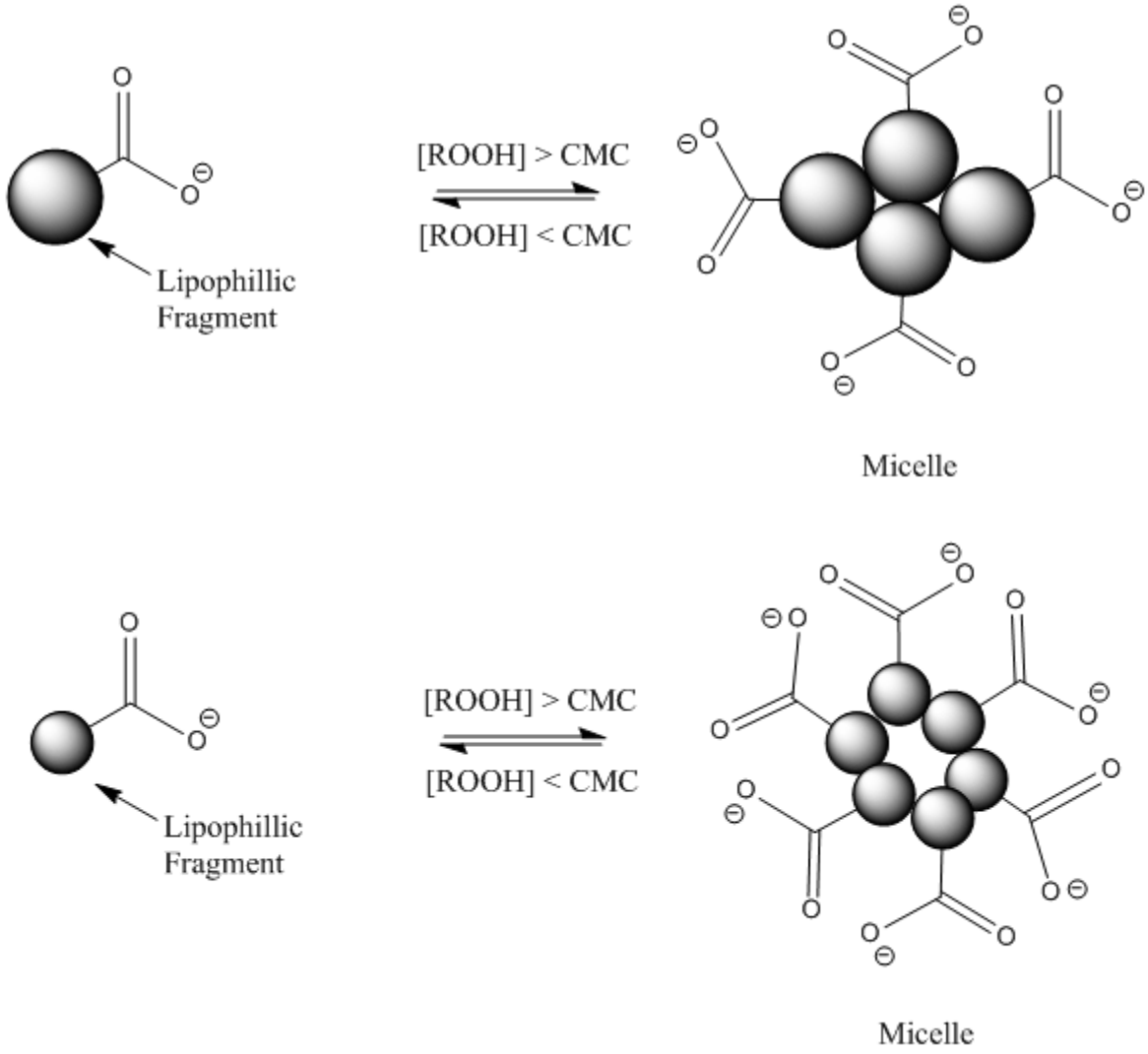

Figure 1.1 Micelle Formation of NAs with varying size of lipophilic fragments

This highlights a problem in the oil sands extraction process. By extracting oil using the Clark caustic extraction process, the toxicity of NAs in aqueous solution is increased due to conversion of more NAs to the water soluble carboxylate anion. Individual components of NAs may have relatively high CMC values such as 50 mM for sodium undecanoate (*24a*) but the CMC of the NAs as a mixture have been reported as low as 154-417 μM (*15*). This could be due to the mixture of carboxylic acids present in NAs (*4*). When more than one surfactant is present the micelles formed is likely a combination of carboxylic acids of varying molecular weight. The resulting CMC of the NAs mixture lies between the cycloaliphatic acids and the aliphatic acids (*25a*). Because of their steric bulk, a lower CMC results (*cf.* Figure 1.1). The elevated salt

concentrations in OSPW may also contribute to the favourable formation of micelles for the large NAs where the occurrence of excess salt (salt content of OSPW is 2200 ppm) in the OSPW can dehydrate the polar head groups or minimize charges between carboxylate groups which encourage formation of micelles (*24a*). Therefore, the toxicity observed may be attributed to micelle formation of the more apolar NAs. Thus, a good method of removing NAs must address the removal of NAs in their ionized and non-ionized forms at variable concentration.

1.1.4 Remediation of NAs

Some NAs in the complex OSPW mixture can degrade naturally and be removed from the OSPW through anaerobic degradation. Unfortunately this process normally takes between 10-15 years (*19, 28*) and a fraction of the recalcitrant high-molecular weight NAs remain unchanged (*29-31*). Therefore, several methods have been developed to address the problem of NAs removal: ozonation, photolysis, bioremediation, and physical adsorption. The most widely used technique in removing NAs is to breakdown the acids using ozonation and UV photolysis. These processes involve conversion of the predominantly large molecular weight NAs into much smaller molecules that may degrade more rapidly. As the molecules have been reduced in size, another method can be introduced that favors the removal of small aliphatic acids. Bioremediation has the advantage of being both natural and economical in terms of energy inputs and ambient temperature conditions. Bioremediation is separated into two categories: phytoremediation (*23*) and microbial remediation. This review on bioremediation will focus on microbial-based bioremediation.

1.1.4.1 Ozonation and Photolysis

This technique employs the usage of the reactive ozone gas and is known to react as a powerful oxidizing agent. One example is its affinity to react with functional groups with double bonds such as alkenes. It can break unsaturated NAs into smaller aldehydes that degrade more rapidly. A fortunate side effect is that the aldehyde forms may be less toxic. This was found by Martin et al. (*27*) when a microtox test using *Vibrio Fischeri* was done on a commercial sample of NAs (Merichem Chemicals and Refinery Services LLC) as well as OSPW samples provided by Syncrude Canada. They monitored the samples for 30 days and found that ozonated samples were degraded by 53% and a higher IC_{20}. This means the toxic inhibitory effect that affects ~

20% of the bacteria population requires a higher concentration of NAs. Therefore, ozonation of NAs appears to render the mixture less toxic. When coupled with bioremediation the half-life of NAs is further decreased. Thus, NAs in natural environments will require years to degrade while ozonation combined with microbial-based bioremediation can reduce the time to ≈ 40 days (*27*). Problems with ozonation are the cost of the ozone synthesis (*4*) and the formation of new pollutants. Ozonation is a radical reaction and a multitude of side reactions are known to occur. These side reactions may form many side products whose toxicological effects are yet to be known. When the commercial NAs and OSPW samples were ozonated to the point where 72% of the NAs was degraded, Martin et al. (*27*) found that the toxicity increases. Secondly, they also found a reduction in toxicity for NAs in OSPW samples are time dependent, thereafter; the IC_{20} decreases after 28 days. Ozonolysis can reduce the amount of larger NAs, reduce the half-life of NAs, and lower the overall toxicity of NAs, at a cost of forming a new and unknown class of toxins as by-products from the degradation of the NAs.

Similar to ozonolysis, photolysis induces radical reactions that can breakdown large molecular weight NAs. The advantage of photolysis over ozonolysis is the half-life of the NAs in OSPW can be reduced to 5-50 hours (*28*). Photolysis and ozonation can be used on a large scale. A disadvantage of photolysis is the generation of a series of side products due to the reactive radical reactions. The side products were determined to be a mixture of hydroxylated radicals and excess hydrogen peroxide, an oxidant that is likely to have toxic side effects (*28*).

1.1.4.2 Microbial-based Bioremediation

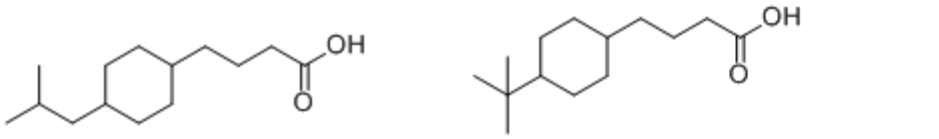

4-(4-*iso*-butylcyclohexyl)-butanoic acid 4-(4-*tert*-butylcyclohexyl)-butanoic acid

Figure 1.2 Model compound NAs studied by Smith et al. (*29*)

Some components of oil sands NAs mixtures undergo a natural bioremediation through aerobic and anaerobic degradation when left in the OSPW. Different bacteria have been shown to vary in degradation reaction rate (*27-29*). Through the inoculum bacterial community, Smith et al. (*29*) have determined the biotransformation of model NAs such as butylcyclohexylbutanoic acid

which can be fully converted to a different form in 1 month. Another model compound such as 4-(4-*iso*-butylcyclohexyl)pentanoic acid was degraded until only 20% remains after a month. When a different bacterial culture was used for another model compound, 4-methylcyclohexylacetic acid, Huang et al. (*30*) also found similar accelerated degradation of NAs.

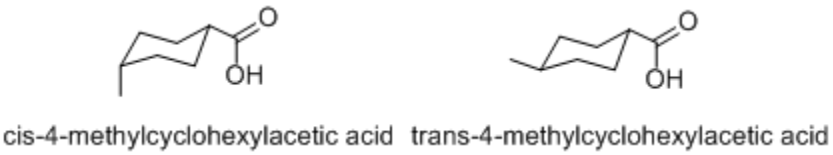

Figure 1.3 Model compound NAs studied by Huang et al. (*30*)

The time required for the model compounds to degrade was found to be 15 hours with different rates of degradation for the different stereoisomers of the model compounds in Figure 1.3. The rate difference is due to changes in conformation where the *trans*-isomer was found to degrade more quickly than the *cis*-isomer. Through these two examples, a problem related to bioremediation can be highlighted. Biodegradation of NAs can depend quite heavily on steric factors such as conformation and substituent bulk. Smith et al. (*29*) found that by increasing the steric bulk from an *iso*-butylcyclohexyl substituent to a tert-butylcyclohexyl substituent there was no perceptible degradation seen for the *tert*-butylcyclohexyl substituent. The persistent problem of other side products also occurs here, i.e. methane formation, depending on the type of bacteria (*31*). The only method of removing NAs that does not convert NAs into another chemical form with potential toxic effects is physical methods such as adsorption.

1.2 Physical Adsorption

1.2.1 General Overview

The term sorption is a broad term that combines two phenomena: absorption and adsorption. Both of the processes involve a material to be adsorbed or absorbed (adsorbate and absorbate, respectively) and a substrate where adsorption or absorption occurs (adsorbent and absorbent, respectively), as shown in Figure 1.4. Absorption is the uptake of absorbates from the bulk phase into the network of the solid (internal surface or pores) where the absorbate proceed

to change the physical properties of the material (*32*). Adsorption is the attraction of the adsorbate from the bulk phase onto the external surface of the material (*24b, 32*). For porous solids, it is often not possible to separate the adsorption from the absorption process therefore, the terms sorption, sorbent, and sorbates are used interchangeably with the above terms.

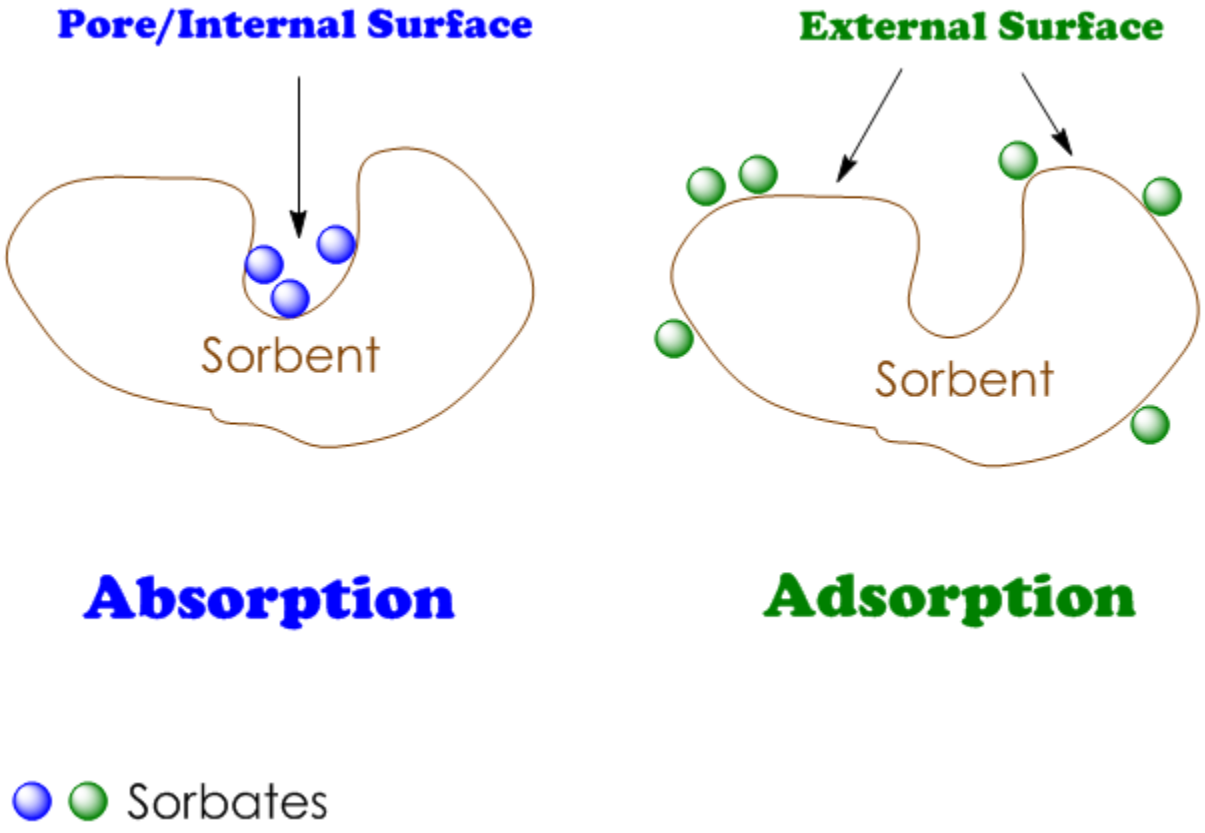

Figure 1.4 Diagram comparing absorption and adsorption is shown above.

Whereas absorption is a volume driven phenomenon, adsorption is a surface driven phenomenon. This interaction at the surface can be driven by multiple intermolecular forces such as van der Waal's, or hydrogen bonding. The former two are examples of a weaker adsorption known as physical adsorption where the process has an enthalpy of desorption ~ 20-40 kJ/mol. Physical adsorption is reversible since the interaction is weak. The molecules are also loosely bound such that rotational motion is still possible (*24b*). Physical adsorption may even be driven by the relative polarity of the solvent in the surrounding according to the relative polarity of the adsorbate molecules. For instance, physical adsorption can be driven by the hydrophobic effect where the hydrophobic adsorbate resides on the surface of the sorbent and this would increase

the entropy of water. A strong intermolecular force that results in irreversible sorption with the substrate itself is given a special category: chemisorption. Chemisorption is characterized by a strong interaction with exothermic heat of adsorption which will render a molecule immobile and irreversibly bound. The enthalpy of desorption for a typical gas chemisorption is 100-400 kJ/mol (*24b*). An example of chemisorption is the oxidation of metals like NAs corrosion of pipes (*5,19b*) while for physical adsorption examples are the many studies involving the adsorption of dyes and NAs by polymeric substrates.

1.2.2) Solution vs. Gas-based adsorption

Sorption onto a solid adsorbent can occur when the adsorbate is a gas or a liquid. The difference between gas adsorption and solution-based adsorption is best encapsulated by the following reaction schemes:

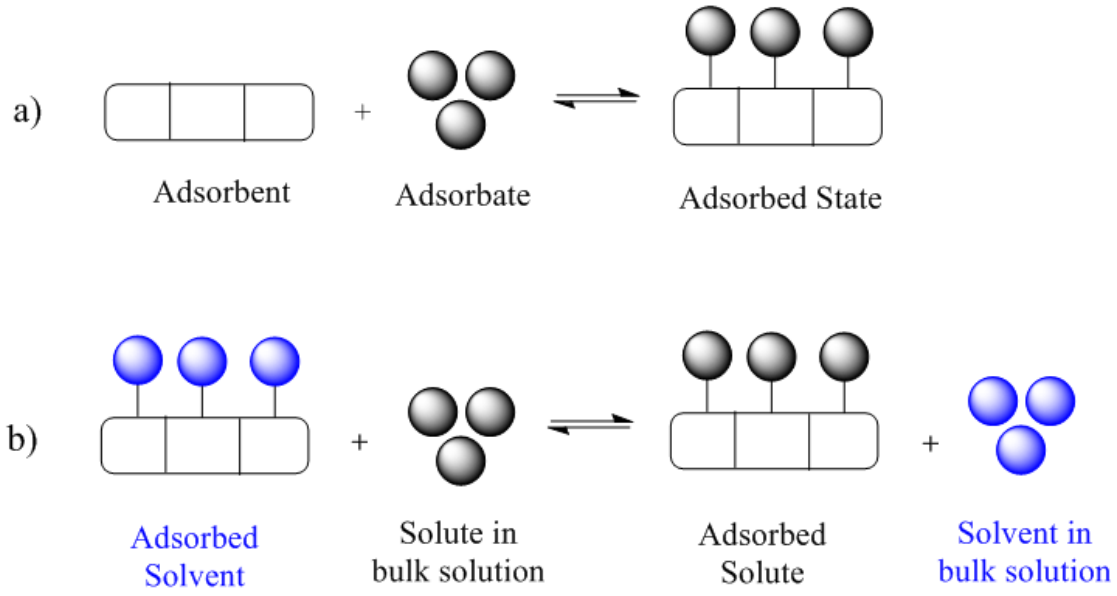

Scheme 1.3 Adsorption processes using a solid substrate with an adsorbate in various phases are illustrated: a) gas adsorption (*24b*), and b) solution-based adsorption (*33*).

For gas adsorption, physical adsorption processes involve noncovalent attachment to a vacant sorption site on the adsorbent. Therefore, the sorption capacity of the material is the amount of adsorbate adsorbed onto the adsorbent.

For solution based adsorption, the assumption that there are vacant sorption sites on the adsorbent is invalid. Instead, all sorption sites are occupied by either a solvent or solute molecule. For a fully desorbed substrate, all sorption sites are occupied by solvent molecules. Thus, the adsorption process in this case is the displacement of solvent molecules by the solute and all models for solution-based adsorption must take into account the activities of the solute and solvent (*33*).

1.2.2.1 Solution-based Sorption Protocol:

Solution phase adsorption on solid adsorbents can be done using a batch equilibrium system or a column chromatography system. A benefit of the batch study approach is the sorption sites in the interior of the adsorbent are accessible and the adsorption process is measured at equilibrium. This method puts the solid adsorbents in the solution phase containing the adsorbate. Once equilibrium is reached, the sorption capacity Q_e can be estimated graphically or by using an appropriate isotherm model. For solution-based adsorption, Q_e is a function of the mole fraction of the solute and the specific surface area of the adsorbent. Assuming ideal-dilute solution condition is obeyed; Q_e can be estimated using the initial concentration of adsorbate (C_0), equilibrium concentration of adsorbate (C_e), mass of the adsorbent (m) and volume of solution (V):

$$Q_e = {(C_0 - C_e)V}/{m} \tag{1.1}$$

In a typical batch study, three variables are held constant. One of the first variables is the temperature. Physical adsorption is an equilibrium process governed by Le Châtelier's principle and temperature will affect the quantity of solute adsorbed. The second variable is the volume of solution because this is the easiest to control. The last variable that is controlled is either the mass of the sorbent or the concentration of adsorbate. Controlling adsorbate concentration has the advantage of being able to obtain adsorption curves relatively quickly as weighing exact sorbent mass is time consuming. Controlling the mass is useful when the amount of adsorbent synthesized can only be obtained in small quantities.

1.2.2.2 Dye Based Method

In the case of solid-solution sorption equilibrium where the sorbent is insoluble, Q_e is evaluated from measuring the residual concentration (C_e) in the supernatant. According to mass-balance for equilibrium conditions, the uptake of adsorbate by the adsorbent can be determined. This decrease in concentration can be measured using the chromophoric properties of the adsorbate according to the Beer Lambert law. For dyes such as *p*-nitrophenol (PNP) the bright yellow color observed is induced by hydrogen bonding with water which reduces the energy gap for the $\pi \rightarrow \pi^*$ electronic transition. When adsorbed into the pores of the copolymer materials the pores are usually small and prevents interaction with the solvent. Without the solvent, PNP will not exhibit its' distinct yellow color and a decrease in absorbance will result. Therefore, one of the most common techniques is to couple batch equilibrium studies for physical adsorption of dyes with UV-Vis spectroscopy. Assuming a large molar absorptivity coefficient, this method is sensitive to dye concentrations in the μM to mM region. Another benefit is that dyes can be used as a way to probe the sorption capacity of the copolymers, analogous to the nitrogen adsorption method. Through the sorption of dyes, the binding affinity, sorption site accessibility, and even surface area of adsorbent can be estimated. Secondly, there are many dyes that can be found that are cationic, anionic, or in an uncharged state depending on the pH and the nature of the dye. Therefore, a dye can be chosen where the sorption capacity of the adsorbent can be evaluated. In the case of naphthenic acids, a model dye compound can be chosen with similar acid-base properties by matching the pK_a of the dye. One such dye is *p*-nitrophenol (PNP) which is an aromatic dye with a pK_a of 7.14 which is close to NAs (pK_a range of 5-6) (*10*). Because of the relative similarity of the pK_a of NAs relative to PNP, the latter will mimic the ionization behaviour of NAs at the alkaline pH conditions of OSPW. At pH conditions < pK_a (PNP), the dye will exist in its' non-ionized form. Above the pK_a (PNP), the dye will exist as an anion. This non-ionized form of PNP has shown a greater adsorption capacity at low pH. Therefore a dye-based methodology to probe the sorption properties of the adsorbent materials can enable tuning of the ionization state of the dye to probe the molecular recognition sites of the sorbent material, according to the pH conditions. As well, pH can be adjusted to simulate OSPW conditions estimate the sorption capacity of the adsorbent materials at field processing conditions.

1.2.3 Types of Adsorption Isotherms

There are six general types of adsorption isotherms defined by IUPAC (*34*). Each type of adsorption isotherm is governed by the surface area and the diameter of the pores. Pore sizes are roughly categorized according to their relative diameter:

1. Macropores: These have a diameter larger than 50 nm.
2. Mesopores: These pores are within the range of 2-50 nm. At this range the pores are large enough to fit more than one gas molecule in the cross-sectional area. Other effects such as capillary condensation also occurs which gives rise to hysteresis loops seen in adsorption and desorption curves
3. Micropore: Pore diameter of 2 nm and less. Only one gas molecule can fit in one cross-sectional area which gives rise to the formation of monolayers seen in the type I isotherm

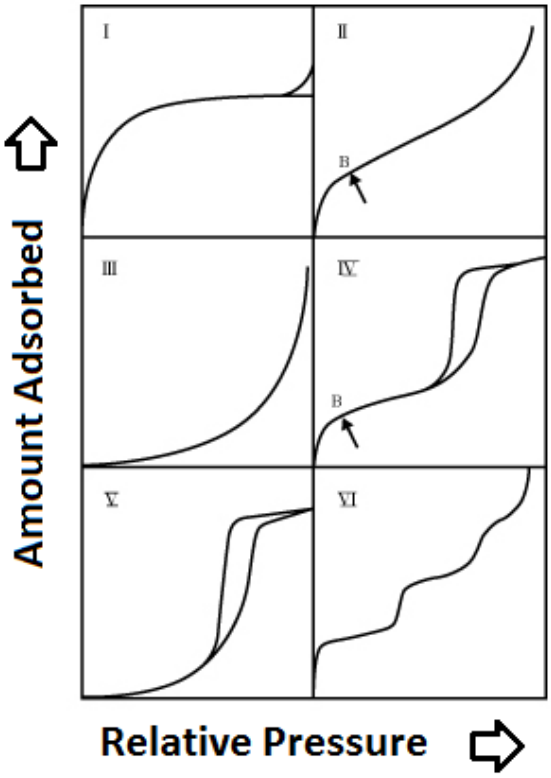

Figure 1.5 Reproduction of the six types of sorption isotherms for gas adsorption. Solution-based adsorption has equilibrium concentration of solute as x-axis. Figure is reproduced with permission from the authors (*35*).

Type I

This curve is a monotonically increasing curve that approaches a specific sorption capacity. Sorbents that follow this behavior tend to be microporous materials where the cross-sectional area of the pores is too small to allow more than one molecule to fit within a pore. Sorbents that follow this type includes GAC or zeolite (*34*).

Type II

Curves of this type can show two extremes in terms of pore size dimensions. This curve can be representative of large macropores where the surface area of the pore is so large that multilayer adsorption can occur without any restrictions. It could also be the type of isotherm for non-porous materials where the only sorption sites are on the external surface.

Type III

This curve occurs due to strong adsorbate - adsorbate interactions where the binding of the adsorbate to itself exceeds the interaction between the adsorbate and adsorbent.

Type IV

Characteristic of mesoporous materials, type IV isotherms are seen for multilayer adsorption processes. Capillary condensation occurs if a hysteresis loop is observed when the adsorbate is desorbed.

Type V

The Type V isotherm is similar to Type III but the interactions between the adsorbates are weaker. This coupled with finite sorption sites enables a plateau to be seen. Hysteresis loops may also be present which suggests the agglomerated particles desorb at once as a collective group.

Type VI

This type of curve shows a step-wise multilayer adsorption profile where one sorption site is filled firstly and then another site is filled. A curve of this type suggests the energy required to adsorb at one site should be very different than at the other site for preferential filling to occur.

1.2.2.1) Hysteresis in solid-gas adsorption/desorption curves

Four types of hysteresis were determined and the definitions are listed below. A typical nitrogen gas-adsorption isotherm is plotted as Q_e against the relative pressure. As the relative pressure approaches unity, condensation occurs inside the pores. The adsorption isotherm obtained can reveal the shape of the pore before condensation. For example: the adsorption isotherm for the H1 is more typical of cylindrical pores whereas H2 is observed for ink-bottle pores (*24b, 34*). As the nitrogen gas has condensed, the desorption process involves an adsorbate in a solution state therefore the desorption-isotherm will be different; hence, the development of a hysteresis loop observed for techniques such as nitrogen porosimetry (*cf.* Figure 1.6).

Type H1

The adsorption isotherm follows Langmuir behaviour. Nitrogen gas adsorbs onto the sides of the pores first before forming multilayers until the pore is filled. This type is associated with cylindrical pores as the filling of the pores can occur uniformly inside the pore which allows for a steep asymptote when condensation occurs.

Type H2

Adsorption into the pores is similar to H1 where capillary condensation is attenuated due to the shape of the pore. The shape associated with this pore is the ink bottle shape where there is a region inside the pore that is difficult to fill (*24b, 34*). This is represented in the elongated region before the asymptote. For the desorption isotherm IUPAC notes that other effects involving the network of pores inside the material is likely a significant factor but the shape of the desorption curve cannot be explained.

Type H3

Beyond the monolayer coverage, interaction between adsorbates on the first layer and the n^{th} layer is relatively weak. This is observed in Figure 2.5 by the broad type III isotherm after monolayer coverage. One type of slit shape that can promote this is a thin slit-like capillary (*34*).

Type H4

The high affinity adsorption isotherm for this type is a distinct indicator of microporosity as the small pore width ensures a strong adsorbent-adsorbate interaction (*34*). The desorption-isotherm is similar to H3 and the pore shape is likely slit-shaped.

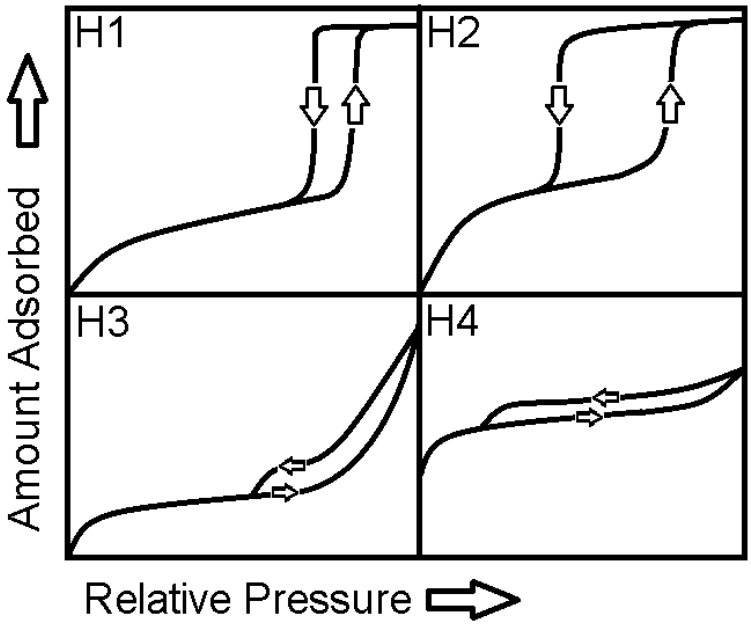

Figure 1.6 The four general hysteresis loops observed for nitrogen adsorption and desorption as defined by IUPAC (*34*)

1.2.4. Models of Sorption Isotherm

1.2.4.1 Langmuir Isotherm

Developed by Irving Langmuir, this isotherm was used to explain, through a simple kinetic model, the adsorption of hydrogen gas on a palladium surface (*36*). Several assumptions

were required; the first is the nature of the material. In the case of palladium, it should have a homogeneous surface. The result is that the sorption sites on the material have similar energy of adsorption and is equally probable for adsorption, regardless of distance between sites. Only a monolayer of adsorbate should form. Lastly, the adsorbate gas should behave as an ideal gas and interaction between the gases within the monolayer are negligible.

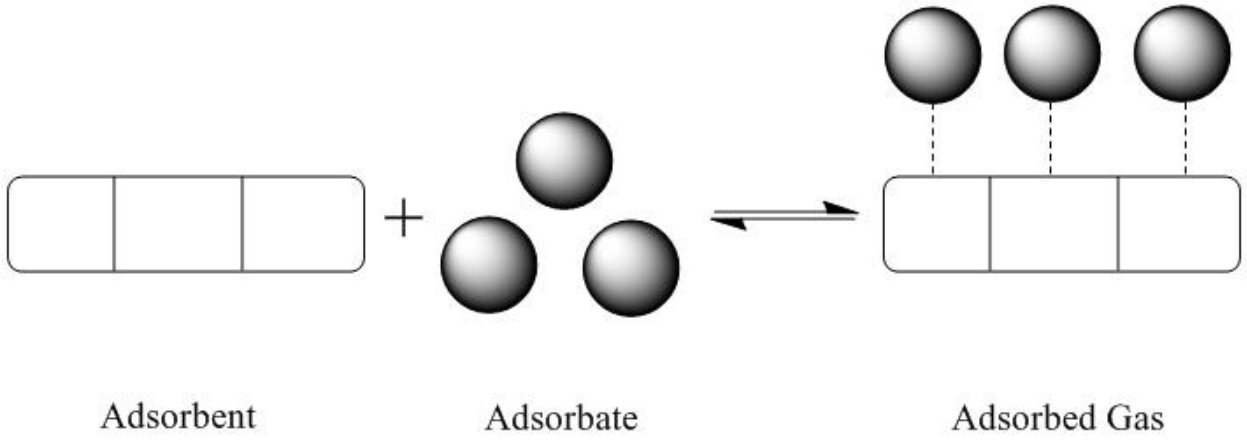

Figure 1.7 Langmuir model of physical adsorption of a gas onto a solid adsorbent

$$\theta = {Q_e}/{Q_m} \tag{1.2}$$

$$\theta = {bC_e}/{1 + bC_e} \tag{1.3}$$

$$b = K_L/a_1 \tag{1.4}$$

θ is the surface coverage factor; Q_e (mmol/g or mg/g) is the sorption capacity or amount of material adsorbed onto a substrate where one gram of the substrate is used. Q_m (mmol/g or mg/g) is the maximum sorption capacity of the material at saturation for one gram of adsorbent/substrate. The term b arises from the consideration of the activity of the solvent (a_1). At dilute solute concentrations (ideal-dilute conditions), the activity of the solvent approaches ideality and b = K_L, the equilibrium constant of the adsorption process (*cf.* Figure 1.7). Therefore, the Langmuir isotherm as interpreted in equation 1.3 requires the equilibrium concentration of the adsorbate (C_e) to be small and preferably obeys Henry's Law. This interpretation holds for the subsequent models where a_1 approaches unity and b = K_x.

1.2.4.2 Freundlich Isotherm

Herbert Freundlich derived his equation by observing that most of the curves do not form horizontal asymptotes as seen in the Langmuir isotherm model. This suggested to Freundlich that the heat of adsorption for every sorption site is not uniform (*cf*. Figure 1.8).

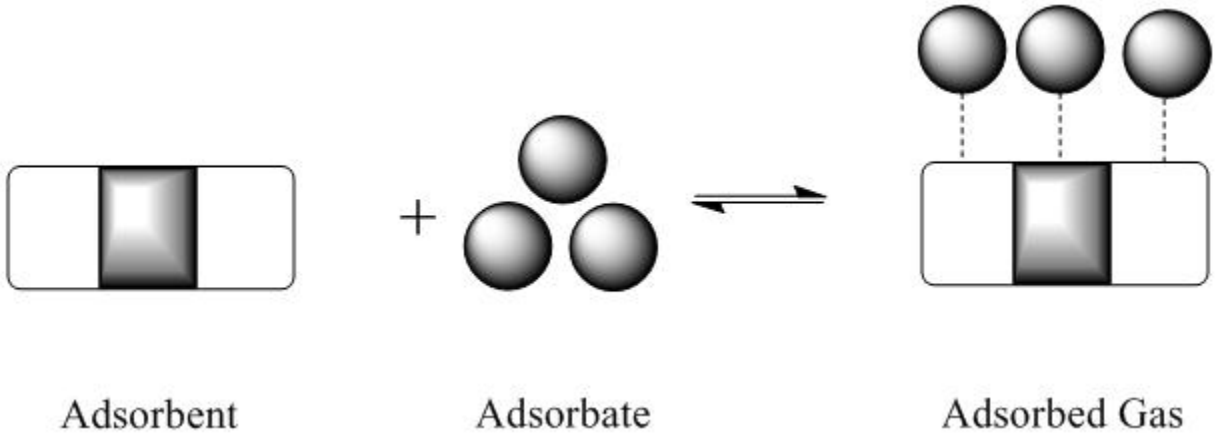

Figure 1.8 The Sips and Freundlich isotherm model of physical adsorption of gas where surface heterogeneity is included.

$$\theta = \left(K_f C_e\right)^{\frac{1}{n_f}} \tag{1.5}$$

The surface heterogeneity is expressed by the parameter $1/n_f$ where the value lies between 0.2 and 1.0 (*37a*). As n_f approaches 1, Henry's adsorption isotherm for dilute solutions is obtained. Again, Freundlich isotherm assumes monolayer coverage. An interpretation of the Freundlich isotherm by Skopp (*38*) using fractal kinetics reveals the meaning of the n_f factor as it approaches zero. According to Skopp (*38*), as n_f approaches zero, the sorption process appears to be independent of the equilibrium concentration of adsorbate and is dependent on the equilibrium constant and the time-dependent rate constants for adsorption and desorption. Unlike the Langmuir isotherm in which the plateau is seen due to saturation of the adsorbent surface, Freundlich isotherm is mainly used for dilute solutions of adsorbates where a plateau is unlikely (*37a*) because many of the sorption sites are unoccupied.

1.2.4.3 Sips Isotherm

Both Langmuir and Freundlich isotherms have similarities and include monolayer coverage. One difference is that the Freundlich isotherm can indicate surface heterogeneity while the Langmuir model does not. By including surface heterogeneity the Langmuir isotherm assumption of constant enthalpy of adsorption at the sorption sites is invalid. Therefore, a general Langmuir-Freundlich isotherm can be developed where the sorption capacity at saturation can be described as a function of the energy distribution of the sorption sites. In cases where this distribution is unity, the Langmuir isotherm (unitary heat of adsorption) is obtained. Specifically, if the heat of adsorption for the sorption sites is distributed in a Gaussian-like manner, the model obtained is the Sips isotherm model (*39*). The n parameter ($n = 1/n_f$) follows the Freundlich isotherm model and reflects surface heterogeneity. The binding affinity of the adsorbate to the sorption sites can be expressed by the equilibrium constant K_s, where a large value indicates adsorption at sites are favored and the sites are readily accessible. As n approaches unity, the model converges to the Langmuir isotherm model where the energy of the sorption site has a singular value. As the concentration of the solution becomes more dilute, the model converges to the Freundlich isotherm. Lastly, this model assumes monolayer coverage when n=1.

$$\theta = {K_s(C_e)^n}\Big/{1 + K_s(C_e)^n} \tag{1.6}$$

This adsorption model is useful in the solution phase due to its ability to simulate both Langmuir and Freundlich conditions, as well as adsorption processes that do not necessarily follow either one (when $0< n<1$).

The Sips isotherm assumptions can be violated from two conditions. The first is strong lateral adsorbate-adsorbate interactions. All three previous isotherms assume ideal solutions where the enthalpy of mixing is zero. One flaw in the Freundlich and Sips isotherms is that the n-parameter only “suggests” the possibility of heterogeneity because lateral interactions between adsorbates can also induce surface heterogeneity. Should the lateral adsorbate-adsorbate interaction dominate (e.g. type III isotherm), the Sips isotherm assumptions can be violated. The second condition that Sips isotherm assumptions do not apply is multilayer formation.

1.2.4.4 Brunauer-Emmett-Teller (BET) Isotherm Model

Whereas the previous three isotherms (Langmuir, Freundlich, and Sips) primarily dealt with monolayer coverage, BET model takes into account multilayer adsorption. Multilayer adsorption is defined for BET where one complete monolayer is stacked on top another through adsorbate-adsorbate interaction (*40*). Depending on the strength of the interaction, Type II-V isotherms can be obtained. This model is useful in providing thermodynamic information such as the enthalpy of adsorption/desorption. If the BET model follows a Type II or IV isotherm, then the sorption capacity of the substrate at the first monolayer can be determined (refer to point B in Figure 1.5).

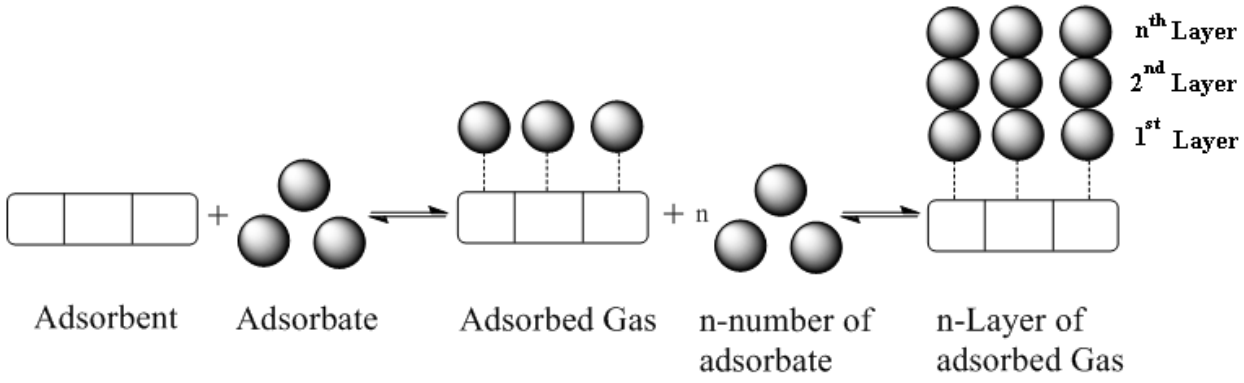

Figure 1.9 BET model of physical adsorption for gas

The thermodynamic data is represented by the constant c (*cf*. Eqn. 1.7). This constant is a function of the enthalpy of adsorption on the first layer and enthalpy of condensation for the gas. A larger c constant value suggests that there is a large enthalpy of adsorption with the adsorbent. This means adsorption on the adsorbent is not favored. This result in molecules adsorbing on the surface of the adsorbent, and subsequent molecules will favor adding onto the layer of adsorbate instead of the adsorbent. Unlike the other isotherms, the initial concentration (C_0) of the adsorbate is required. The BET isotherm model predicts that at saturation, a droplet of gas adsorbate will form on the surface of the adsorbent. The origin of this droplet comes from the BET assumption that the formation of n-layers of adsorbate continues until the adsorbate is fully adsorbed on the adsorbent surface and condensation occurs.

$$\theta = {cC_e}\Big/{(C_0 - C_e)\left(1 + (c-1)\left(\frac{C_e}{C_0}\right)\right)} \quad (1.7)$$

1.3 Applications of Physical Adsorption: Clay, Calcite, Mica, and Activated Carbon

1.3.1 General Overview

Depending on the nature of the adsorbent materials, the adsorption capacity can differ greatly (*41-47*). Adsorption shares one advantage in that NAs are physically removed from the aqueous solution and no side products are formed. This removal of NAs coupled with the fact that the sorbents are in their solid phase that can be physically removed from the solution phase by mechanical means makes this method attractive. Once removed from OSPW, the adsorbate can be removed from the sorbent through desorption processes whether by heating under anaerobic conditions (as was the case with activated carbon) or by desorption with an appropriate solvent. The latter is a less energy-intensive advantage shared by carbohydrate-based copolymers such as β-CD and chitosan copolymers. The sorbent materials can also be modified by cross-linking macromolecules with various linker units that can modify physical properties such as solubility, hydrophobicity, and swellability. With this flexibility, it is possible to enhance the sorption capacity of the materials by careful synthetic modification. Lastly, the sorbents can be made from materials that are economical and may be produced on an industrial scale to match ozonolysis and photolysis. Two of the sorbents, clay (*43*) and petroleum coke (*45*), are by-products of the oil sands extraction process and are generated at scales in the millions of tonnes. Cyclodextrins derived from bacteria are produced on an industrial scale (*44*). The same can be said about chitosan which originates from chitin found in the shells of crustaceans such as crabs and shrimp.

1.3.2 Calcite and Mica

Rezaei Gomari et al. (*42*) analyzed mica and calcite and reported that sorption occurs with preference towards aliphatic carboxylic acids such as stearic and oleic acid. Unfortunately, they did not obtain sorption isotherms and the sorption capacity parameters are unknown. Secondly, OSPW NAs mixtures are predominantly bicyclic and tricyclic carboxylic acids which

mean there is limited benefit in materials that display selectivity toward aliphatic carboxylic acids assumptions can be violated.

1.3.3 Clay

In the oil sand extraction process there is already an abundant amount of clay sedimentation that causes problems in refining the bitumen because of their adsorptive properties and the formation of stable colloidal suspensions. These colloidal suspensions or tailings can be classified as either thin fine or mature fines depending on the particle size but the fact that clay sorbents have strong adsorptive properties towards organic molecules makes them suitable candidates for physical adsorption of NAs. A study by Zou et al. (*43*) where Na-Kaolinite, Na-montmorillonite, and Na-illite were chosen demonstrated sorption capacities of 0.0081 mmol/g, 0.383 mmol/g, and 0.244 mmol/g, respectively. These studies show the potential of clay as a sorbent. The pH of the OSPW is not considered in these studies since OSPW has a pH of 8 which means NAs are in their naphthenate form. The solvent used in the sorption of clay is toluene. The adsorption capacities of clay, although high in toluene, cannot be compared to aqueous solutions. Lastly, a preference for aliphatic carboxylic acids versus cycloaliphatic carboxylic acids is not practical for the NAs in OSPW which are predominantly bicyclic (*4*).

1.3.4 Granular Activated Carbon and Petroleum Coke

Another example of industrial waste sorbent recycled for treatment of OSPW is petroleum coke. Coke is a crude form of activated carbon containing impurities such as sulphur and is a side product of the fluid coking process required in oil sands production (*45*). It has the benefit of being produced in massive quantities (over 50 million tonnes currently (*45*) as well as being a good sorbent towards NAs. Petroleum coke has an affinity towards NAs regardless of the size of NAs present in the mixture. The decrease in NAs concentration due to petroleum coke adsorption was between 67-99% depending on the size of the NAs. An OSPW sample initially contained a concentration of 75.0 mg/L of NA which decreased to 5.7 mg/L after it was treated with petroleum coke. Larger sized NAs with Z = -8 have been adsorbed preferentially with a 90% decrease and the NAs with fewer unsaturation (Z = -2) had a reduced uptake of NAs ~ 67% (*45*). Coke has one advantage over clay in that petroleum coke favors cycloaliphatic carboxylic acids. Secondly, the EC_{20} of the OSPW after being treated with petroleum coke increased from

20% of the OSPW volume required to cause a 20% effect to 91% of OSPW volume. This shows that petroleum coke has the ability to render OSPW relatively non-toxic. A disadvantage of petroleum coke is related to the leaching of impurities from the coke; where sulphur contents can range from 5.7 to 6.8%. A second disadvantage is the quantity needed to adsorb 69.3 mg of NAs in 1L of OSPW (7% uptake of NAs). A 22% by weight sample was used by Gamal El-Din et al. (*45*) which suggests that if 1L of OSPW is used for treatment then the amount of petroleum coke needed is 220 g (*45*). Thus, petroleum coke is a relatively inefficient material used for the removal of NAs. The sorption capacity of petroleum coke can be further improved if we converted the coke to granular activated carbon through carbonization.

When the impurities such as hydrogen, oxygen, and other trace metals are removed through a process of carbonization, which heats the petroleum coke up to 800^{o}C, granular activated carbons (GAC) is obtained. These highly porous materials can have surface area of 1100 m^2/g (*46-47*). The porous structure of GAC can also improve the sorption of NAs as there is more surface area for the NAs to adsorb. By converting petroleum coke into GAC the result was that every 1g of GAC, the amount of NAs adsorbed onto the material is 159mg (*41*) (16% uptake of NAs).

Although GAC is an improvement over petroleum coke, there is still one disadvantage that limits its potential application. GAC has surface functional groups such as alcohols, carboxylic acids, and carbonates; determinable through Boehm titration as described by Kwon and Wilson (*35*). Depending on the source of the coke the relative amount of surface groups can vary. All three of these surface attachments would deprotonate near pH of 8-9 similar to NAs in OSPW. Therefore, GAC is an anionic adsorbent and has an electrostatic repulsion towards NAs at alkaline pH. GAC, although a good adsorbent, cannot adsorb NAs to the potential occurrence of electrostatic repulsions. Thus, a material that has a neutral zeta-potential at high pH while being just as porous as GAC will be an ideal candidate for the removal of NAs from OSPW. A potential sorbent would be carbohydrate-based copolymers.

1.4. Applications of Physical Adsorption: β-Cyclodextrin-based materials

Cyclodextrins (CD) are cyclic-oligosaccharides that are produced by bacteria (*44*). The three most common forms (α-, β-, and γ-CDs) are shown in Figure 1.10. CDs have a toroidal

cavity that may adsorb molecules as large as steroids and as small as *p*-nitrophenol. CDs have demonstrated chiral recognition of one enantiomer preferentially over another (*48*). Thus, a CD copolymer would be an ideal sorbent for NAs because CDs can be tuned to adsorb molecules of various sizes according to their diverse structure and properties.

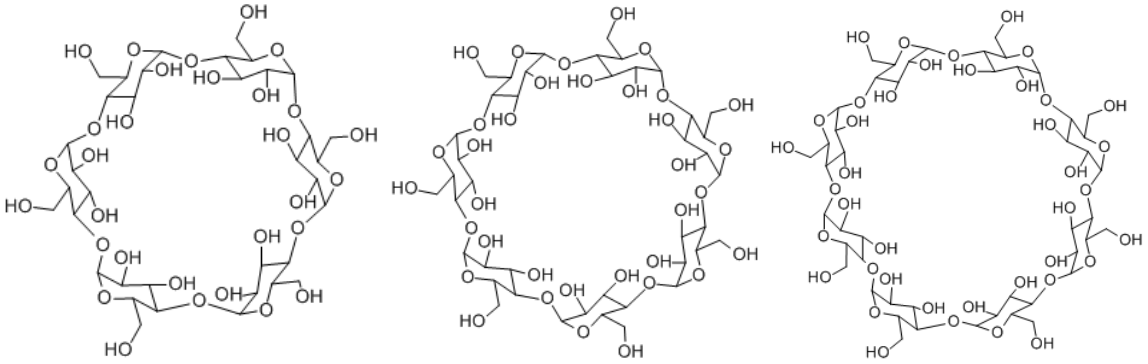

Figure 1.10 Molecular structures of cyclodextrins left: α-cyclodextrin; middle: β-cyclodextrin; right: γ-cyclodextrin

CD-based copolymers can have a variety of properties that can be tuned by controlling the amount of cross-linking and the type of cross-linkers. Highly polar CD copolymers with peracylated linkers were synthesized by Hirayama et al. (*49*) which can increase the solubility of the copolymers for use in the field of drug delivery but are of limited use in wastewater remediation. Isocyanate-based CD copolymers have low water solubility which makes such copolymers suitable for physical adsorption of NAs (*10*). Polyurethane-CD copolymers are suitable for the removal of NAs and areformed by direct addition of diisocyanate linkers to β-Cyclodextrin (β-CD) in anhydrous dimethylacetamide or other suitable solvents. Several linkers were chosen (see Figure 1.11) to reflect different functional groups such as: aliphatic (HDI, CDI), and aromatic (NDI, MDI, PDI) units.

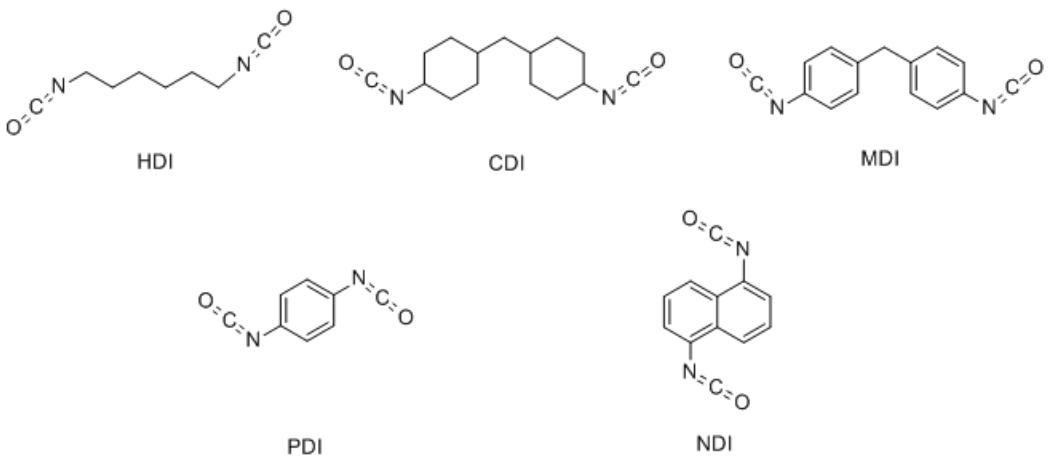

Figure 1.11 Molecular structures of diisocyanate cross-linkers used by Mohamed et al. (*41*)

Each copolymer was made at variable different ratios from a 1:1 β-CD to linker mole ratio to 1:6. The results were compared to the sorption capacity of GAC at pH 9.00 (147 mg/g). It was found that the aliphatic linkers had the highest overall sorption capacity. HDI had a sorption capacity of 70-75 mg/g while CDI had a sorption capacity of 70.4 mg/g. The aromatic linkers had a sorption capacity range of 21-57 mg/g.

The results indicate that the greater sorption capacity of the urethane-based copolymer was observed for aliphatic linkers when compared with the aromatic linkers. This can be due to several factors with accessibility to the sites being a contributing factor. Mohamed et al. (*41*) determined the % accessibility to the β-CD sorption sites and found PDI and CDI had the highest. When coupled with the high K_S value it can be concluded that PDI and CDI exhibited high sorption capacity and this was understood by the relative access of the β-CD inclusion sites. A disadvantage of the aliphatic linker is the accessibility to the sorption sites decreases rapidly as the amount of linkers increase. This was illustrated by the decrease in the equilibrium constant, K_S. As the linker content increased from PDI-1 to PDI-2 the K_S value drops from 0.118 to 0.0323; whereas, the K_S value for CDI-1 was 0.0147. For the aromatic linker compounds, the K_S value did not drop as rapidly for MDI-1; K_S value of 0.0729 *vs.* the K_S value for MDI-2 being 0.0673. Therefore, one benefit of the aromatic linkers for β-CD copolymers was the lack of steric hindrance that may account for the smaller drop in K_S value when compared to the aliphatic linkers. While aliphatic linkers had the overall higher sorption capacity, it was the aromatic

linkers, with an attenuated decrease in K_s that can retain these NAs inside the copolymer networks.

1.5 Applications of Physical Adsorption: Chitosan-based materials

1.5.1 Origin and Properties of Chitosan

Chitosan was first discovered in 1859 by Rouget when chitin was boiled in concentrated potassium hydroxide and the subsequent product was shown to be soluble in acids (*50a*). Unlike chitin, chitosan is rarely found in nature. Chitosan is a polysaccharide containing two types of monomers: 2-acetamido-2-deoxy-D-glucopyranose and 2-amino-2-deoxy-β-D-glucopyranose. The monomers have β-linkages and chitosan has a "stretched", linear structure in solid state (*50a*). This is also true for chitosan in solution where the charge repulsion between ammonium groups between the 2-amino-2-deoxy-D-glucopyranose ensures coiling is minimized (*50b*). This has the effect of increasing viscosity of chitosan in dilute solutions unless ionic strength is increased to neutralize the repulsive ammonium charges (*51*). Chitosan is known to be stable in air and inert in most solvents. It does not degrade unless rigorous conditions such as concentrated acids which can cause chitosan to depolymerize (*51*). The pK_a of chitosan is ~ 5.5-6.5 depending on the degree of deacetylation. Average molecular weight of chitosan can vary over a wide range from (1-5) x 10^5 g/mol.

At different pH conditions chitosan can undergo physical or chemical changes. At low pH under 3, chitosan can depolymerize via hydrolysis. At higher pH at 3.6, chitosan is soluble in acidic aqueous solutions this distinction is how chitosan is differentiated from chitin and also defined. At neutral and basic pH conditions chitosan can be precipitated out when pH > pK_a because the primary amine groups are neutral and less polar relative to their ammonium ion forms.

1.5.2 Solubility

Chitosan is defined as being an N-deacetylated derivative of chitin such that it is soluble in dilute aqueous acids like formic acid; whereas chitin is insoluble (*52a*). According to Muzzarelli et al. (*52a*) chitosan requires deacetylation of 85% of the glucopyranose monomers but varying degrees of deacetylation have been used in commercial samples ranging from 75-85%

deacetylation (*53-55*). A trade-off of lower deacetylation ratio is that solubility becomes more limited and a stronger concentration of acid may be necessary. Although chitosan is soluble at low pH (4.1 (*55*)), it can undergo hydrolysis and depolymerize back to its monomer form if the pH is below 3. This makes it attractive towards pharmaceutical industry where chitosan can be used as a disintegrant or carrier. The drug puracetamol was carried in the gel form of chitosan and when it reached the stomach (pH 1.5-3.5) the gel disintegrated into the non-toxic monomer (*56*).

Chitosan is insoluble in most non-aqueous solvents unless a small amount of acid is present which is used to alter the protonation state of the chitosan monomers. Chitosan may dissolve depending on the molecular weight, degree of deacetylation, type of acid, and the strength of the acid. 2% acetic acid solution can dissolve chitosan as long as chitosan is within 2% (w/v) (*55*). Chitosan has also been shown to be soluble in a 10% citric acid solution (*52a*). For organic solvents, chitosan has been shown to be highly soluble in a dimethylformamide/dinitrogen tetroxide solution (*50a*); dimethylformamide has a pK_a of -0.01 which shows it is an organic acid. The addition of acid to increase the solubility of chitosan can be explained through the acid-base properties of the primary amine group. Chitosan has a pK_a of 6.5, and chitosan is soluble at pH values < 4.1 where much of the amine group are in their protonated ammonium form. The increased charge repulsion between amine groups in chitosan enlarges the volume so that the ammonium groups are more exposed to polar solvents such as water. This will cause ion-dipole interaction to form preferentially between the ammonium cation and water (*52b*).

1.5.3 Gelation

Chitosan and chitosan copolymers have been known to form gels and the synthesis of chitosan copolymers in their powder form takes advantage of the gelation processes (*52a*, *55*). A gel is a network of aggregated particles or polymers that can trap liquid through surface tension effects (*57*). Gels consist of a continuous solid phase where the polymer network encompasses the solvent phase. It also consists of the dispersed solution phase which is a liquid trapped by the network of polymers. Therefore gel formation is a spontaneous process if the polymer is large enough, and contains multiple bonding sites. If the polymer chain length is small, then solvent can be driven off to reduce the volume and increase the interaction of the polymers (*58a*). Gels

can be quantitatively measured using two parameters: viscosity, and shear modulus. As the polymer forms networks, the solution should become more viscous. At the start of gelation, one molecule of chitosan will form intermolecular interactions with either itself or another cross-linker where the interactions are primarily through hydrogen bonds (*59*). Then the dimer that is formed will interact with another dimer and form oligomers until a fibrous network is obtained and the solvent is trapped in the interstitial pores of these fibers resulting in a gel (*57*). This acceleration in gelation is mirrored in the viscosity of the solution. The viscosity of the solution increases exponentially until gelation occurs where the solution can no longer flow (*58a*). Once gelation occurs, an aging process may set in.

1.5.3.1 Aging Process in Gelation

The aging process is the gradual hardening of the gel network from the gel point. At the gel point, there are enough polymers to solidify into a gel but there are still sites in the gel interior that can still interact through intermolecular forces such as hydrogen bonding or chemically cross-link and make the network more rigid. This hardening of the gel network is another way to characterize gels. By testing the shear modulus of the gel, information of the amount of cross-linking in the interior of the gel can be elucidated. The aging process will be crucial in the synthesis of chitosan-glutaraldehyde (Chi-Glu) copolymers.

Three possible processes can occur during the aging process: polymerization, coarsening, and phase transformation. For Chi-Glu copolymers, the polymerization process are of relevance (Further information of the other two processes can be found in literature (*58b*)). Polymerization is the increased interconnectivity of the cross-linkers due to chemical reactions. For silica gel, the reaction is the condensation reaction between two hydroxyls while for Chi-Glu systems, the reaction is amine-catalyzed aldol condensation involving the amine on the chitosan and the aldehyde on glutaraldehyde (*55*). As more chitosan is cross-linked there is greater interconnectivity and hardening of the gel.

1.5.4 Chitosan Production

Chitosan is normally not found in abundance in nature but can be obtained from chitin which is an industrial by-product of fisheries around the world. Each year, approximately 20 million tonnes of shrimp, lobster, and crab shells are discarded as waste (*60*). Depending on the organism, the amount of chitin in crustacean shells may range from 14% to 75% chitin (*60*). This makes obtaining chitosan from waste products such as crustacean shells appealing. There are several methods that chitosan can be synthesized from crustacean shells with chemical and enzymatic processing are two examples (*60*). As much of the shells contain a mixture of $CaCO_3$, proteins, and chitin; it is necessary to separate the three components using either of the methods. Proteins can be removed through a mild treatment of an alkali solution. This dissolves the proteins while leaving the chitin. $CaCO_3$ can be removed through the addition of dilute acid which causes CO_2 to evolve and Ca^{2+} to be dissolved in water (*60*). Lastly, chitosan is obtained through deacetylation of chitin using an alkali solution. The temperature of the deacetylation step determines the molecular weight of the resultant solution. Although high temperature can cause a greater degree of deacetylation, it can also cause hydrolysis and depolymerisation chitosan, resulting in lower molecular weight products (*60*).

1.5.5 Chitosan Copolymer Synthesis and Applications

Much of the application of chitosan copolymers employs cross-linkers to change the physical structure of chitosan through a reaction at the primary amine and hydroxyl substituents. After deacetylation, chitosan may have a powder or flake form depending on the mechanical treatment of chitin during production (*59*). After cross-linking, chitosan copolymers can be tuned to a multitude of morphological forms such as chitosan beads, hydrogels, powders, and films/membranes. Each one of these various forms has seen applications ranging from self-repairing materials (*61-62*), filtration material of protein (*62*), wastewater and dye remediation (*63-65*), and drug delivery (*66-69*). For wastewater and dye remediation, two forms show promise: chitosan copolymer beads and powders.

Synthesis of chitosan copolymers undergoes a similar process for each of the materials. Chitosan is dissolved in dilute acid forming an aqueous solution and cross-linkers are added. To obtain beads, the mixture is then added dropwise into an alkali solution where the droplets are

precipitated. As the precipitation process occurs rapidly, the resulting beads will have uniform diameters (*64*). For the other types, the viscosity of the chitosan-cross-linker solution increases over time until the gel point is reached where the chitosan-cross-linker solution becomes a gel. This gelation process depends on various factors but it can be accelerated by neutralizing the pH so that the solution is close to the pK_a (*55*). An aging process sets in where the shear modulus of the gel increases and the gel hardens (*55*). An insoluble cross-linked copolymer is obtained when the gel network is broken by adding an alkali solution to precipitate out the copolymer followed by air drying.

1.6 Applications of Chitosan Copolymers

1.6.1 Chitosan Copolymer Beads

Chitosan is a semi-crystalline polymer due to the presence of abundant hydroxyl and amine groups. Both of these groups undergo hydrogen bonding and can result in crystalline structures (*59*). This crystalline structure is favored when water is driven from the chitosan network. Therefore, chitosan copolymer beads are popular in wastewater treatment and dye remediation due to the small surface area which can attenuate the drying of beads and result in the slowing of crystallization in chitosan copolymers (*59*). Linkers that have been often used for the formation of chitosan copolymer beads such as glutaraldehyde (Chi-Glu) (*63, 55*) and epichlorohydrin (ChiECH) (*63*). When comparing the chitosan copolymers synthesized from epichlorohydrin (ECH) and glutaraldehyde (Glu), Chiou et al. (*63*) observed that higher sorption capacity of reactive red 189 (RR) in the epichlorohydrin. The sorption capacity of ChiGlu towards RR was 1000 mg/g while ChiECH was 1800 mg/g. Epichlorohydrin preferentially bonded at the hydroxyl substituents on chitosan. This left available primary amine sites as the main sorption site in chitosan that were bound with the dye. Chiou et al. (*63*) tested the effects of increased molecular weight in the chitosan sample and was found to be negligible. Various molecular weights of chitosan were chosen from 150 kDa to 600 kDa with the content of amino groups are constant. The sorption capacity remained the same on the chitosan copolymer beads regardless of their molecular weight.

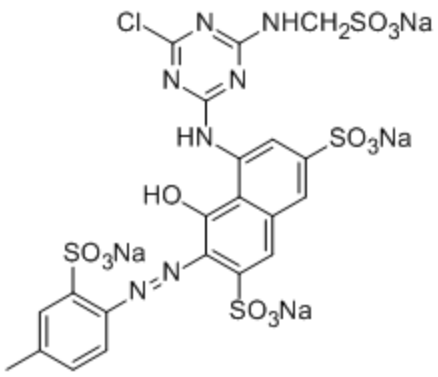

Figure 1.12 Molecular structure of reactive red 189

A disadvantage of chitosan beads is that sorption in chitosan is determined by two factors that the bead form does not remedy. Sorption of dyes on chitosan can occur on the surface where the surface area of the particle dictates the number of sorption sites. While less crystalline, the surface area of beads is smaller than large particles, and therefore, greater sorption capacity is expected (*59*). Secondly, sorption can also occur in the internal sites where intraparticle diffusion is a key factor. Accessibility to these sites was found to be inversely proportional to particle size. As the particle size increased, the sites became less accessible and equilibrium time increased (*59*).

1.6.2 Chitosan Copolymer Powder Application

The powder form of chitosan copolymer has been studied mainly as a sorbent for metal species such as copper, and as a vessel for drug delivery (*66-69*). This form has the advantage of greater surface area and sorption capacity. Average particle size were shown to be ~ 4-24 nm for chitosan-N-poly(ethylene)glycol particles while chitosan-tripolyphosphate (*66*) have been shown to be ~ 2-3 μm. Through this powder form, there is a greater ability to tune the physical properties of chitosan. Jafarinejad et al. (*66*) chose the powder form over beads due to its' higher solubility of the drug itraconazole onto the chitosan-tripolyphosphate copolymer. One disadvantage of the particulate system is the particles are of small size and have a tendency to aggregate which can reduce the surface area (*69*). The small size of the particles was not suitable for a batch study because the particulates may form a colloidal suspension if they are not aggregated (*69*).

1.7 Summary: A Good Adsorbent for sorption of NAs

In order to physically remove NAs, a toxic component of OSPW, without making potentially toxic side products, a suitable sorbent material is required. There are four requirements of a good adsorbent:

1. Scale: The adsorbent must be made from materials that can be produced on a large scale that have good Sorptive uptake of OSPW NAs.
2. Cost: The adsorbent must be made from materials that are economical or its applications to industry will have limited usage
3. Reusability: Adsorbent should be designed so that recyclability is possible with minimal energy inputs.
4. High Adsorption Capacity: This ensures the adsorbent efficiently removes NAs

The first two criteria have been satisfied by a diverse range of materials such as clay, activated carbon, cyclodextrins, and chitosan. For reusability, chitosan and cyclodextrin based materials have shown this (*59, 69*). The last criteria of high sorption capacity using cyclodextrin and chitosan based copolymer materials will be the focus of this thesis. One method for obtaining high sorption capacity is to increase the surface area in the material. An overall increase in the surface area will increase the number of sorption sites and an increase in sorption. This can include increasing the exterior surface area and the number of pores that make up the interior surface area. Another method could be activating sites that are normally inaccessible by increasing the intraparticle diffusion. Both of these methods can be done by tuning the copolymers through the addition of linker agents.

From the review of the different materials, chitosan-based copolymers in powder form would be a good candidate because of the high surface area. The pK_a of chitosan is high and can have multiple cationic ammonium sites that favor binding with the anionic naphthenates. This is also true for β-CD copolymers that have shown enhanced sorption with dyes and NAs (*41*). By taking advantage of the hydrophobic effect which favors NAs adsorption, a non-polar linker such as glutaraldehyde would be an ideal linker to cross-link with chitosan. The hydrophobic nature of the sorbent can be varied by adjusting the level of cross-linking and the nature of the cross-linker.

1.8 Research Objectives

Therefore the following hypothesis-driven objectives will be investigated in this thesis:

1. Can the mole ratios of linkers affect the sorption capacity of the copolymers? Chitosan and β-cyclodextrin based materials have been synthesized and characterized at various mole ratios.
2. Can the mechanism and sorption capacity of NAs be elucidated through the adsorption of *p*-nitrophenol (PNP) and carboxylic acids with varying z-components? Through the dye sorption method, an absolute maximum for the sorption capacity have been determined with relative ease and the carboxylic acids revealed the effects of steric hindrance on adsorption.
3. Lastly, are the chitosan and β-cyclodextrin copolymers applicable to the removal of NAs in OSPW environments? Sorption of NAs using the commercial samples (Fluka and Acros) was studied at pH 9.0 to investigate the utility of the copolymers for the removal of NAs from OSPW.

CHAPTER 2

MATERIALS AND METHODS

2.1 Introduction

For this section, instruments used in this project will be described. Materials and a synthesis protocol for both of the β-CD and ChiGlu copolymers conclude this chapter. For further background on the instruments see references (*78-89*)

2.2 Instrumental Analysis

2.2.1 ^{1}H NMR

The ^{1}H NMR spectra were obtained at 500 MHz using a 3-channel Bruker Avance (DRX) spectrometer. The internal chemical shift standard is tetramethylsilane (TMS) with a chemical shift of 0 ppm. Solvents used were deuterated DMSO (DMSO- d_6), deuterium oxide (D_2O), and deuterated chloroform ($CDCl_3$).

2.2.2 FT-IR

Fourier Transform IR spectra were obtained using a double beam spectrophotometer (Bruker, model Tensor 27). The sample chamber was purged with nitrogen gas and solid samples were analyzed as KBr pellets in transmission mode. In the case of liquid samples, they were analyzed as a liquid film using a NaF cell.

2.2.3 UV-Vis

UV-Vis absorbance spectra were obtained using a double beam Varian-Cary (Cary 100) spectrophotometer. Samples were analyzed in solution using quartz cuvettes. A calibration curve of absorbance *vs*. concentration of dyes is made to determine the linear response region of the Beer-Lambert law and the molar absorptivity of PNP at various pH and concentration conditions.

2.2.4 TGA

Thermalgravimetric analysis (TGA) of samples was obtained with a TA Instruments TGA (Model Q50). Nitrogen gas was used for cooling and purging of the sample compartment.

Samples were analyzed in open aluminum pans over the temperature range between 30^{o}C to 500^{o}C at a heating rate of 10^{o}C.

2.2.5 Porosimetry

Nitrogen adsorption isotherms were obtained using a Micromeritics ASAP 2000 V2.05 surface area pore size analyzer. Samples were weighed to ± 0.1mg and within the range of 0.8 to 1.0 with a precision of ± 0.0010 g. The sample compartment was degassed at 70^{o}C with pumping until a stable outgas rate of <10 μmHg was reached.

2.2.6 CHN Analysis

Carbon, Hydrogen and Nitrogen elemental content was obtained using a Perkin Elmer 2400 CHN Elemental Analyzer. The combustion oven temperature was above 925^{o}C while the reduction oven had a temperature over 640^{o}C. The instrument was purged using a mixture of pure oxygen and helium gas. The calibration standard was acetanilide. Both precision and accuracy of the results are within 3%.

2.2.7 Mass Spectrometry: ESI-MS

The instrument used for obtaining electrospray mass spectra was a Quattro Ultima mass spectrometer (Micromass, UK) coupled to a Waters 2695 advanced separation system (Milford, MA). The eluent was a 50:50 mixture of acetonitrile: water with 0.1% of NH_4OH. The sample is directly injected into the separation system. The mass analyzer used was a linear quadrupole and the detector was optimized to measure fragment ions in negative ion mode. The source temperature was 90^{o}C, while the desolvation temperature was set at 220^{o}C. The cone gas used was N_2 with a flow rate of 147 L/hr and the capillary voltage setting was 2.63 kV with a cone voltage set at 62 V. The mass resolution was set to 14.0 and the ion energy was 1.7 eV. Entrance voltage was 96 V and the exit voltage was 56 V with collision energy of 13 eV. The multiplier was set at 410 V. The full scan range (100-550 m/z) was employed and the software used for analysis of the results was MassLynx version 4.1.

2.3 Materials

β-CD was obtained from Alfa Aesar (Ward Hill, MA, USA). Anhydrous

dimethylacetamide (DMA) was obtained from EMD (Edmonton, AB) . Terephthaloyl chloride (TCl), sebacoyl chloride (SCl), diphosphorus pentoxide (P_2O_5), sodium hydroxide, potassium phosphate monobasic, *p*-nitrophenol, low molecular weight chitosan (85% deacetylated, molecular weight range: 50,000-190-000kDa), 50 wt.% glutaraldehyde in water, glacial acetic acid, and various HPLC grade solvents (acetone, methanol, and diethyl ether) was obtained from Sigma-Aldrich Canada Ltd. (Oakville, ON). Granular Activated Carbon (GAC*;* Norit Rox 0.8) was obtained from Norit America and used as received. GAC materials were subsequently dried under vacuum. All other chemicals were used as received unless specified otherwise.

TCl and β-CD were dried prior to synthesis using a pistol dryer under vacuum with P_2O_5 as the desiccant. The dried reagents were stored in a desiccator containing activated molecular sieves as the desiccant until required.

2.4 Synthesis

2.4.1 Cyclodextrin Copolymers

A combined mass of 2.00 g β-CD and TCl were dispensed such that the mole ratios of β-CD to linker (1:1, 1:2, and 1:3) were obtained. Once the β-CD and TCl solids were under argon gas, 20 mL of anhydrous DMA was added to the round bottom flask with stirring until complete dissolution. The reaction was then heated to 60^{o}C for 48 h. After the reaction, the solvent was removed under vacuum until a gel was formed. The gel was then washed with a polar aprotic solvent such as acetone. A white to light yellow solid product was isolated using vacuum filtration. The product was washed in a Soxhlet extractor with acetone for 48 h. After subsequent drying at 50^{o}C in a vacuum oven, a second cycle of washing in the Soxhlet extractor with diethyl ether was carried out for 48 h. In the case of 1:6 and 1:9 copolymers, methanol was used in place of acetone. The percentage yields were calculated according to initial amount of β-CD and the cross-linker, according to Figure 2.1.

Table 2.1 Mass of β-CD, SCl, and TCl used in reaction

Copolymer Product	Mass of β-CD (g)	Mass of TCl (g)	Volume of SCl* (ml)
1:1 TCl	1.6965	0.3035	
1:2 TCl	1.4730	0.5270	
1:3 TCl	1.3015	0.6985	
1:6 TCl	0.9647	1.0353	
1:9 TCl	0.7663	1.2337	
1:1 SCl	1.6514		0.31
1:2 SCl	1.3038		0.62
1:3 SCl	1.2254		0.69
1:6 SCl	0.8833		1.0
1:9 SCl	0.6905		1.2

*density of SCl is 1.121 g/L.

2.4.2 Chitosan-Glutaraldehyde (Chi-Glu) Copolymers

6.00g of Low molecular weight chitosan (50,000-190,000 g/mol) was dissolved in 600 mL of aqueous acetic acid (5% v/v). Once the chitosan was fully dissolved, glutaraldehyde was diluted with an additional 20mL (5% v/v) aqueous acetic acid (pH 3.3-3.9) and then added to the chitosan solution. The amount of glutaraldehyde added is dependent on the mole ratio. The solution was stirred overnight until a light yellow to orange coloured gel was obtained. Should gelation not occur within 24h, *in vacuo* removal of water was done (gentle heating was applied at 25-30^{o}C). Upon gelation, the gel was given 24h to allow the aging process to occur. Once aging has completed (*cf.* Figure 4.3b or 4.5a) a solution of 1M NaOH was added slowly to the gel. Rigorous stirring was done using a spatula while 1M NaOH was added. The gel will undergo

three stages (see Figure 4.5) until an insoluble brown precipitate was observed and the pH of the supernatant solution was 7.0. The suspension was left in the solution overnight to facilitate aldol condensation and a dark brown precipitate was obtained. This precipitate was then isolated using vacuum filtration. A swollen, dark brown hydrogel was obtained (*cf*. Figure 4.8. right-side). This new gel was cut into pieces by a spatula, and ground gently with a mortar and pestle. Gentle drying was done using an oven for 1 hour at 60^{o}C and at ambient pressure. The product is removed and grounded again using the mortar and pestle. This procedure is repeated until the final product was a fine brown powder which was dried overnight at ~ 25-30^{o}C. The product obtained was further grounded and sieved (40-mesh) followed by washing in a Soxhlet extractor with methanol for 24h. Finally, a vacuum oven at a temperature of 45^{o}C and reduced pressure (25 mmHg) was used to remove any solvents from the final product.

Table 2.2 Mass of Chitosan and Glutaraldehyde used in reaction

Copolymer Product	Mass of Chitosan (g)	Volume of Glutaraldehyde* (ml) 50% *w/v* Solution
1:400 ChiGlu	6.0000	3.6
1:700 ChiGlu	6.0000	6.3
1:1000 ChiGlu	6.0000	9.0

*density of glutaraldehyde solution is 1.106 g/L

2.5 Solubility and Hydrolysis Measurements

A gravimetric approach was used to determine the solubility of the co-polymers in deionized and distilled water (resistivity at 25^{o}C: 18.2 Ωcm). Approximately, 60 – 100 mg of copolymer was added to a vial and 7.00mL of water was then added. The mixture was mixed on a shaker table for 24 h to ensure equilibrium. The particles were then isolated using a centrifuge. 1.00 mL of the supernatant solution was added to a pre-weighed sample vessel. After gentle air drying, the gravimetric differences provide estimates of the solubility.

Hydrolysis of the polyester materials were tested using the same procedure stated above in aqueous buffer solutions (0.10 mM KH_2PO_4 buffer at pH 4.60 and 0.10 mM $NaHCO_3$ buffer at pH 9.00). 3M NaOH was used to adjust the pH of the buffer solutions. The salt content of the buffers were accounted for in the determination of solubility of the copolymer materials.

2.6 Sorption Measurements:

2.6.1 *p*-Nitrophenol (PNP) adsorption

The molar absorptivity (ε) of *p*-nitrophenol (PNP) was estimated using the Beer-Lambert calibration plot (λ_{max} = 325 nm at pH 4.60). The value for ε was 10,176 $Lmol^{-1}cm^{-1}$ at pH 4.60, in agreement with the literature (*35*). Deviations from the Beer-Lambert law occur when [PNP] > 0.18mM; therefore, all supernatant solutions from the solid-solution isotherms were analyzed in the linear region and diluted accordingly. The sorption of PNP was carried out for copolymers which had negligible solubility and limited hydrolysis at pH 4.6, as determined in section 2.5**.** In a typical sorption experiment, 20.0 ± 0.2mg of copolymers (for chitosan copolymers: 50.0 ± 0.2 mg; GAC: 2.0 ± 0.2 mg) were added to each of the 15 vials. A series of vials without sorbent were used as blanks. A stock solution of PNP in 0.10 mM KH_2PO_4 buffer at pH 4.60 was serially diluted over a range of concentrations (0.6 mM – 60.0 mM) as required. 7.00mL of PNP solution at variable concentration were added to each vial containing sorbent and blank. The samples were mixed for 24 h at 295 K and then the supernatant measured using UV-Vis spectroscopy, as outlined above. At high pH 9.00, the procedure was the same where the buffer was 0.10 mM $NaHCO_3$ solution. The molar absorptivity was 18,552 $Lmol^{-1}cm^{-1}$ at pH 9.00 (λ_{max} = 400nm). For neutral pH 7.0, two forms of PNP exist and calculations of the molar absorptivity are not as straight forward and are outlined in section 6.3.2. The molar absorptivity of the anionic form is 22194 $Lmol^{-1}cm^{-1}$ at pH 7.00 (λ_{max} = 400nm) and for the neutral (or protonated) form it is 9904 $Lmol^{-1}cm^{-1}$ at pH 7.0 (λ_{max} = 325nm).

2.6.2 Single component carboxylate anion adsorption

A stock solution of a single component carboxylates was prepared at concentrations below the critical micelle concentration (cmc) value to avoid micelle formation.

Table 2.3 Table of CMC values of the carboxylic acids obtained from Tensiometer measurements from Mohamed et al. (*10*)

Carboxylates (See section 1.1.1 for definition of z)	Critical Micelle Concentration CMC (mM)
2-Hexyldecanoic acid (z = 0)	0.035
trans-4-pentylcyclohexylcarboxylic acid (z = -2)	0.55
Dicyclohexylacetic acid (z = -4)	4.5

The carboxylates were mixed and their pH is maintained at 9.00 to simulate OSPW conditions. The pH is raised using a 1mM ammonium hydroxide solution to facilitate ion formation for ESI-MS analyses. The solution preparation and experimental conditions were outlined in section 2.12.3. The analysis of residual carboxylate concentration for single components and their mixtures is done using ESI-MS wherein the residual adsorbates at equilibrium after sorption (C_e) were diluted to concentrations between 1-10 ppm (mg/L) for ESI-MS analysis.

2.6.3 Naphthenate (NAs) adsorption

The range of NAs concentration prepared was in the range of 10-110 mg/L to reflect OSPW conditions[1]. A preparation of the samples was similar to the single component carboxylate systems.

2.7 Swelling of Chitosan Copolymers

The swelling behaviour of the Chi-Glu copolymers in water was determined using a gravimetric approach. A clean, lidless, pre-weighed vial was obtained and 40-50 mg ± 1 mg of chitosan copolymers was added into the vial. 6.00 mL of deionized water was added to the vials and the materials were shaken for 48 hours at 160 rpm. The materials were then removed and using a pre-weighed filter paper, the swelled copolymers were isolated and tamped dry to remove excess water prior to obtaining sample weights. The filter paper, and vial were air dried for 12 hours. Both the filter paper with the copolymer and the vial containing residual copolymers were weighed. The difference between the mass of the hydrated copolymer relative to the dried copolymer is related to the degree of swelling of the copolymer. The amount of percentage swelling (S) is given by the following equation:

$$S = [(m_s - m_d)/m_d]\, x\, 100\% \quad (2.7)$$

Where m_s the mass of the hydrated polymer and md is the mass of the dry polymer

2.8 Surface Coverage

To determine the specific surface area (SSA; m^2/g) of the material a surface coverage equation is used. The maximum sorption capacity at the monolayer (Q_m) is needed as well as Avogadro's number (N). The surface area of an individual adsorbate (σ) is needed as well. As the number of sorption sites is dependent on surface area, one adsorbate molecule can take up twice as much sorption sites as another due to differences in σ. The coverage factor (Y) is calculated by the number of layers the adsorbate forms on the adsorbent (for PNP and adsorbates that form monolayers, Y = 1):

$$SSA = {Q_m N \sigma}/{Y} \quad (2.8)$$

Therefore, if the maximum sorption capacity of nitrogen on the adsorbent can be measured then the specific surface area of the material can be estimated.

2.9 Error Analysis of Sorption Isotherms

Determination of a good fit were done using R^2 and root mean square error (RMSE) to determine if there was a good fit between the Sips model and the experimental results.

$$RMSE = \sqrt{\sum(Q_e - Q_T)^2/N} \tag{2.9}$$

$$R^2 = 1 - \sum(Q_e - Q_T)^2/\sum(Q_e - Q_{Av})^2 \tag{2.10}$$

Q_e is the experimental sorption capacity (*cf*. Eqn. 2.9) and Q_T is the calculated sorption capacity according to Sips isotherm (*cf*. Eqn. 2.10) and according to the best-fit adjustable parameters (i.e. Q_m, K_s, and n). Where Q_{Av} is the average experimental sorption capacity and N is the number of data points. The best fit can be determined as R^2 approaches unity and RMSE to zero.

CHAPTER 3

RESULTS AND DISCUSSIONS: β-CD COPOLYMER SYNTHESIS AND CHARACTERIZATION

3.1 Synthesis

The synthesis of polyester copolymers described in Scheme 3.1 was adapted from a previous study (*90*) that varied the relative mole ratio of β-CD and the cross-linker units. The yields for this reaction are listed in Table 1 and calculated according to Scheme 3.1. A 1:1 ratio in Table 3.1 means one molecule of cross-linker was attached to one molecule of β-CD. The mechanism of the reaction follows a typical nucleophillic substitution at the carbonyl group of the acid chloride containing cross-linker where a direct addition of the β-CD nucleophile was followed by displacement of HCl (*cf.* Scheme 3.2) (*91a*).

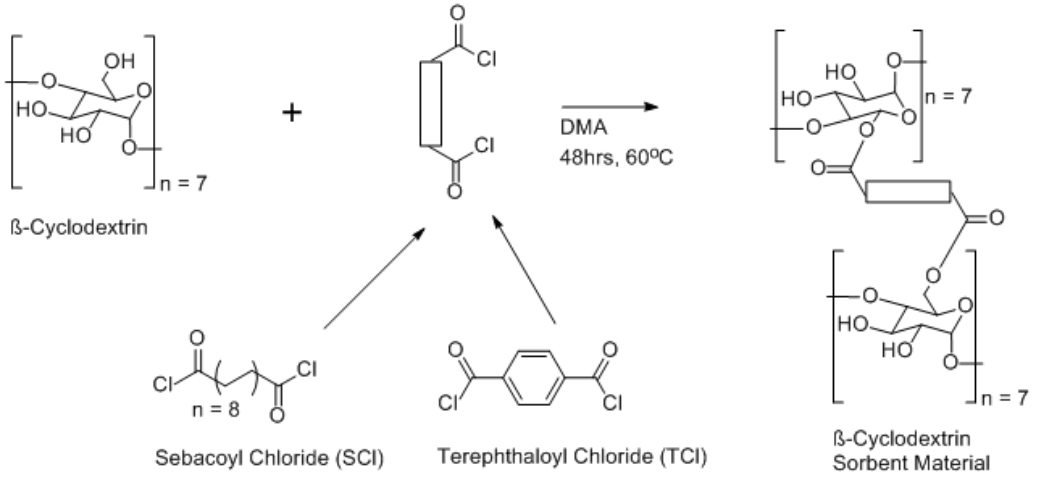

Scheme 3.1 The overall reaction scheme for the cross-linking of TCl and SCl to β-CD is shown.

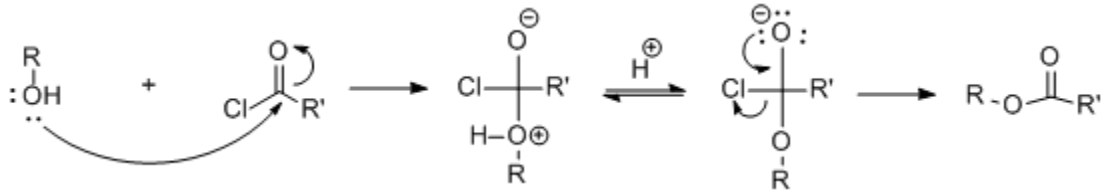

Scheme 3.2 Mechanism for the step-wise polymerization of β-CD (R-OH) with the linkers containing acid chloride groups (e.g., TCl or SCl = R').

The various copolymers exhibit similar physical appearance where the resulting products were a white powder. The product yields were respectable according to **Table 3.1** and were not affected significantly by the presence of residual water/solvents in the reaction mixture with the exception of the higher mole ratios of β-CD and cross-linker (*e.g.*, 1:9 SCl and TCl) where water appeared to facilitate actual gel formation instead of a viscous liquid, as described in the materials and methods chapter. In some cases, the reduced yields were related to loss of product due to partial solubilization in the solvent mixtures during the isolation and purification steps. Given that HCl was a by-product from this copolymer synthesis method, the basicity of the solvent was anticipated to affect the overall product yields due to potential acid hydrolysis of the products. DMA is considered a weak base (pK_a = 0.19); whereas, triethylamine is a stronger base and has been used in the Schotten-Baumann process (*92*). DMA was chosen as the most appropriate solvent because of the favorable solubility of the starting materials required for the synthesis.

Table 3.1 Yield results for the polyester copolymers according to Scheme 3.1 are shown.

Copolymer	**Yield (%) Copolymer**	**Copolymer**	**Yield (%) Copolymer**
1:1 SCl	69	1:1 TCl	51
1:2 SCl	70	1:2 TCl	80
1:3 SCl	64	1:3 TCl	66
1:6 SCl	40	1:6 TCl	50
1:9 SCl	70	1:9 TCl	66

3.2 FT-IR Spectroscopy

The structural characterization of the copolymers was carried out using spectroscopic (FT-IR and ^{1}H NMR) and TGA methods. Direct evidence in support of the product identity was provided by the IR-spectra (*cf.* Figure 3.1 and 3.2) obtained for the copolymers where the carbonyl vibrational band seen was observed in the range of 1683-1727 cm^{-1} (TCl copolymers) and 1725-1745 cm^{-1} (SCl copolymers) and were consistent with the range observed for ester linkages (*79*). The symbol v denotes vibrational modes involved with the stretching of bonds

while δ denotes the bending or deformation of bonds. Subscripts "as" denotes asymmetry while "s" denotes symmetrical vibrational modes.

3.2.1 β-CD, TCl, and SCl Starting Materials

3.2.1.1 β-CD

FT-IR spectra of β-CD can be seen in Figure 3.1 and 3.2. Characterization of the IR absorption bands for β-CD can be separated by the functional groups: alkanes, alcohols, and ethers. Typical C-H stretching bands at 2927 cm^{-1} determines the presence of saturated methylene and methine groups. According to reports in the literature (*79*), v_{as}(C-H) for methine was observed at 2890 cm^{-1} while v_{as}(C-H) and v_s(C-H) for the methylene groups were at 2930 cm^{-1} and 2850 cm^{-1}. By merging these bands, the resulting v(C-H) band for β-CD resulted in a broad band located at 2927 cm^{-1}. The broad spectral features was also observed in the combination band at 1418 cm^{-1} which constituted the various δ_s(C-C-H) of the methine groups of the glucopyranose units of β-CD with the $\delta_s(CH_2)$ methylene groups. For the C-C skeletal bands, the pre-dominant band was the v(C-C) skeletal band at 1653 cm^{-1}. Normally, skeletal bands are weak (*79*) but due to the presence of oxygen in the glucopyranose units the dipole change and the resulting transmittance was greater. Secondly, inductive effects caused by the hydroxyls and oxygen substituents will also increase the wavenumber values of the v(C-C) skeletal bands. The presence of R-OH groups were found in the v(O-H) band at 3394 cm^{-1} and the v_{as}(C-O-H) at ~1207 cm^{-1}. If steric interactions are considered, it is possible to estimate the location of the v_{as}(C-O-H) band for secondary and primary alcohol functional groups. According to the literature, secondary alcohols were found at higher wavenumbers when compared with primary alcohols. Combined with inductive effects of nearby hydroxyls, the IR band at 1207 cm^{-1} was attributed to a secondary alcohol. As indicated in Scheme 3.2, primary alcohols were considered the main nucleophile which can be elucidated from the copolymer structure where a minimum is seen at ~1100 cm^{-1} (*79*). Therefore, v_{as}(C-O-H) for primary alcohols is located at ~1100 cm^{-1}. Using these two bands and the δ_s(C-C-H) band as a standard IR signature band, it is possible to qualitatively determine whether cross-linking occurs at the primary alcohol, the secondary alcohol, or both. Lastly, ether bonds can be observed through the v_{as}(C-O-C) absorption band at 1027 cm^{-1}.

3.2.1.2 Terephthaloyl Chloride (TCl)

A preliminary analysis of the IR-spectra for TCl indicates that there was some scattering due to the Christiansen effect (*79*). This accounts for the asymmetry of the IR band shapes. Two reasons can account for the Christiansen effect: poor grinding and high refraction index between the embedding matrix and the analyte. As TCl was already grinded and sieved, it would be prudent to use a different matrix (e.g. NaCl or CsI) for future characterization. These cells would reduce the Christiansen effect and the long wavelength is similar to KBr (625 cm^{-1} and 165 $cm^{-1}$for NaCl and CsI, respectively). The small 3500 cm^{-1} is the v(O-H) without intermolecular hydrogen bonding and can only be seen if the concentration of the hydroxyl groups are small. Therefore, hydrolysis of TCl to terephthalic acid had been kept to a minimum. To explain the broad peak at 1740 cm^{-1}, it was necessary to refer to the resonance structures that can be formed by TCl (*cf.* Figure 3.3).

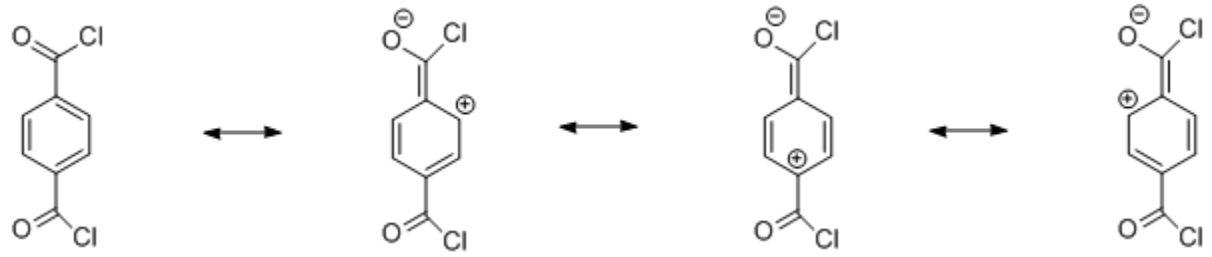

Figure 3.1 Resonance contributing structures of TCl

For di-substituted aromatic compounds like TCl with electron withdrawing carbonyl groups, it is ideal if the two substituents are in the meta-position to provide resonance stabilization for both carbonyls. Since TCl contains para-substituted carbonyls, only one of the carbonyl groups will undergo resonance stabilization. Therefore, the v_{as}(C=O) for TCl should have two values, one for the resonance stabilized acyl chloride (1740cm^{-1}) and one without resonance (1786 cm^{-1}). The resonance structure of TCl contains olefin v_{as}(C=C) IR signature. In combination with the v_{as}(C=C) of the aromatic resonance structure, the two forms can explain the broad peak ranging down to 1600 cm^{-1}.

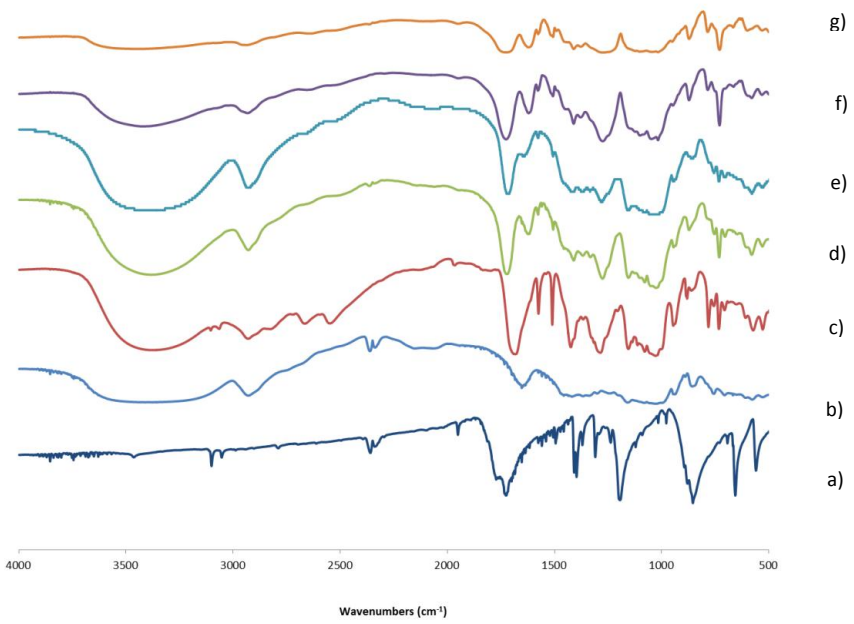

Figure 3.2 FT-IR Spectra of TCl copolymers and initial reagents obtained using KBr pellet technique: a), β-CD; b), TCl; c), 1:1 TCl; d), 1:2 TCl; e), 1:3 TCl; f), 1:6 TCl; and g), 1:9 TCl.

3.2.1.3 Sebacoyl Chloride (SCl)

In comparison with TCl, the absence of a broad v(O-H) band at 3300 cm^{-1} is indicative of minimal hydrolysis of SCl (*cf.* Figure 3.2). The doublets at 2838 cm^{-1} to 2931 cm^{-1} can be assigned to v_s(C-H) and v_{as}(C-H) of the methylene groups of SCl, respectively. The absorption band v_{as}(C=O) is located at 1796 cm^{-1} and is typical of acyl chlorides (*74*). Lastly, the $\delta_s(CH_2)$ scissoring band is located at 1465 cm^{-1} and is close to the predicted 1470 cm^{-1} for saturated alkanes (*74*).

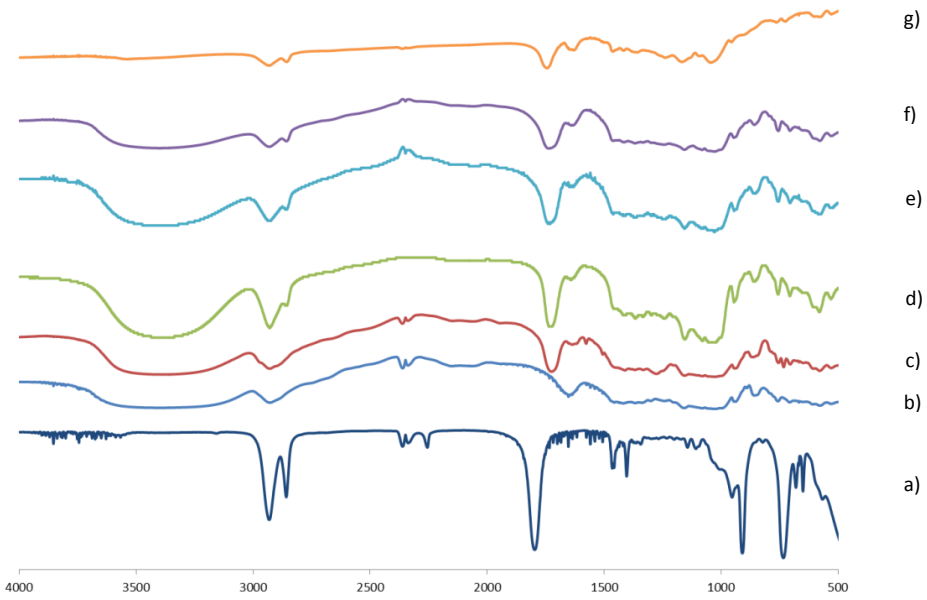

Figure 3.3 FT-IR Spectra of SCl copolymers and initial reagents (SCl spectra was obtained as a neat liquid applied on a KBr cell): a), β-CD; b), SCl; c), 1:1 SCl; d), 1:2 SCl; e), 1:3 SCl; f), 1:6 SCl; and g), 1:9 SCl.

3.2.2 SCl and TCl-based copolymers

According to a previous report (*87*), an increase in the cross-linking resulted in a decreased intensity of the v(O-H) due to increasing substitution of the hydroxyl groups of β-CD in the annular hydroxyl region. Each cross-linker reacts with two equivalents of hydroxyl groups of β-CD (*cf.* Scheme 3.1). The effect can be seen in Figure 3.1 and 3.2 by comparing the relative intensity of the carbonyl and hydroxyl vibrational bands. As the relative mole ratio approaches 1:6, the intensity of the hydroxyl vibrational band decreases relative to the carbonyl band, as a result of the formation of greater numbers of ester linkages. For the copolymer ratio 1:9, the intensity of the absorption band for v(O-H) reaches a minimum for this copolymer and indicates that cross-linking has reached an upper limit. From Table 3.2, the decrease in the wavenumber position for the carbonyl band of the acyl chlorides at 1772 cm^{-1} (TCl) and 1796 cm^{-1} (SCl) to 1683-1727 cm^{-1} for TCl co-polymers and 1725-1745 cm^{-1} for SCl copolymers provides strong support of the formation of ester linkages (*93*).

Table 3.2 Numerical wavenumber values for select absorption bands of TCl and SCl-based copolymers and monomer precursor materials.

	ν_{as}(C-O-C) (Low v) and ν_{as} (C-O-H) (High v)	$\delta_s(CH_2)$ and δ_s(C-C-H) Scissoring	ν(C-C) Skeletal	ν_{as}(C=O)	ν_{as} and ν_s (C-H)	ν(O-H)
β-CD hydrate	1027 1207	1418	1653	NA	2927	3394
SCl†	NA	1465	NA	1796	2858 2931	NA
1:1 SCl	1029 1206	1418	1645	1725	2861 2931	3412
1:2 SCl	1030 1191	1412	1653	1732	2859 2931	3396
1:3 SCl	1031 1190	1413	1649	1733	2859 2930	3384
1:6 SCl	1028 1198	1416	1639	1737	2858 2931	3403
1:9 SCl	1043 1203	1417	1630	1745	2857 2932	3540
TCl	NA	1408	1653*	1740-1786	3053 3100	NA
1:1 TCl	1029 1167	1424	1683*	1683	2930	3375
1:2 TCl	1027 1169	1410	1624*	1723	2929	3385
1:3 TCl	1027 1173	1411	1623*	1721	2929	3377
1:6 TCl	1017 1172	1411	1622*	1726	2934	3409
1:9 TCl	1017 1181	1411	1622*	1727	2939	3428

† Analyzed as a liquid film where SCl is dissolved in deuterated chloroform and applied on a KBr cell

*Includes the δ_s (C=C) aromatic ring-bending mode for TCl

Another metric for characterization of the copolymers is the relative intensity of the aromatic ring bending modes ~ 1624 cm^{-1}. As the TCl content of the copolymer increased, the C-C vibrational band would also increase in intensity relative to signatures that are attributed to β-CD such as the aliphatic C-H stretching bands ~ 2930 cm^{-1}.

3.2.2.1 Regioselectivity

Using the v_{as}(C-O-H) of the primary and secondary alcohols it is possible to determine where the cross-linking occurs. As the cross-linking increased, a minimum was observed at 1100 cm^{-1} which correlates to v_{as}(C-O-H) of primary alcohols (also influenced by neighboring hydroxyls) (*79*). At high mole ratios of β-CD: cross-linker (i.e. > 1:1), the absorption band at ~1170-1200 cm^{-1} (v_{as}(C-O-H) for secondary alcohols) decreased in intensity when compared with the $\delta_s(CH_2)$ band at 1420 cm^{-1}. Two possible conclusions were drawn from these results. Firstly, the cross-linking reaction occurs mainly at the primary hydroxyl groups of β-CD because of the lack of steric hindrance at these sites. The second possibility was that secondary hydroxyl groups also participate in the cross-linking reactions even when primary hydroxyl groups are available. In Figure 3.4, it can be seen that as more primary hydroxyl groups undergo cross-linking, one side of the β-CD cavity becomes more sterically hindered such that the annular face becomes more sterically hindered relative to the annular face with secondary hydroxyl groups. Thereafter, the secondary hydroxyl group undergo cross-linking and is supported by the IR-spectra where a sudden decrease of the v_{as}(C-O-H) band for secondary alcohols at 1170-1200 cm^{-1}. This occurs for both TCl and SCl-based copolymers at higher mole ratios (1:6 and 1:9). Similar trends in reactivity have been reported for the reaction between β-CD and various diisocyanate linkers by Mohamed et al. (*87*).

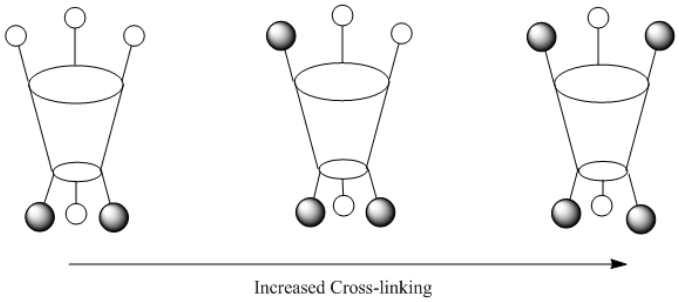

Figure 3.4 Adapted from Mohamed et al. (*72*) Diagram of the cross-linking reaction with β-CD is shown where linkers will first attach to the primary hydroxyls (narrow side of the cavity). Attachment is shown with the shaded spheres while the empty spheres are unreacted hydroxyl groups. Not all the primary hydroxyl groups will react due to steric hindrance, according to the steric bulk of the cross-liner unit, and this result in further cross-linking at the secondary hydroxyl sites (wider side of the cavity).

3.3 ^{1}H NMR-Spectroscopy

3.3.1 β-CD, TCl, and SCl

Characterization of the β-CD bands have been done using a combination of NMR-spectroscopy techniques such as ^{1}H NMR, ^{13}C NMR, HSQC, COSY, and HMBC and have been compared to literature (*93*) (Results not shown). The ^{1}H spectral parameters are listed in Table 3.3. For the NMR characterization of SCl, H_{12} and H_{13} is relatively simple. H_{13} is least affected by the inductive effects of the electronegative carbonyl groups as evidenced the singlet at 1.25 ppm. The H_{12} group is closer to the carbonyl group and is less shielded, resulting in an upfield chemical shift (1.50 ppm). H_{11} is split into many signals but each band is a triplet. From the IR-spectra, it is noted that a small amount of the SCl undergoes hydrolysis to form the corresponding acid. Since the carboxylic acid substituent exerts less deshielding when compared to the acyl chloride groups, H_{11} should become more shielded. Hydrolysis can also explain the multiplet signals observed for H_{ar} since a singlet is predicted due to symmetry.

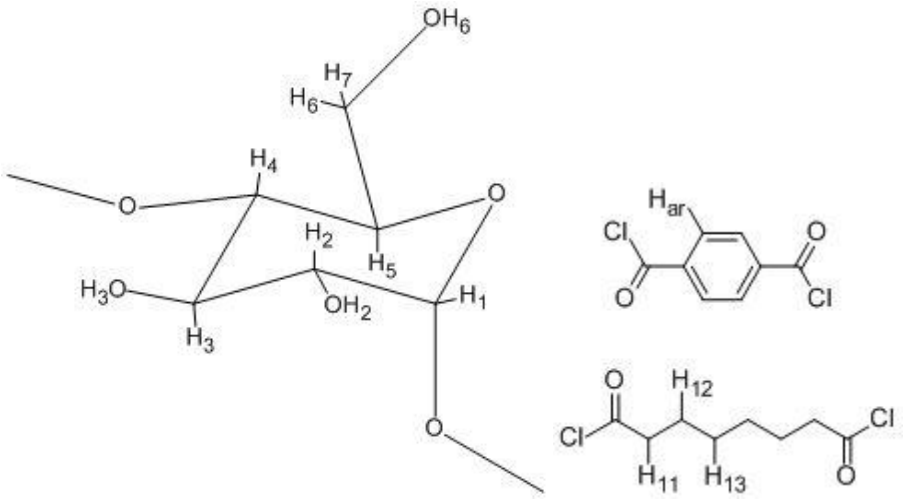

Figure 3.5 Numbering Scheme used for ^{1}H nuclei of β-CD and cross-linkers. Left: A monomer of β-CD; Right: The linkers SCl and TCl.

Table 3.3 [1]H NMR data for SCl and TCl Copolymers and co-monomers in DMSO-d_6 at 500 MHz and 295 K are shown. The chemical shifts are relative to TMS (δ=0 ppm) where the multiplicity, and integrated peak areas are provided.

	H_1 (ppm)	**H_2-H_7 (ppm)**	**OH_6 (ppm)**	**OH_2,OH_3 (ppm)**	**H_{11} (ppm)**	**H_{12} (ppm)**	**H_{13} (ppm)**	**H_{ar} (ppm)**
β-CD hydrate	4.83, s,7	3.32-3.65, m, 42	4.46, t, 7	5.70, m, 14				
SCl					2.30, t, 4	1.50,t, 4	1.25, s, 8	
1:1 SCl	4.83, m,7	3.32-3.60, m, 42	4.46,m,6	5.54,s,14	2.30,m, 8	1.50,s, 8	1.25,s,16	
1:2 SCl	4.84, m,7	3.32-3.60, m, 42	4.46,m,2	5.54,s, 14	2.30,m, 12	1.50,s,12	1.25,s,24	
1:3 SCl	4.84, m,7	3.32-3.60, m, 42	4.46,m,7	5.54,s, 14	2.30,m, 16	1.50,s,16	1.25,s,32	
1:6 SCl	4.84, m,7	3.32-3.60, m, 42	4.46,m,7	5.54,s, 14	2.30,m, 30	1.50,s,30	1.25,s,56	
[1]TCl								8.25, s, 4
1:1 TCl	4.83, m, 7	3.32-3.60, m, 28	4.46, m, 6	5.54, s, 14				8.07, m, 4
1:2 TCl	4.84, m, 7	3.32-3.60, m, 28	4.46, m, 2	5.54, s, 14				8.10, m, 8
1:3 TCl	4.84, m, 7	3.32-3.60, m, 28	4.46, m, 7	5.54, s, 14				8.07, m, 14

s = singlet, t = triplet, and m = multiplet.

[1]TCl NMR solvent was $CDCl_3$ relative to TMS (δ=0 ppm)

3.3.2 SCl and TCl-based copolymers

From the NMR spectra in Figures 3.6 and 3.7, the resonance lines of β-CD (~3.3 to 3.7 ppm) become increasingly broadened as the linker content of the copolymer increases. This is attributed to the reduced motional dynamics of the β-CD monomers with increasing cross-link density of the co-polymer, in agreement with literature (*72*). Product formation can be determined by the shielding effects and the chemical shift values of the H_{ar} and H_{12} bands to higher field (*cf.* Figure 3.6 and 3.7). For TCl (1:2 TCl copolymer ^{1}H NMR spectra is not shown), the chemical shift values illustrate shielding effects from 8.25 ppm for the reactant to 8.07-8.10 ppm for the copolymers. H_{12} shifts from a range of 2.1-2.4 ppm and converges to a broad band at 2.3 ppm. Both H_{ar} and H_{12} are located adjacent to the carbonyl and are most sensitive to the inductive electron withdrawing effects of the acyl group. As cross-linking occurs, acyl group replaced with an ester linkage and the β-hydrogen atoms becomes more shielded.

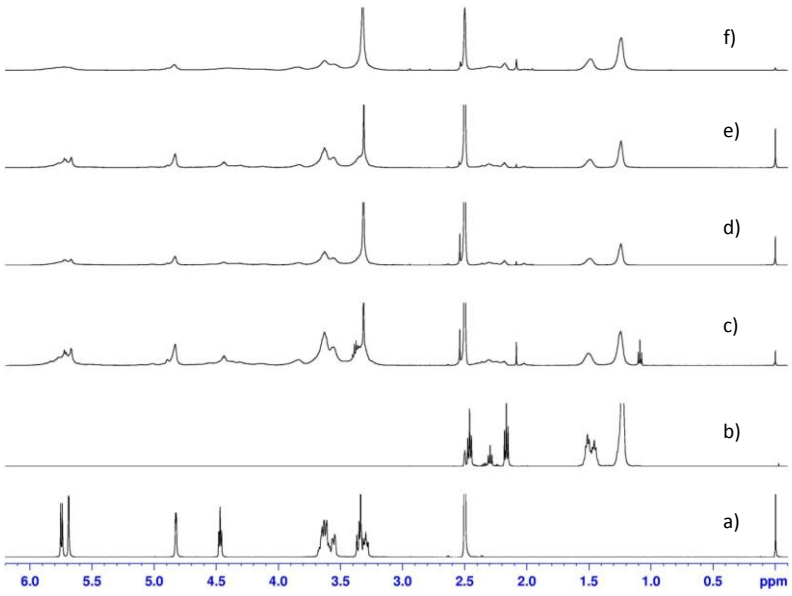

Figure 3.6 ^{1}H NMR spectra of SCl and its copolymer materials at 295 K in DMSO-d_6 at 500 MHz are shown. a), β-CD; b), SCl; c), 1:1 SCl; d), 1:2 SCl; e), 1:3 SCl; f), 1:6 SCl. All spectra were obtained in DMSO-d_6 and chemical shifts were referenced to TMS. *Note the residual solvent (i.e. diethyl ether) is seen at 1.09 ppm.

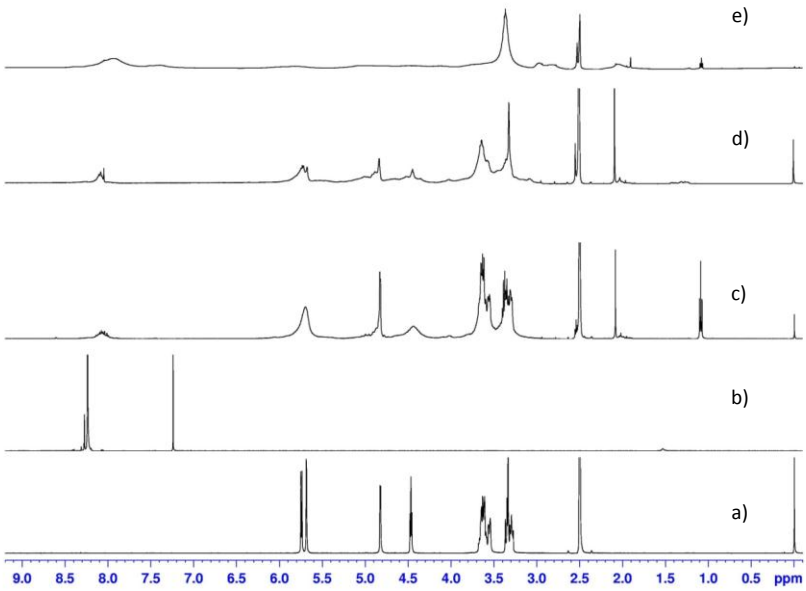

Figure 3.7 1H NMR spectra of the TCl products are shown. a), β-CD; b), TCl; c), 1:1 TCl; d), 1:3 TCl; e), 1:6 TCl. All spectra were obtained in DMSO-d_6 except for the reagent TCl which is obtained in $CDCl_3$ and chemical shifts were referenced to TMS. *Note the residual solvent (i.e. diethyl ether) is seen at 1.09 ppm.

3.3.3 Synthetic Mole Ratio

Table 3.4 lists the ^{1}H NMR parameters of selected nuclei for β-CD and the cross-linker units at variable mole ratios. Using Figure 3.3, the H_1 hydrogen atom of β-CD is located near the glycosidic bond and is unaffected by cross-linking. H_1 is then a suitable reference for quantitative analysis of the integrated values for the host nuclei. The integration of the aromatic nuclei of TCl (H_{ar}) and methylene groups (H_{12}) of SCl, relative to the H_1 nuclei of β-CD afford the relative composition of the copolymer. For the TCl copolymer at the 1:1 mole ratio, there are approximately 4-^{1}H nuclei (H_{ar}) of TCl nuclei per 7 ^{1}H nuclei of β-CD (H_1). A similar integrated ratio is observed for the 1:1 copolymer of SCl for the ratios of H_{12} of SCl and H_1 nuclei of β-CD. The calculated values are in good agreement with the stoichiometric synthetic ratios, according to the monomer ratios employed in the copolymer synthesis. In the case of copolymers prepared at higher ratios (i.e. 1:6 TCl, 1:9 SCl, and 1:9 TCl) these products were generally insoluble in the solvents investigated and their analysis was precluded from the results listed in Table 3.4.

Table 3.4 Experimental Mole Ratio using ^{1}H NMR results of selected copolymer nuclei in DMSO-d_6 at 295 K

Co-polymers	Chemical Shift (ppm, DMSO)	Integration	Calculated Mole Ratio via NMR (values in bracket not rounded to nearest integer)
1:1 TCl	4.83, m 8.00, m	7.00 4.54	1:1 (1:1.1)
1:2 TCl	4.83, m 8.00, m	7.00 9.70	1:3 (1:2.8)
1:3 TCl	4.83, m 8.00, m	7.00 15.14	1:4 (1:3.8)
1:1 SCl	4.83, m 1.52, m	7.00 6.91	1:2 (1:1.7)
1:2 SCl	4.83, m 1.52, m	7.00 9.00	1:2 (1:2.2)
1:3 SCl	4.83, m 1.52, m	7.00 16.86	1:4 (1:4.2)
1:6 SCl	4.83, m 1.52, m	7.00 17.98	1:5 (1:4.5)

3.3.4 Hydrolysis

Since polyester copolymers are known to undergo basic hydrolysis (*80*)**,** it is appropriate to determine the conditions at which the products undergo hydrolysis at various pH conditions. The NMR spectra in Figure 3.8 illustrate that the 1:3 SCl copolymer undergoes hydrolysis at alkaline pH and appears to be more stable in D_2O at ambient (pD ~ 6) conditions. The hydrolysis of the copolymer is evidenced according to the sharpening of the broad resonance lines upon addition of base. As well, there is a pronounced sharpening of the nuclei corresponding to SCl (~0.7-2.5 ppm) and β-CD (~3.5-4 ppm) with upfield chemical shifts of the α-CH_2 group of SCl. Although the results are shown only for the 1:3 SCl copolymers, hydrolysis also occurs for the TCl co-polymers in acidic solution (pH ~ 4.60). The copolymers at higher mole ratio (> 1:6) undergo attenuated hydrolysis and display favourable properties as solid phase sorbents in aqueous solution. Thus, sorption studies were carried out for selected copolymers of SCl and TCl-systems at higher mole ratios (1:6 and 1:9), and are described in Chapter 5.

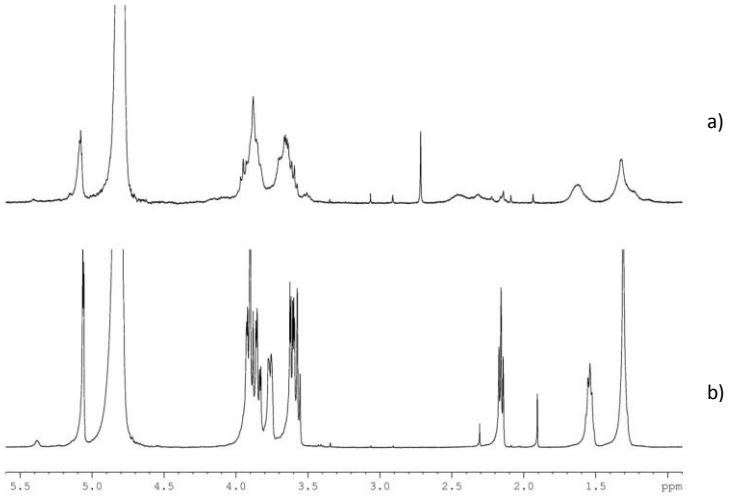

Figure 3.8 a) 1:3 SCl in D_2O, and b) 1:3 SCl in D_2O after adding one drop of 3 M NaOH.

3.4 Solubility

The linker units are relatively apolar in nature relative to the hydrophilic regions of β-CD. Increased cross-linking and substitution of the annular hydroxyl groups of β-CD is anticipated to reduce the accessibility of solvent, copolymer solubility, and hydrolysis of the copolymer (*47, 87*). This effect is observed according to the reduced solubility of the copolymers relative to β-CD where a decrease in solubility occurs as the CD: linker mole ratio approaches higher values (i.e. 1:6). The consistent decrease in solubility parallels the increased cross-linking (*cf.* Table 3.5) of the copolymer framework. By adding additional linkers to β-CD and the formation of copolymers, the solubility drops from 1:1 mole ratio to 1:9 mole ratio. The greater solubility observed for TCl compared to SCl may be due to differences in solvent accessibility. Rigid aromatic linkers in TCl cannot undergo coiling as in the case of aliphatic linkers in polar solvents such as water. The higher solubility values of the copolymer could also be influenced due to potential hydrolysis which has been shown to occur (*cf.* Section 3.3.4**)**. In turn, hydrolysis would break down the copolymer framework into its constituent water soluble monomers. For SCl copolymers, aliphatic linkers may cause steric effects upon coiling to reduce their relative apolar surface area in water which attenuates accessibility of solvent into the micropore domains of the copolymer framework.

Table 3.5 Solubility values for the copolymers in water at 22^{o}C according to a gravimetric-based method

Sample	Solubility (g/L)	Sample	Solubility (g/L)
1:1 TCl	12.5	1:1 SCl	7.00
1:2 TCl	7.07	1:2 SCl	6.66
1:3 TCl	6.22	1:3 SCl	4.06
1:6 TCl	0.24	1:6 SCl	0.19
1:9 TCl	0.51	1:9 SCl	ND*
β-CD Pure **[39]**	18.5		

*This value could not be determined

3.5 TGA

In Table 3.6, the TGA results are provided for the copolymers and the co-monomers. In general, two transitions are observed and attributed to the thermal decomposition processes of the copolymer framework, according to thermal breakdown of the respective subunits (i.e. cross-linker and β-CD). The assignment of TGA transitions are consistent with urethane copolymers reported previously. (*87*) The decomposition temperature of β-CD in its monomer and its copolymer form vary slightly according to the nature of the linker and the relative monomer content. The SCl-based copolymer appears to have greater thermal stability relative to the TCl-based copolymers. The differences are attributed to the conformational motility of TCl and SCl which may affect the relative heat capacity of the copolymer materials accordingly. Differences in framework flexibility of the framework are evidenced by the swelling behaviour of aliphatic- and aromatic-based linkers in aqueous solution. The greater conformational freedom of SCl may result in enhanced thermal stability due to its greater degrees of freedom that result from conformational changes of the aliphatic linker relative to the more rigid TCl unit. The greater thermal stability observed for the SCl copolymers is evidenced by with the relatively high stability observed for the 1:9 SCl copolymer. The potential occurrence of self-inclusion of the SCl aliphatic linker may also contribute, in part, to its greater thermal stability since such types of host-guest interactions have been reported previously (*91*).

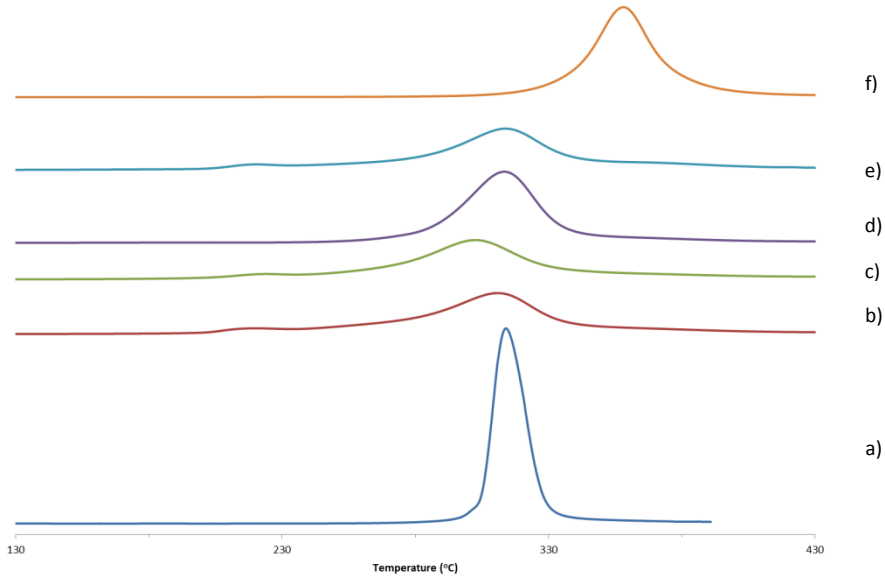

Figure 3.9 DTG of the SCl-based copolymers: a) β-CD; b) 1:1 SCl; c) 1:2 SCl; d) 1:3 SCl; e) 1:6 SCl; and f) 1:9 SCl.

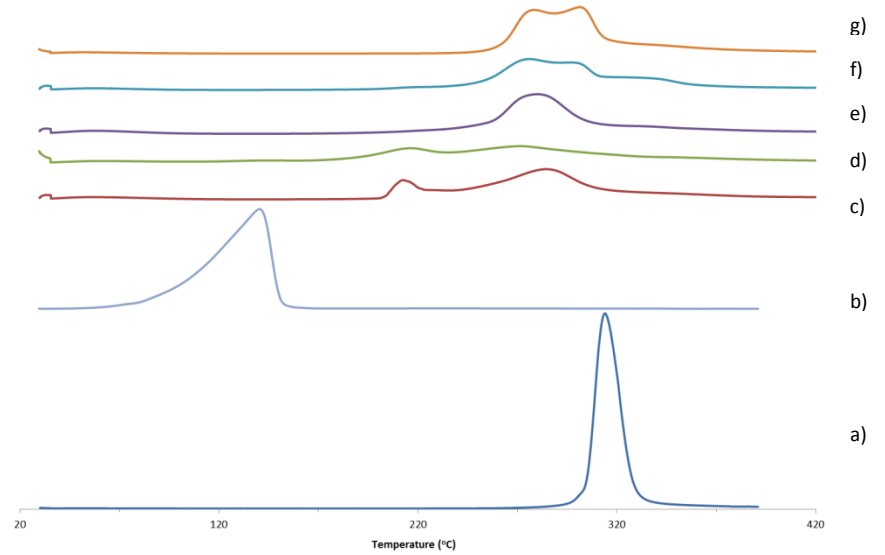

Figure 3.10 DTG of TCl based copolymers: a) β-CD; b) TCl; c) 1:1 TCl; d) 1:2 TCl; e) 1:3 TCl; f) 1:6 TCl; and g) 1:9 TCl.

Table 3.6 Differential thermal gravimetry (DTG) results of the β-CD copolymers.

Sample	**Decomposition Temperature (^oC)**	**Sample**	**Decomposition Temperature (^oC)**
β-CD hydrate	314	TCL	140
1:1 SCl	311	1:1 TCL	212, 285
1:2 SCl	302	1:2 TCL	215, 272
1:3 SCl	314	1:3 TCL	279
1:6 SCl	314	1:6 TCL	275, 298 326
1:9 SCl	358	1:9 TCL	279, 299

Another result is the relative temperature shift for the 1:6 and 1:9 copolymers for SCl and TCl linker units. In Figure 3.4, the respective copolymers have different framework structural characteristics compared with those materials with reduced cross-link density (*i.e*. 1:1, 1:2 and 1:3 TCl). The reduced thermal decomposition temperatures for copolymers with lower cross-linker content contribute to their reduced thermal stability. As the mole content of linker increases, the intensity of the peak at 139^{o}C for the TCl copolymers decreases while another peak at 274^{o}C increases, and may be related to the formation of more densely cross-linked copolymers (*cf.* Table 3.6, Figure 3.9 and 3.10). For SCl copolymers, as the mole content of SCl increases, the peak at 318^{o}C broadens and shifts to a higher temperature ~ 358^{o}C.

3.6 CHN Analysis

The use of CHN analysis to β-CD copolymers is similar in principle to the use of ^{1}H NMR where the composition of the copolymers can be elucidated. Through an empirical formula, the mole to mole ratio between copolymer and linker can be calculated. The benefits of CHN analysis over ^{1}H NMR are that the former is a solid state technique therefore, solubility and hydrolysis of the sample is not a concern. Therefore, experimental cross-linker ratios for insoluble copolymers such as 1:9 SCl can be obtained. A disadvantage is that the mass percentages are highly influenced by the presence of residual solvents. Residual water, for example, can lead to an underestimation of %C and an overestimation of %H and %O. Corrections for residual water can be done, in part, by integrating the thermogram at 100^{o}C to obtain the percent mass of the residual water. Dimethylacetamide residues can be corrected using ^{1}H NMR (*87*) but a simpler method is to use the percent by mass of nitrogen. The final polyester copolymer should not contain any nitrogen atoms and any non-zero percent by mass value for nitrogen will be attributed to the presence dimethylacetamide residues. To calculate %O, the cross-linkers are assumed to be fully cross-linked and any remaining chlorine atoms are removed during the Soxhlet extraction process.

Using the cross-linking reaction in Scheme 3.1, an assessment of the CHN values is listed in Table 3.7. The first general trend is that as the mole ratio increases from 1:1 to 1:9 the mass percent of carbon increases which agrees with literature (*87*). This trend in elemental analyses provides additional support of increased cross-linking. Even after correcting for solvent and water, the values the %C are smaller than the theoretical CHN results.

Table 3.7 Mass percentages of C, H, and N obtained for TCl and SCl-based copolymers. The monomer β-CD was calculated theoretically. All values were adjusted for dimethylacetamide content and residual water.

	Experimental				Theoretical			
Sample	%C	%H	%N	%O[†]	%C	%H	%N	%O[†]
β-CD* (Theoretical)					44.5	6.22	0.0	49.3
1:1 SCl	43.5	6.73	0.0	49.7	48.0	6.50	0.0	45.5
1:2 SCl	48.1	6.53	0.0	45.4	50.8	6.73	0.0	42.5
1:3 SCl	47.5	6.97	0.0	45.5	52.9	6.91	0.0	40.1
1:9 SCl	59.7	7.56	0.0	32.8	60.3	7.51	0.0	32.2
1:1 TCl	46.4	6.58	0.0	47.0	47.5	5.74	0.0	46.8
1:2 TCl	46.7	6.09	0.0	47.2	49.9	5.35	0.0	44.7
1:3 TCl	45.4	6.32	0.0	48.3	52.0	5.02	0.0	43.0
1:6 TCl	52.7	4.71	0.0	42.6	56.4	4.32	0.0	39.2
1:9 TCl	55.1	4.91	0.0	40.0	59.4	3.85	0.0	36.8

[*] From the TGA profile in Figure 3.9, there does not appear to be a thermal event at 100°C associated with residual water. Therefore, β-CD sample is assumed anhydrous.

[†] Calculated by summing the percentages for C, H, and N and subtracting by 100%.

3.6.1 Experimental Determination of Cross-Linker Ratio

In a β-CD copolymer a single monomeric unit is the result of y-number of β-CD cross-linking to x–number of linkers. This is represented in the three equations below where the contributions to each element come from both β-CD and the linkers. C_{mon}, H_{mon}, and O_{mon} are the number of carbon, hydrogen, and oxygen atoms in a single monomer of the copolymer.

$$C_{mon} = yC_{\beta-\mathrm{CD}} + xC_{linker} \quad (3.1)$$

$$H_{mon} = yH_{\beta-\mathrm{CD}} + xH_{linker} - 2x \quad (3.2)$$

$$O_{mon} = yO_{\beta-\mathrm{CD}} + xO_{linker} \quad (3.3)$$

$C_{\beta\text{-CD}}$, $H_{\beta\text{-CD}}$, and $O_{\beta\text{-CD}}$ are the number of carbon, hydrogen, and oxygen content of a β-CD molecule, respectively. C_{linker}, H_{linker}, and O_{linker} are the number of carbon, hydrogen, and oxygen atoms for a linker molecule, respectively. A note about hydrogen is that the cross-linking reaction will cause the loss of 2 hydrogen atoms for every one linker that is attached. Therefore, what is to be determined is the number of linkers (x) and β-CD (y) in a monomer. To determine them, the total atomic composition of the monomer (C_{mon} ,H_{mon} ,O_{mon}) must also be found. One assumption can be made to simplify the variable y. From the mechanism in Scheme 3.2, β-CD molecules only react with the cross-linkers and not with other β-CD molecules. Therefore, each monomer should contain only one β-CD; thus, y = 1. Now only the total atomic composition of the monomer remains to be determined and then the number of linkers attached to a β-CD molecule can be determined. The former can be resolved through an empirical formula using the data from the CHN analysis. By definition, an empirical formula is the simplest ratio between each element. When multiplied by an integer (z), the atomic composition of the monomer can be derived from the empirical formula (C_{Em} ,H_{Em} ,O_{Em}).

$$zC_{Em} = C_{mon} = C_{\beta-\mathrm{CD}} + xC_{linker} \quad (3.4)$$

$$zH_{Em} = H_{mon} = H_{\beta-\mathrm{CD}} + xH_{linker} - 2x \quad (3.5)$$

$$zO_{Em} = O_{mon} = O_{\beta-\mathrm{CD}} + xO_{linker} \quad (3.6)$$

Table 3.8 Solutions to z and x using **eqn. 3.4-3.6** for all three methods

	Method 1 (C and O)		Method 2 (C and H)		Method 3 (H and O)	
	z	x	z	x	z	x
TCl	$z = \frac{98}{4O_{Em} - C_{Em}}$	$x = \frac{zO_{Em}}{2} - 17.5$	$z = \frac{238}{4H_{Em} - C_{Em}}$	$x = \frac{zH_{Em}}{2} - 35$	$z = \frac{35}{H_{Em} - O_{Em}}$	$x = \frac{zO_{Em}}{2} - 17.5$
SCl	$z = \frac{133}{5O_{Em} - C_{Em}}$	$x = \frac{zO_{Em}}{2} - 17.5$	$z = \frac{8}{\frac{5}{7}H_{Em} - C_{Em}}$	$x = \frac{zH_{Em}}{14} - 5$	$z = \frac{135}{7O_{Em} - H_{Em}}$	$x = \frac{zO_{Em}}{2} - 17.5$

As there are 3 linearly independent equations with two unknowns the problem can be solved using basic linear algebra. Only 2 of the 3 equations are needed for a solution which means several methods can be employed. For method 1 in Table 3.8, the solution was derived by solving for z and x using the equation for carbon and oxygen. Method 2 solved for z and x using the equations for carbon and hydrogen. The last method involves solving the equations using hydrogen and oxygen. The calculated experimental number of linkers is listed in Table 3.9.

Table 3.9 Calculated experimental mole ratios using the three types of calculation methods and ^{1}H NMR results are also listed.

Sample	Experimental Cross-linker Ratio			
	Method 1 (C and O)	Method 2 (C and H)	Method 3 (H and O)	Results from ^{1}H NMR
1:1 SCl	ND*	1 : 0.83	1 : 0.53	1:2 (1:1.7)
1:2 SCl	1 : 1.0	1 : 3.5	1 : 1.0	1:2 (1:2.2)
1:3 SCl	1 : 0.9	1 : 1.5	1 : 1.6	1:4 (1:4.2)
1:9 SCl	**1 : 8.4**	**1 : 8.7**	**1 : 8.7**	
1:1 TCl	1 : 0.76	ND*	ND*	1:1 (1:1.1)
1:2 TCl	1 : 0.75	1 : 0.44	ND*	1:3 (1:2.8)
1:3 TCl	1 : 0.32	1 : 0.02	ND*	1:4 (1:3.8)
1:6 TCl	1 : 3.3	1 : 3.9	1 : 5.6	
1:9 TCl	1 : 5.1	1 : 3.9	1 : 1.0	

*Could not be determined

The accuracy of the cross-linker ratio calculated using CHN data is questionable. Most of the ratios are smaller than the predicted values with the smallest being 1:3 TCl. Each method had at least one cross-linker ratio where the calculation yielded a negative cross-linker ratio which is not possible and therefore, denoted as not determinable (ND). When comparing the cross-linker ratios calculated from ^{1}H NMR and CHN analysis, ^{1}H NMR appears to be more accurate as the ratios are closer to the theoretical ratios. Solvent peaks in ^{1}H NMR are clearly resolved and well separated from the H_1, H_{11}, and H_{ar} bands used to calculate the ratios while for CHN analysis this

is not true. The best example of the effect of solvent is in the results obtained for 1:9 SCl. From TGA, the DTG for 1:9 SCl reveals minimal DMA (200^{o}C) and water residues. Therefore, the results for 1:9 SCl are the most accurate among the various cross-linker ratios investigated using CHN analysis, regardless of the method. CHN analysis is concluded to be relatively reliable for determination of the cross-linker ratios; however, the copolymers must be free of solvent. Finally, the relative sensitivity of the method inherently relies on large differences in CHN of the various subunits which comprise the copolymer.

CHAPTER 4

RESULTS AND DISCUSSIONS: CHITOSAN - CHARACTERIZATION

4.1 Mechanistic interpretation of cross-linking reaction:

4.1.1 Imine formation: amine-catalyzed aldol condensation

In aqueous solution, chitosan can only be dissolved under acidic conditions, the Chi-Glu copolymer reaction is bound to obtain multiple products if the reaction conditions are ideal for catalyzing a cross-linking reaction involving multiple aldehyde and amine reaction sites. Secondly, the complexity of the cross-linking mechanism of glutaraldehyde to chitosan is compounded by an inability to track, *in situ*, the reaction as the Chi-Glu solution undergoes gelation before precipitating. Therefore, mechanistic studies on this reaction done by various groups often occur before the transition to gel phase (*55, 94*). Two general reaction schemes have been proposed for the cross-linking of glutaraldehyde to chitosan, as shown in Scheme 4.1.

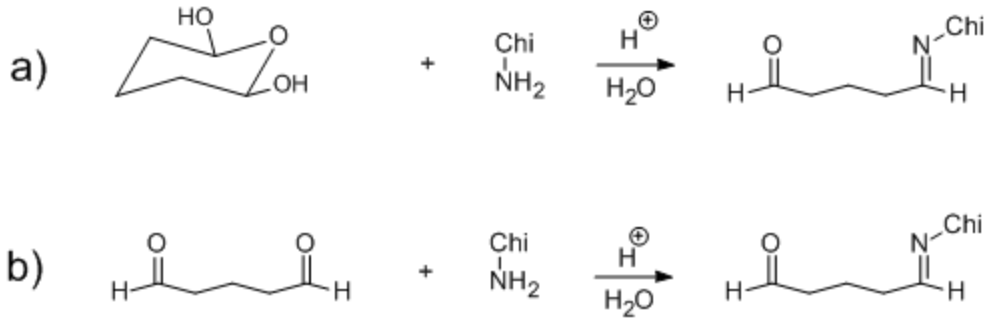

Scheme 4.1 Cross-linking reaction schemes involving chitosan (Chi-NH_2) and glutaraldehyde: a) cyclized glutaraldehyde reacting with chitosan as proposed by Knaul et al. (*94*) (Note that the above form is only one of several isomers of cyclic glutaraldehyde); b) Direct addition of chitosan followed by imine.

The first reaction scheme is proposed by Knaul et al. (*94*) where the reaction of glutaraldehyde appears to follow an acid-catalyzed ring opening reaction followed by imine formation. Their reaction scheme did not appear to be fully correct because the mechanism they determined required breaking the octet rule and C-H cleavage at room temperature. Therefore, a plausible mechanism has been proposed to explain the cross linking observed by Knaul et al. (*94*) (*cf.* Scheme 4.2) Cyclized glutaraldehyde is no different than a hemiacetal as Knaul et al.

(*94*) noted, and the mechanism is expected to be similar. Therefore, the first step is to re-form the carbonyl followed by a nucleophillic attack of the amine from chitosan. Then an imine is formed and the ring breaks. Now a diol is present and in the presence of acids, it will form the aldehyde and the cross-linking is complete.

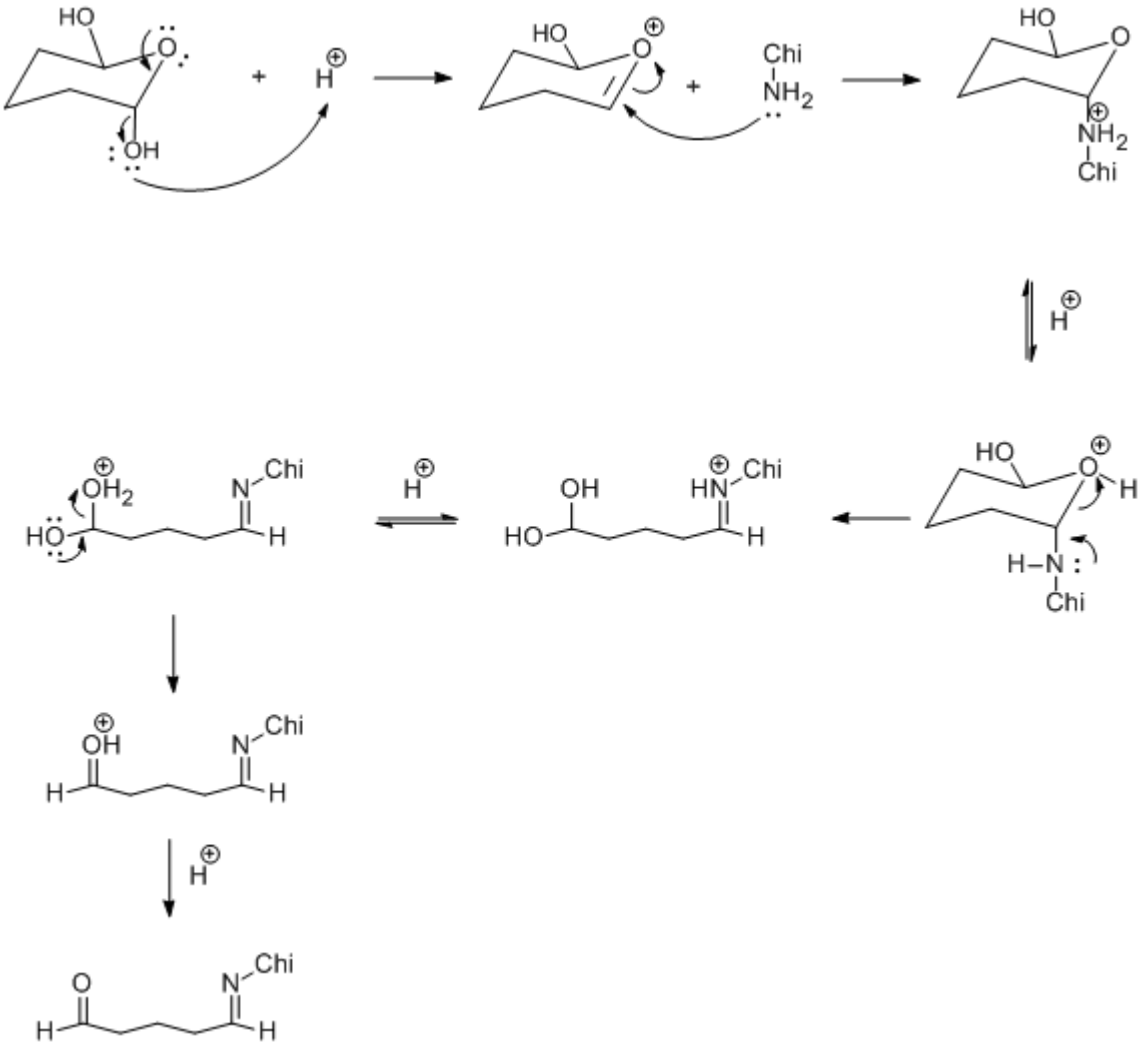

Scheme 4.2 Proposed mechanism for the cross-linking of cyclized glutaraldehyde to chitosan (Note that the above form is only one of several isomers of cyclic glutaraldehyde)

This ring opening reaction was verified by Kildeeva et al. (*55*) using ^{1}H NMR spectroscopy and determined the same result but at an attenuated rate of reaction. As reported by Kildeeva et al. (*55*) the cyclized glutaraldehyde is a minor component as compared to the free aldehyde. As the pH is increased to 5.6, the amount of cyclized glutaraldehyde decreases while cross-linking

increases. Therefore, this reaction scheme is not the primary mechanism of the cross-linking reaction. The most widely accepted cross-linking scheme involves the direct addition of the primary amines to chitosan followed by imine formation (Scheme 4.1). Amines are nucleophillic with pK_a ranges from 10 (primary amines) to 11 (tertiary amines) (*91b*). They also readily form imines at low pH and room temperature with an acid catalyst like acetic acid (*95*). Amines, primary (*96, 97*) and secondary (*98-101*), catalyze aldol addition reactions through the formation of an enamine (*cf.* Scheme 4.3**).**

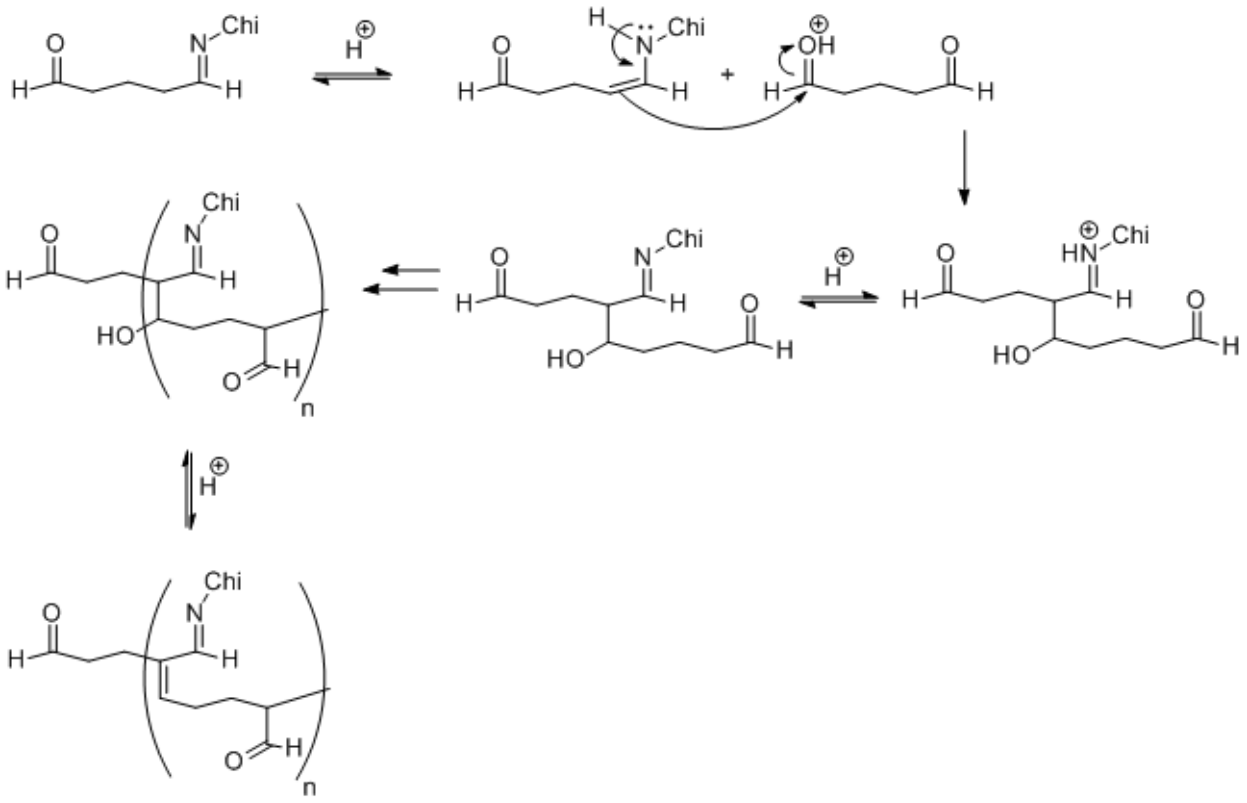

Scheme 4.3 Proposed mechanism of the aldol addition and polymerization of glutaraldehyde on chitosan. Reaction is done at room temperature and pH 3.3-3.9.

This reaction pathway bypasses the requirement for an enol which is the rate determining step for both acid- and base-catalyzed aldol additions (*98*). A consequence, aldol additions occur with high enantioselectivity (*96, 97, 100*) and can be achieved at room temperature. Since there are two aldehyde groups per glutaraldehyde, the amine also catalyzes the polymerization of glutaraldehyde as shown in Scheme 4.3 where the process repeats itself until all accessible amines have reacted. Note that the current aldol product is the major product but only kinetically

stable (*91c*). Long reaction times, elevated temperatures, acidic, or basic pH conditions will cause the aldol to eliminate the secondary alcohol and form the thermodynamically stable α,β-unsaturated product (*91b, 98*). One of these products (*cf.* Scheme 4.3) is from an acid-catalyzed dehydration of the secondary alcohol to form the unsaturated imine predicted by Monteiro Jr. and Airoldi (*102*). The second product is an unsaturated enal predicted by Kildeeva et al. (*55*).

4.1.2 Stability of Imine bond

Recently, chitosan has been applied as a catalyst for aldol additions (*103*). If chitosan follows the mechanism seen in Scheme 4.3 through to the condensation product then the final step in the amine-catalyzed aldol condensation involves hydrolysis of the imine (*98*). The amine on chitosan is the catalyst, and by definition, should be regenerated at the end (*103*). But if the amine is regenerated then the glutaraldehyde molecule is no longer cross-linked with chitosan. A second problem associated with the cross-linking mechanism is how chitosan is able to cross-link with glutaraldehyde if the imine bond is hydrolyzed readily. There are two possible explanations. The first is the steric interaction at the reactive sites. Imines are nitrogen analogues of carbonyl compounds and therefore access to the Bürgi-Dunitz trajectory is a good indicator of the reactivity of the imine. The imine is bonded to polymerized glutaraldehyde and chitosan. Both are large molecules that can prevent access to the trajectory and hinder hydrolysis.

The second explanation is an alternate reaction pathway where the formation of an N-heterocyclic and O-heterocyclic intermediate occurs. Aniline reacting with glutaraldehyde forms 2,6-disubstituted tetrahydropyran (*104*). For other amines, a 2,6-disubstituted pyridine or 2,6-disubstituted piperidine have been isolated (*104-107*). The 2,6-disubstituted piperidine intermediate that is formed is a known intermediate in the total synthesis of piperidine alkaloids (*106*) and has been applied to proteomic analysis (*105, 107*). In a similar reaction involving adenosine with glutaraldehyde, Olsen et al. (*105*) isolated the proposed 2,6-dihydroxypiperidine through mass spectrometry. This structure is relatively unstable and will reverse the reaction reform the imine (*105, 107*). If the dialdehyde is unsymmetrical, then intramolecular *trans*-imination can occur in the reaction (*cf.* Scheme 4.4).

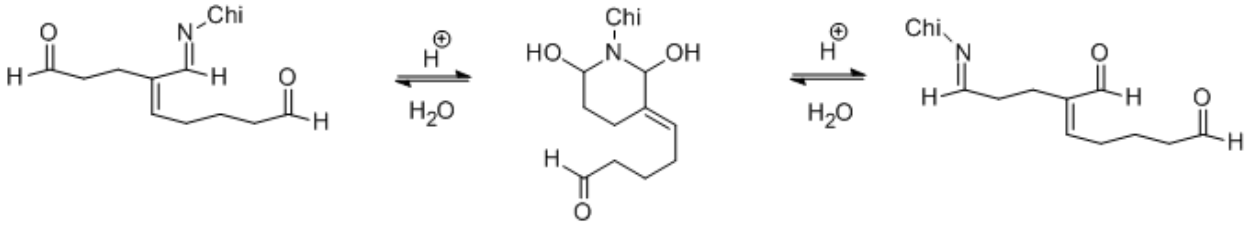

Scheme 4.4 Proposed reaction scheme for the *trans*-imination of chitosan based on several studies (*104-108*)

This process is usually associated with pyridoxal phosphate and the aminotransferase process but studies done by Kovaříček and Lehn (*108*) has shown the feasibility of *trans*-imination occurring in small diamine molecules. Through *trans*-imination of dialdehydes, water can react with the imine and form an aldehyde while the nitrogen concurrently attacks the second aldehyde to re-form an imine (*cf.* Scheme 4.4). Through this alternate reaction pathway, the total level of cross-linking does not decrease since glutaraldehyde is still bound to chitosan.

If the *trans*-imination process moves the imine to saturated aldehyde then it is free to continue the polymerization reaction which can explain the relative lack of free aldehyde signals (~1720 cm^{-1}) in the FT-IR spectra. Kildeeva et al. (*55*) measured the rate of polymerization between two glutaraldehyde molecules with and without the addition of chitosan. A key result they found was that enal formation was greater in the presence of chitosan as compared to the absence chitosan. This indicates that a portion of the enal species that are formed as a product of the amine-catalyzed cross-linking reaction. But Scheme 4.3 shows that the amine-catalyzed process should not generate enals unless the imine is hydrolyzed and the cross-linker is detached from chitosan. Therefore, *trans*-imination of the imine seen in Scheme 4.4 can explain the increased formation of enals due to the presence of an amine.

4.2 Synthesis

4.2.1. Addition of Glutaraldehyde

Syntheses of the Chi-Glu copolymers have been adapted from a similar study done by Wilson and Xue (*73*). When dissolved in acetic acid (pH 3.6-3.9), the resulting aqueous solution had a light yellow color. The color was likely due to oxidized astaxanthin (*109, 110*) in the sample obtained from the manufacturer (Sigma Aldrich). Another effect that had been observed was the increase in viscosity of the aqueous chitosan solution. This increase in the viscosity was due to

the polyelectrolyte effect where the charge repulsion of the ammonium groups linearizes the conformation of the chitosan polymer. By linearizing the polymer chain, the polymeric backbone had more exposed ammonium sites available for ion-dipole interactions between the ammonium group and the solvent (i.e. water).

When glutaraldehyde was added to the chitosan solution, the solution turned from a pale yellow color to a darker yellow. This was indicative of the start of the cross-linking reaction involving chitosan and glutaraldehyde; specifically, the color indicates the presence of unsaturated aldol condensation products. The presence of unsaturated aldehyde was determined by Kildeeva et al. (*55*) using UV-Vis spectrophotometry. By measuring the absorbance of a solution similar to that in Figure 4.1b, Kildeeva et al. (*55*) extrapolated a spectral band with a λ_{max} = 233 nm that was indicative of unsaturated aldehydes. Judging by the intensity of the color in Figure 4.1 the concentration of unsaturated imine and aldehydes was quite small. This was consistent with the mild reaction conditions because it was not favorable for the dehydration of alcohols and the formation of enals or conjugated imines (*55*).

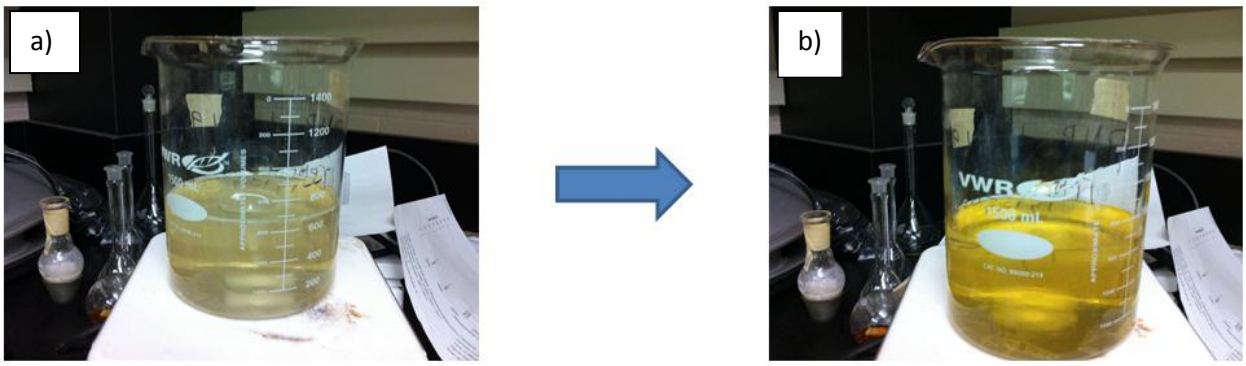

Figure 4.1 Addition of glutaraldehyde to the chitosan solution at pH3.3 and 298 K (Pictured: 1:1000 Chi-Glu): a) Chitosan dissolved in 2% aqueous acetic acid; b) 5-6 hours of stirring after the addition of glutaraldehyde to the chitosan solution

4.2.2 Gelation and Aging

After gentle stirring for 24h, the Chi-Glu solution began to gel as seen in Figure 4.3. The rate of gelation was found to depend on the concentration of glutaraldehyde which agreed with literature (*58b*). Although a gel was formed, it was crucial to allow the gel to age as seen in Figure 4.3. At the gel point, there was sufficient amount of cross-linked glutaraldehyde to form the gel but not enough to keep the network rigid (*cf*. Figure 4.2). Therefore, the Chi-Glu gel still flowed at the gel point but after 24h the gel started to stiffen.

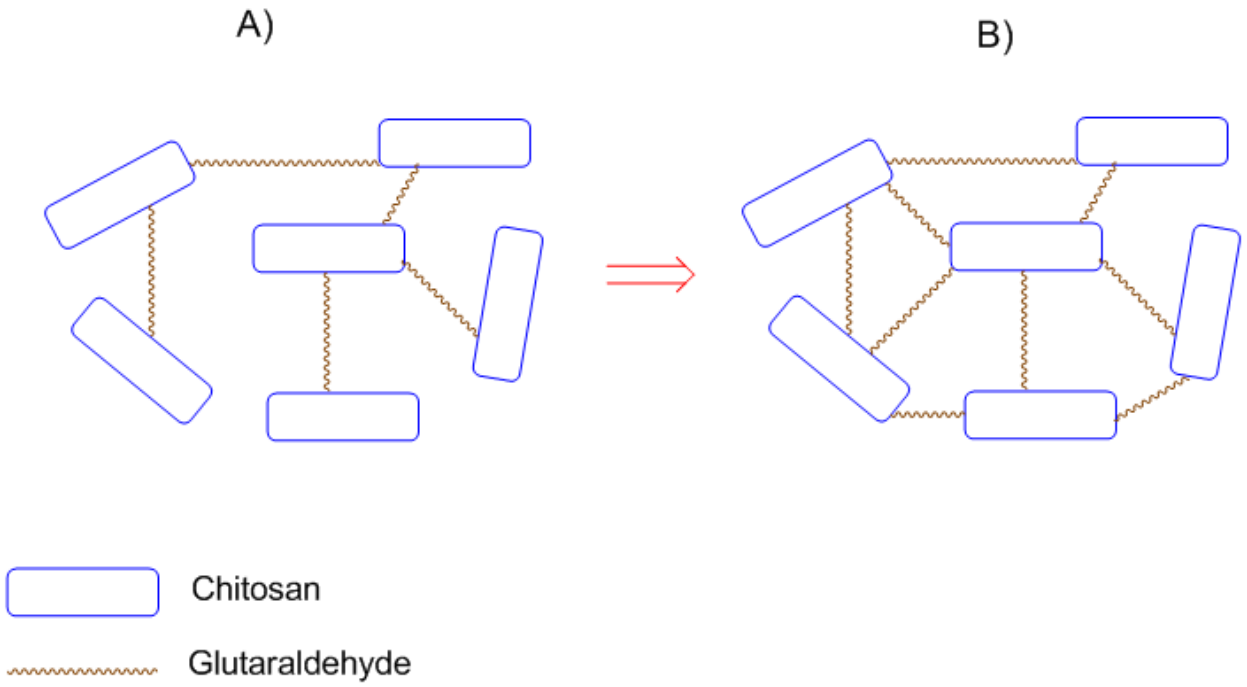

Figure 4.2 Diagram of the Chi-Glu copolymer during the aging process: A) near the gel point; B) after aging

This aging process as noted in a previous section (Section 1.5.3.1) was affected by three processes with polymerization being the crucial one. As more glutaraldehyde was cross-linked and polymerized with chitosan, it increased the interconnectivity of the disparate strands of chitosan forming the network which strengthened it through increased cross-linking. The polymerization as mentioned before formed mainly aldol products under mild conditions. As each aldol monomer contributed one hydroxyl group, the longer the polymer chain, the more hydrophilic the cross-linker chain became. This accounted for the sheer volume of water that was

absorbed by the gel. But since the aldol product was kinetically stable, a long period of reaction time ultimately converted more aldols into the thermodynamically stable enals or α, β-unsaturated imines. This accounted for the consistent darkening of the yellow color when comparing Figure 4.1b with Figure 4.3.

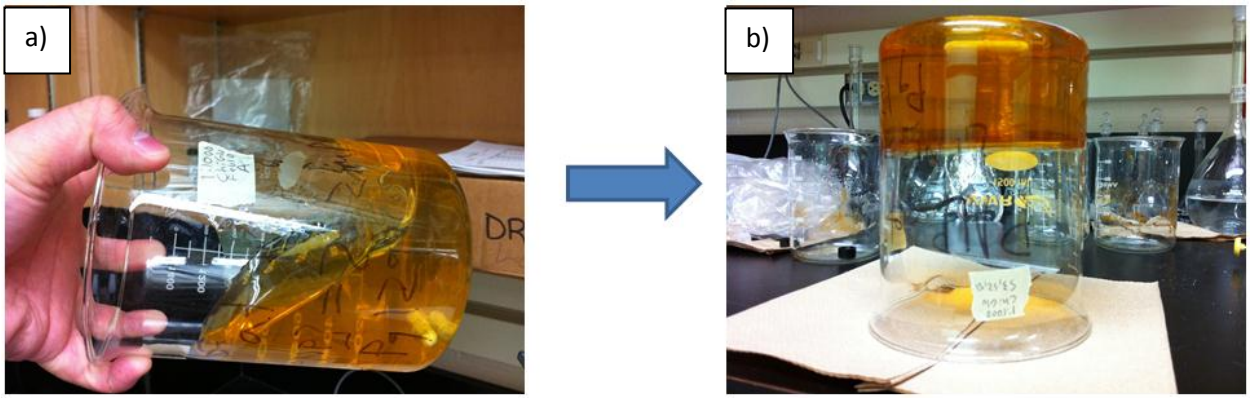

Figure 4.3 Aging of a 1:1000 Chi-Glu copolymer gel at ambient temperature and pressure: a) 1:1000 Chi-Glu at the gel point where some flow can be observed. b) After 24 h the same gel stiffens and has enough surface tension in the network to withstand gravitational flow.

4.2.2.1 Effects of volume and temperature

For the 1:400 Chi-Glu copolymer, and occasionally, the 1:700 Chi-Glu copolymer, there was an excess of aqueous acetic acid solution that prevented the formation of the polymeric network needed for gelation. Therefore, two methods were chosen to evaporate water and acetic acid to allow gelation to occur. The first method involved mild heating of the Chi-Glu solution (50-60^{o}C). Ideally, this method reduced the volume of water but increased the gelation time according to the Arrhenius equation (*57c*) (Figure 3.4). The temperature could be reduced afterwards to increase the rate of gelation. While increasing temperature did reduce the volume of water and acetic acid, this had the unintended effect of catalyzing the aldol condensation between glutaraldehyde and chitosan. At elevated temperatures, most of the aldol underwent elimination to the more hydrophobic enal and α, β-unsaturated imines. This was seen by the intense dark brown color emitted by these conjugated products. Secondly, dehydration of the alcohols to form enal reduced the number of hydrogen bonding sites which suggested that the volume of water required for removal- for gelation to occur- had increased. Lastly, the primary amines of chitosan acted as a catalyst in the aldol condensation reaction. By increasing the

temperature the primary amine catalyst ended up being "re-generated" and decreased the cross-linking between chitosan polymer units. Therefore, elevated temperature exacerbated the problem of excess solution. This verified the results observed in Figure 4.3 where, on the left, 1:700 Chi-Glu gelled with all 600ml of aqueous acetic acid inside the porous gel network. On the right, a similar 1:700 Chi-Glu sample was heated to 60^{o}C (333 K), where ~ 200-250 ml of aqueous acetic acid remained before gelation occurred.

Figure 4.4 1:700 Chi-Glu gels obtained at pH 3.3 and at various temperatures. On the left, 1:700 Chi-Glu was gelled at room temperature. On the right, 1:700 Chi-Glu was heated to 60^{o}C.

The second method was to depress the boiling points of water and acetic acid through reduced pressure and evaporate off the solvents. This method was documented in the 1:400 Chi-Glu copolymers by subjecting the 1:400 Chi-Glu solution with a rotary evaporator attached to a vacuum pump. Very gentle heating at 30^{o}C was applied to accelerate the process. The reaction resulted in the condensation of aldol as the resulting gel retained a dark brown color (Figure 4.5a). But when the final product was characterized using TGA (see Section 4.3), the thermal profile was similar to a 1:1000 Chi-Glu copolymer that gelled at room temperature. The same cannot be said of the thermal profile of the 1:700 Chi-Glu copolymers that underwent heating at 60^{o}C when compared to another 1:700 Chi-Glu copolymer that gelled at room temperature and pressure. Therefore, *in vacuo* removal of water at 30^{o}C was the preferred method for accelerating gelation.

4.2.3 Precipitation of Chi-Glu Copolymers

As various studies in the synthesis of Chi-Glu copolymers (*73, 102*), fibers (*94, 111*), and beads (*53, 112*) have indicated, an alkaline solution was introduced into the gel network to facilitate precipitation. The capillary pressure caused by an increase in cross-linking prevented diffusion of the aqueous alkali solution into the gel network. Therefore, rigorous mechanical stirring using a spatula became necessary to facilitate exposure of the polymeric network in the gel to the NaOH solution. This was seen in Figure 4.5 going from the gel in step a) to step b). In b) bubbles can be seen and heat was evolved during the reaction. The latter can be attributed to the exothermic acid-base reaction between NaOH and acetic acid. Evolution of the bubbles is more complex as no gas was observed to have been evolved during the reaction. One possible explanation for the appearance of a gas is the increased presence of Na^+ salts from NaOH that can decrease the solubility of carbon dioxide. A second explanation is the shrinkage of the gel network induced by NaOH causes syneresis (expulsion of solution). One effect of syneresis is that porosity of the copolymer is increased and sites for nucleation of the bubbles could be formed by the evacuation of water from the porous network (*58b*).

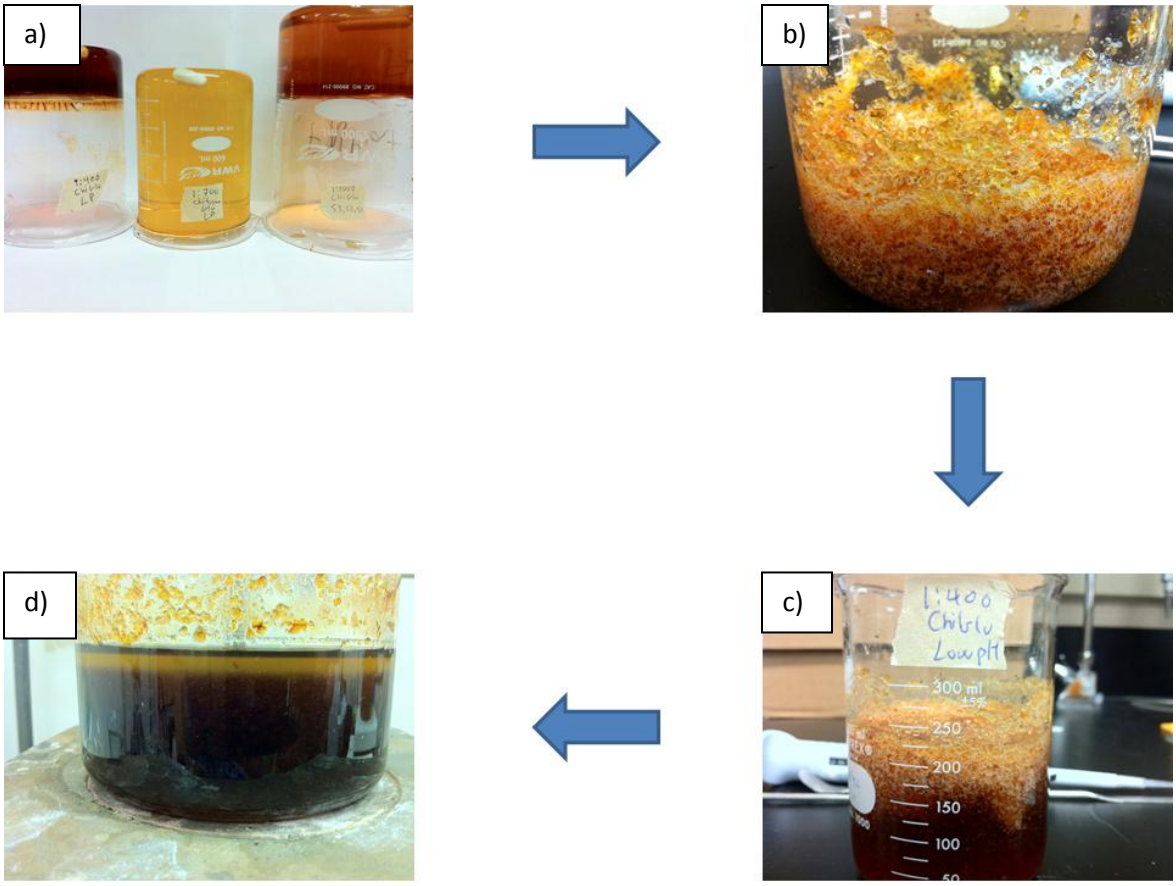

Figure 4.5 The four stages observed during the precipitation of Chi-Glu copolymers: a) Aged gel for 1:400 Chi-Glu (left), 1:700 Chi-Glu (center), and 1:1000 Chi-Glu (right) at 298 K; b) After addition of 3-4 ml of NaOH and rigorous stirring with a spatula (Pictured: 1:1000 Chi-Glu). c) The solution currently has a pH 5-6 which is close to the pK_a. Stirring was done with a magnetic stir bar (Pictured: 1:400 Chi-Glu). d) The resulting suspension after 24 h of stirring. The recorded pH was 6.9 (Pictured: 1:1000 Chi-Glu).

As NaOH was introduced into the network many of the positively charged ammonium groups on the chitosan deprotonated into the uncharged amine group. As more amine groups were deprotonated, many of these groups underwent further cross-linking with glutaraldehyde. This can be observed by the darkening of the copolymer product color as seen in Figure 4.5 b) to d). As the copolymer becomes more hydrophobic through increased cross-linking, a decrease in the attractive forces between water and the pore surfaces ensues. The result was the disappearance of the ordered layer that facilitated the opposing dipole interaction that kept the gel in a hydrated and swelled state. Instead, greater cooperative ordering between water

molecules occurs (*cf.* Figure 4.6) (*58d*). This reduction of the repulsive dipole interaction results in a shrinkage of the pores and the evacuation of the water.

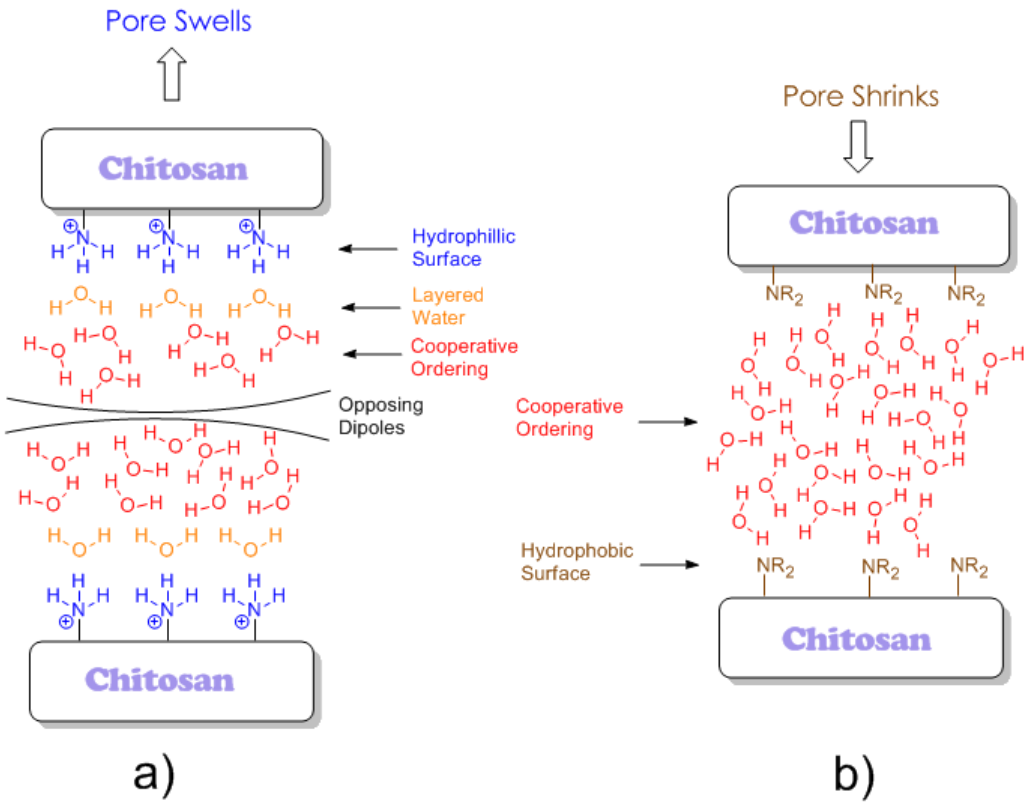

Figure 4.6 Cross-sectional view of a pore structure showing interaction of the surface with water (adapted from Brinker and Scherer (*58d*)): a) water interacting with a hydrophilic surface; b) water is interacting with a hydrophobic surface.

4.2.4 Effect of reaction time after addition of NaOH

As more glutaraldehyde was cross-linked to chitosan, the surface of chitosan becomes more hydrophobic. This was seen in Figure 4.5 where the transition from c) to d) resulted in a separation of phases. Step d) itself was divided into two stages depending on the reaction time. Figure 4.7 demonstrated the amount of time needed in step d) to complete the cross-linking of glutaraldehyde and chitosan. The swelling and the darkening of the precipitate were indicators that the reaction had gone to completion as the majority of the aldol had been converted into the UV-active enal or α, β-unsaturated imine. From these two examples, it was concluded that

polymerization of the glutaraldehyde was ongoing and filtration of the product prematurely will reduce the cross-linking efficiency of glutaraldehyde.

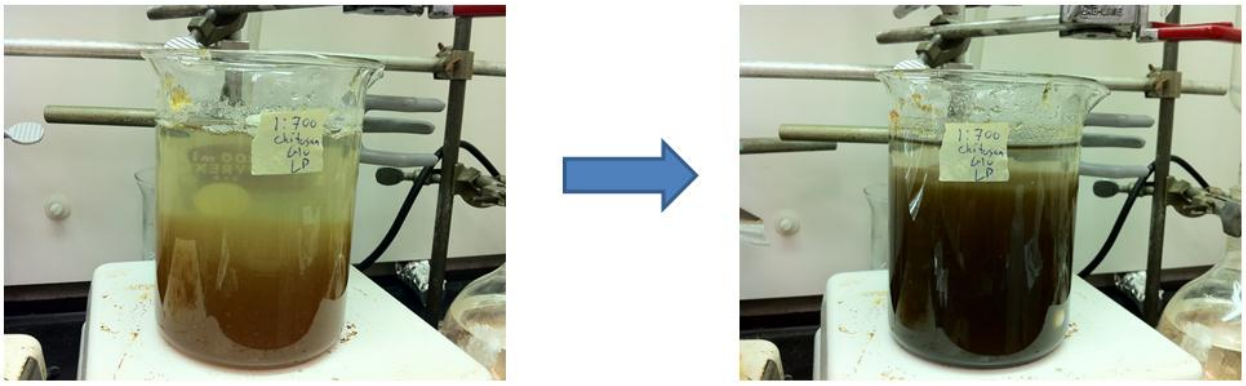

Figure 4.7 1:700 Chi-Glu copolymer precipitated at 298 K. The solution retained a pH value of 6.9. Left: After 5-6 h of stirring after the addition of NaOH and right: After 24 h of stirring.

The changes in the physicochemical properties due to reaction time after the addition of NaOH have been studied by Wilson and Xue (*73*). From the TGA results obtained by Wilson and Xue (*73*), only one band is apparent and was assigned to low levels of cross-linked chitosan to oligomers of glutaraldehyde. In Figure 4.8, the physical appearance of the copolymer was noteworthy. The physical appearance of the 1:1000 Chi-Glu copolymers resembled the texture of the CP-1 material synthesized by Wilson and Xue (*73*). Differences in the physical properties such as relative swelling ratios in aqueous solution and the thermal stability have been evaluated and will be described further in later sections.

Figure 4.8 1:1000 Chi-Glu copolymers were precipitated using 1M NaOH at 298 K and pH 5.6-7.0; left: Isolated after 5 h of stirring; right: Isolated after 24 h of stirring

4.2.5 Effect of excess NaOH

Adapting the synthetic protocol by Wilson and Xue (*73*), the Chi-Glu copolymers were isolated as precipitates after addition of base such that the final pH of the solution was at pH 7. This poses an intriguing hypothesis: Does excess NaOH affect the morphology and physicochemical properties of Chi-Glu copolymers? In this study, a 1:400 Chi-Glu copolymer was synthesized and isolated such that the supernatant solution had a pH of 12.8. The physical appearance was a dark brown color (*cf.* Figure 4.9).

Figure 4.9 Physical appearance of a 1:400 Chi-Glu copolymer prepared out at 298 K. The reaction was stirred for 24 h in the solution at pH 12.8.

4.2.6 Yield and Characteristics of the Chi-Glu copolymer powder

The yield was calculated assuming that all the glutaraldehyde was cross-linked with chitosan; either through an aldol condensation or an amine-catalyzed aldol addition. Both reactions resulted in the loss of 2 water molecules lost for every molecule of glutaraldehyde cross-linked. Therefore, the molar mass of the product ($M_{Chi\text{-}Glu}$) was calculated using Equation 4.1. Equation 4.1 was derived using the reaction depicted in Scheme 4.5.

$$M_{Chi-Glu} = M_{Chi} + nM_{Glu} - 2nM_w - M_{res} \quad (4.1)$$

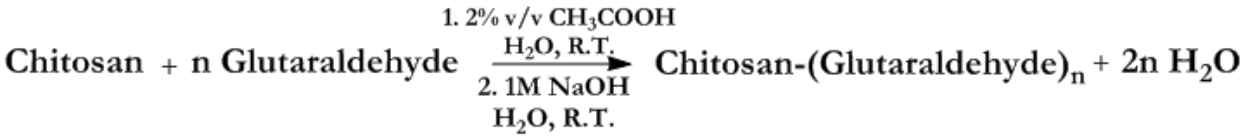

Scheme 4.5 Stoichiometry of reaction scheme for the cross-linking of chitosan with glutaraldehyde is shown.

Molar mass of chitosan (M_{Chi}) was between 50,000-190,000 g/mol and an average of 120,000 g/mol was used. Unreacted glutaraldehyde (M_{Glu}) had a mass of 100.1012 g/mol and since there was more than one glutaraldehyde added the total molecular weight was multiplied by the number of glutaraldehyde molecules added (n) for a single chitosan. For example: 1:400 Chi-Glu had 400 moles of glutaraldehyde for every one mole of chitosan therefore, n = 400. Assuming every single glutaraldehyde had reacted then every glutaraldehyde molecule should lose 2 molecules of water due to cross-linking. If there was n-number of glutaraldehyde than there was 2n number of water molecules lost. Therefore, the molecular weight of the water lost was $2nM_w$. Lastly, residual solvents (M_{res}) remaining in the polymer was considered and this can be determined using TGA. The results are listed in Table 4.1.

Table 4.1 Experimental Yields of various Chi-Glu copolymers were gelled at 298 K and precipitated at pH 7.0 unless stated otherwise.

Chi-Glu Copolymers[1]	Mass of Copolymer (g)	Theoretical Yield[2] (g)	% Yield
1:400 Chi-Glu	5.8924	7.3102	81
1:400 Chi-Glu at pH 12.8*	4.9971	7.2874	69
1:700 Chi-Glu	7.6356	8.3122	92
1:700 Chi-Glu at T = 333 K†	6.4820	8.2489	79
1:1000 Chi-Glu	7.2560	9.2148	78

[1]The ratios are indicative of the Chitosan to Glutaraldehyde mole ratio. For example: 1:400 means for every 1 mole of chitosan, 400 moles of glutaraldehyde was added

[2]Calculated according to Scheme 4.5

*pH of the supernatant solution after precipitation using NaOH (See Section 4.2.5)

† Temperature of the Chi-Glu solution before gelation (See Section 4.2.2.1)

Overall, the yield obtained for the copolymer products ranged from 70-92%, and was comparable to values reported by Wilson and Xue (*73*). The loss of product had been attributed to the loss of low molecular weight cross-linked copolymers of Chi-Glu with small particle sizes during filtration of products.

The color of the final copolymer product was a dark brown color with subtle variations that can be seen according to pH conditions and relative ratio of glutaraldehyde employed. Products with darker color were observed as the content of the glutaraldehyde increases; with all other reaction conditions held constant. 1:400 Chi-Glu appears to be the lightest and 1:1000 Chi-Glu being the darkest coloured copolymer material. An exception to this trend occurs when reaction conditions are changed. The darkest color would now be assigned to 1:700 Chi-Glu at 333 K.

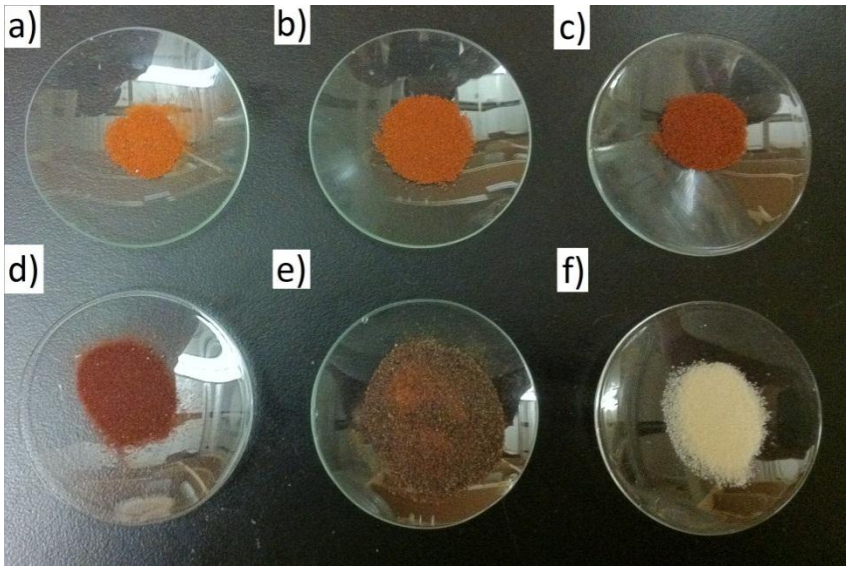

Figure 4.10 Physical appearances of the dried copolymer products: a) 1:400 Chi-Glu; b) 1:700 Chi-Glu; c) 1:1000 Chi-Glu; d) 1:700 Chi-Glu at T=333 K; e) 1:400 Chi-Glu at pH 12.8, and f) as received Chitosan.

This can be explained by the promotion of condensation at elevated temperature which converts more aldol into the enal and α,β-unsaturated imine form. The four copolymers at various Chi-Glu mole ratios all consistently show one color whereas the 1:400 Chi-Glu copolymer precipitated at pH=12.8 had a heterogeneous mixture of color. The mechanism for the formation of Chi-Glu at basic pH conditions accelerated the polymerization of aldol on the surface of the copolymer only. The reactions in the pores were slower due to poor intra-particle diffusion (*54*). This uneven polymerization explained the multiple colors seen in 1:400 at pH 12.8 (*cf*. Figure 4.10e). If the surface of the 1:400 Chi-Glu became relatively nonporous due to heavy amounts of cross-linking then cross-linking of glutaraldehyde in the interior of the particle became discouraged. Therefore, the amount of cross-linking in the interior of the particle was less than the surface and has a light color. Synthesis of the 1:400 Chi-Glu copolymer at high pH conditions yielded a heterogeneous mixture of compounds but also highly crystalline Chi-Glu copolymers. These characteristics, as observed by Crini and Badot (*59*), occur when sufficient water was driven away from chitosan. Without water, the gel network collapsed and this caused compaction of the chitosan copolymers.

4.3 FT-IR Spectroscopy

The FT-IR spectra of chitosan, 1:400 Chi-Glu, 1:700 Chi-Glu, and 1:1000 Chi-Glu synthesized at pH 7.0 and at 298 K are shown in Figure 4.9. The symbol v denotes vibrational modes involved with the stretching of bonds while δ denotes the bending or deformation of bonds. Subscripts "as" denote asymmetry while "s" denotes symmetrical vibrational modes. Characterization of chitosan using FT-IR is complicated since many of the functional groups of both chitosan and the Chi-Glu copolymers contribute absorption bands with similar wavenumbers. Consequently, this means that the various bands in the spectra for chitosan and the copolymers are combination bands contributed by various functional groups.

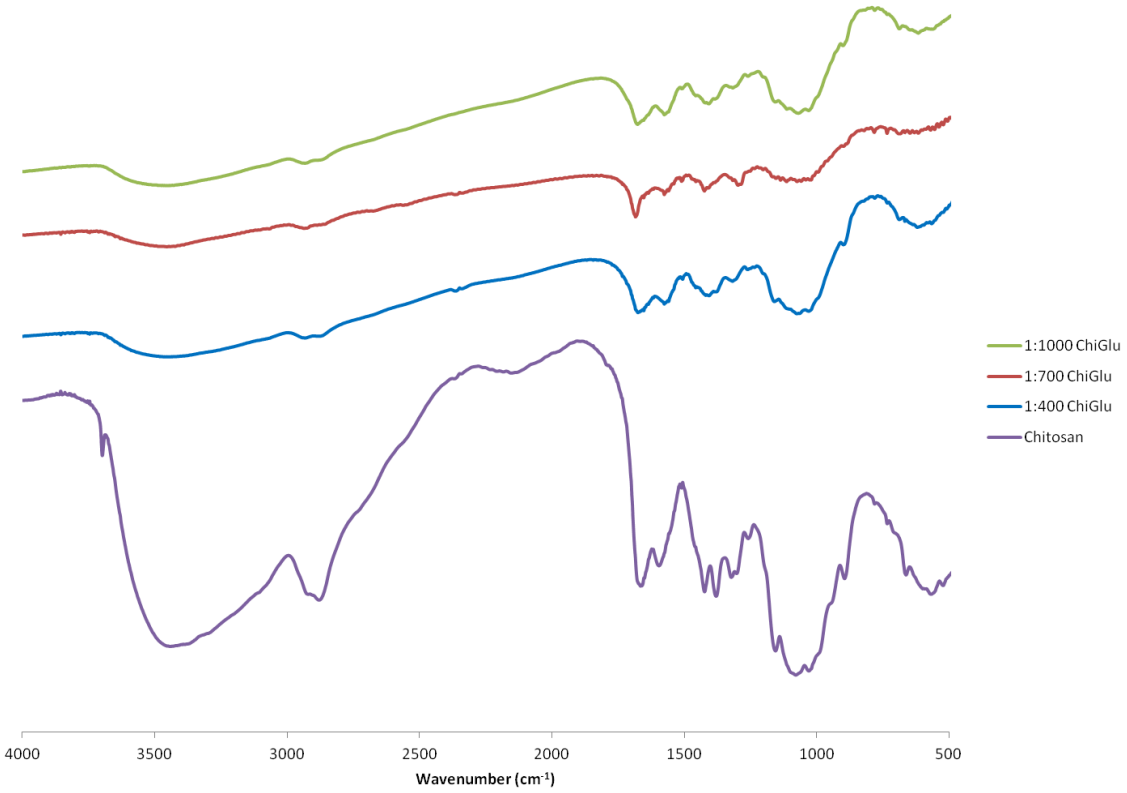

Figure 4.11 FT-IR spectra of chitosan and Chi-Glu copolymers at pH 7.0 and 298 K.

4.3.1 Chitosan

The broad absorption band seen in Figure 4.11 for chitosan ranges from ~2500 cm^{-1} to 3600 cm^{-1} is too broad to simply correspond to the stretching band of O-H (v(O-H)). According

to the literature[26], a typical range for hydrogen bonded ν(O-H) should be between the region 3200 cm^{-1} to 3400 cm^{-1} with the wavenumber of the minima dependent on the degree of hydrogen bonding between the hydroxyls. The range of values from 2500 cm^{-1} to 3200 cm^{-1} can be accounted for by combination bands seen for ammonium groups are included. Therefore, the broad band at 3440 cm^{-1} observed for chitosan is attributed by both the hydroxyls (3200-3600 cm^{-1}) and by ammonium cations (2500-3200 cm^{-1}). The doublet seen at 2878 cm^{-1} and at 2920 cm^{-1} corresponds to the symmetric stretching ($\nu_s(CH_2)$) and asymmetric stretching of the methylene groups ($\nu_{as}(CH_2)$), respectively.

Table 4.2 IR bands (cm^{-1}) of Chi-Glu copolymers gelled at 298 K and precipitated at pH 7.0 unless specified otherwise.

Material	**Combination Bands:** ν_{as} (C-O-C) ν_{as} (C-O-H) ν_{as} (C-N-H) $\delta(CH_2)$	**Amide III**	**δ_s (CH_3)**	**δ(C-H) Methine Deformation** (Low ν) δ(H-C=N) (High ν)	**δ(NH_2), and Amide II** (Low ν) ν_{as}(C=N) (High ν)	**Combination Bands:**	**$\nu_s(CH_2)$** (Low ν) and $\nu_{as}(CH_2)$ (High ν)	**ν(O-H) ν(NH_3^+)** Stretch
Low MW Chitosan	1079	1323	1380	1424	1596,1665	2259	2878,2920	3440
1:400 Chi-Glu	1074	1318	1383	1406,1420	1576,1675		2900,2939	3457
1:400 ChiGlu pH 12.8 (Powder)	1071		1385	1424	1576,1685		2881-2929	3456
1:400 ChiGlu pH 12.8 (Crystal)	1075		1384	1424	1575,1683		2903-2923	3454
1:700 Chi-Glu	1075			1424	1576,1684		2899,2939	3454
1:700 ChiGlu T = 333 K	1075			1425	1576,1685		2901-2933	3456
1:1000 Chi-Glu	1084	1317	1382	1408,1420	1576,1676		2899,2932	3446

The combination band at 2259 cm^{-1} is indicative of the presence of primary ammonium cations and is a combination of several fundamental vibrational modes. Changes in the intensity of this combination band will indicate reactions involving the ammonium cation. Presence of an amide is assigned to the band at 1665 cm^{-1} (ν_{as}(C=O)). An absorption band at 1596 cm^{-1} corresponds to a combination of deformations of the primary amine groups ($\delta(NH_2)$), deformation of the primary ammonium cation, and the asymmetric stretching of C-N in the amide (ν_{as}(C-N), amide II). The foregoing assignment of IR bands agrees with characterization done by Lazaridis et al. (*113*) However, the only disagreement is the band at 1424 cm^{-1} where Lazaridis et al. (*109*) assigned it to the amine group. This spectral band is attributed to a methine deformation of the glucopyranose ring of chitosan and is also characteristic of saccharides as this band is also observed for cyclodextrins. (*114, 115*) It is the sole absorption band that should remain the same. For comparisons between band intensities, this unchanging methine deformation band would be a good standard. The absorption band at 1380 cm^{-1} is the symmetric deformation of the methyl groups on the amide. The doublet seen at 1323 cm^{-1} corresponds to the amide III band but the vibrational modes for this band cannot be accurately assigned (*79*). This band, along with amide I, amide II, and $\delta_s(CH_3)$ can only be affected if the amide functional group undergoes either a physical or chemical change. Therefore these bands are a good indication of any reactions involving amides. The last absorption band of significance is the broad band seen at 1079 cm^{-1}. This is a combination band of various asymmetric stretching originating from ether bonds within the chitosan ring (ν_{as}(C-O-C)), alcohol substituents (ν_{as} (C-O-H), and primary amines (ν_{as} (N-H)). Contributions from the twisting and rocking deformations from methylene groups are included here.

4.3.2 Chi-Glu Copolymers

To characterize the copolymers it is necessary to recall the various reactions that have occurred throughout the synthesis. The first reaction involved the cross-linking of glutaraldehyde to chitosan to form an imine. This reaction can be supported by numerous changes seen on the FT-IR spectra. From Scheme 4.1, the product of the cross-linking reaction of the amine group to form imine. This can be observed by the disappearance of the $\delta(NH_2)$ band at 1596 cm^{-1} and the formation of the imine band ν_{as}(C=N) at 1675-1680 cm^{-1} for the various copolymers. The attenuation of the combination band at 2259 cm^{-1} combined with a decrease in the $\delta_s(NH_2)$ band

is attributed to deprotonation of the ammonium cation and cross-linking with glutaraldehyde (*cf.* Figure 4.2). As more glutaraldehyde is cross-linked, more Schiff base contributions to the copolymers result as evidenced by the new band at 1400 cm^{-1} for the copolymers. This band is analogous to the deformation of the C-H band observed for aldehydes but in this case it is the C-H deformation band for a Schiff base. These results provide support of imine formation.

The presence of products derived from an aldol condensation is determined by the presence of the v_{as}(C=C) band at 1576 cm^{-1} as seen for the various copolymers. According to Monteiro Jr. and Airoldi (*112*), the intensity of the band at 1576 cm^{-1} relative to v_{as}(C=N) can be used to obtain semi-quantitative estimates the amount of glutaraldehyde cross-linked to chitosan. Therefore, 1:700 Chi-Glu should have the least amount of glutaraldehyde cross-linked while 1:400 Chi-Glu and 1:1000 Chi-Glu would have the most. When compared with the CHN data, this is proven to be not true as the mass percentage of carbon is highest in 1:700 Chi-Glu. According to Monteiro Jr. and Airoldi (*112*), a high carbon mass percentage should indicate a high degree of cross-linking. Thus, FT-IR analysis concludes that the 1:700 Chi-Glu copolymer has the lowest level of cross-linking while CHN analysis concludes the opposite. The explanation of this contradiction can be found in the broadness of the 1576 cm^{-1} absorption band. The broadness of the band suggests multiple vibrational modes contribute to this band. Therefore, contributions to this band are likely from both the amide II band as well as v_{as}(C=C).

4.3.3 Deacetylation

From Figure 4.11, the broadness of the v_{as}(C=N) band seen for 1:400 and 1:1000 Chi-Glu copolymers is correlated to the unreacted amide chitosan monomers at 1665 cm^{-1}. For 1:700 Chi-Glu at various temperatures (*cf.* Figure 4.12, and Section 4.2.2.1), the band sharpens to a maxima at 1684 cm^{-1} with a reduction of the v_{as}(C=O) for amide or the amide I band at 1665 cm^{-1}. Coupled to this result is the reduction of the amide II (1576cm^{-1}), $\delta_s(CH_3)$ (1380 cm^{-1}), and the amide III band (1320 cm^{-1}). The reduction of the intensity of the four bands seen for the 1:700 Chi-Glu copolymers at elevated temperatures suggests deacetylation occurs at these conditions (*cf.* Figure 4.12). In Figure 4.13, the 1:400 Chi-Glu were precipitated at pH 6.9 and 12.8. At high pH=12.8, 1:400 Chi-Glu also shows an attenuation of the intensity of the four bands associated with amides. Therefore, high concentrations of base will similarly cause deacetylation. The hydrolysis of amides is not kinetically favored but since the reaction is irreversible it may be

possible to drive the reaction thermodynamically by manipulating the concentration of base (*91d*). In Section 4.1.4, 1M NaOH was added until the solution had a final pH of 6.9. Therefore, high concentration of base was introduced to the gel network and this could drive deacetylation. A more interesting question is why deacetylation occurs for 1:700 Chi-Glu as opposed to 1:400 and 1:1000 Chi-Glu copolymer. This result is surprising and cannot be explained.

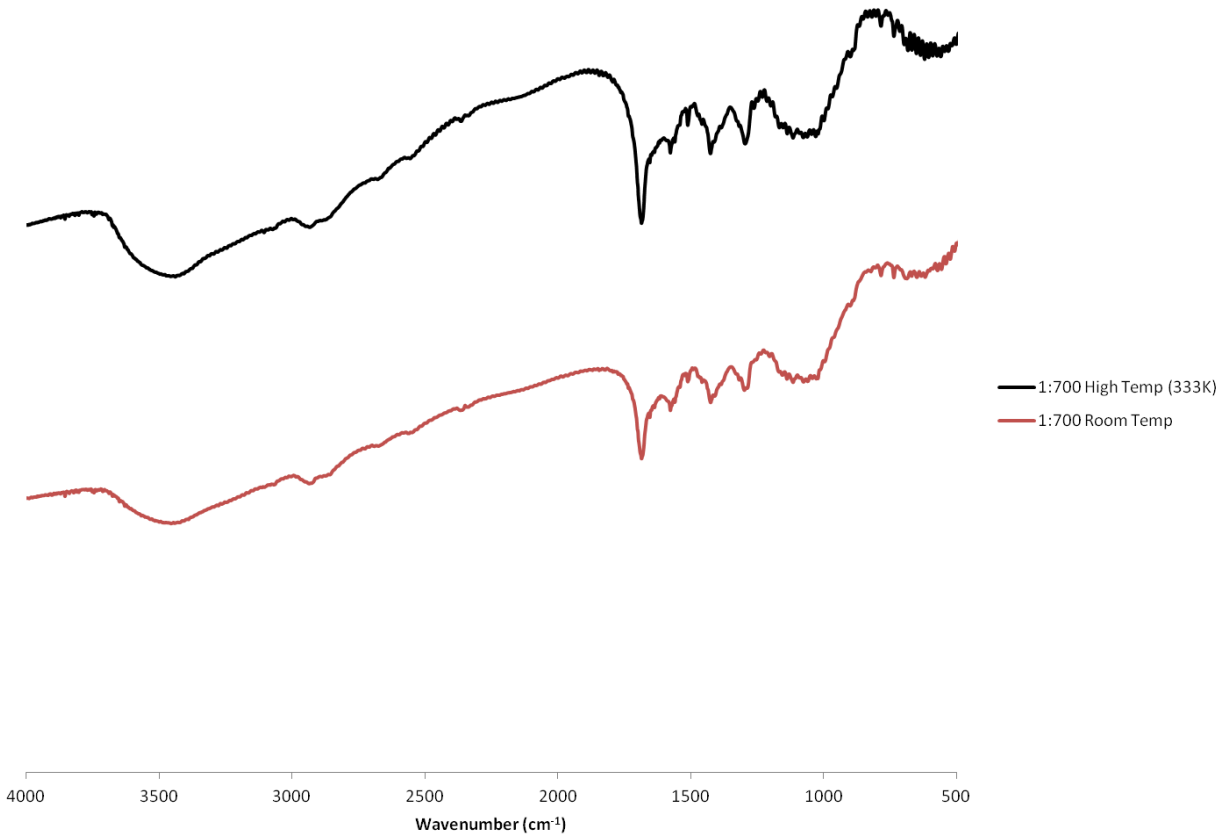

Figure 4.12 FT-IR spectra of the 1:700 Chi-Glu copolymers where the Chi-Glu solution temperature were at 298 K and 333 K before gelation

4.3.4 Effects of pH

The cross-linking of glutaraldehyde has been shown by various groups to undergo multiple reactions (*55, 73, 112*). Mechanistically, the reaction at higher pH demonstrates the same deacetylation as determined for 1:700 Chi-Glu at neutral pH. The FT-IR spectra in Figure 4.12 illustrate that there is an apparent decrease in amide I, amide II, $\delta_s(CH_3)$, and amide III

bands when comparing the spectra for the neutral pH 1:400 Chi-Glu and the 1:400 Chi-Glu copolymer. This result supports the premise that the amide hydrolysis in Chi-Glu copolymer is base-catalyzed. Another interesting result is the decrease in the number of free amine and ammonium groups. When contrasting the spectra for 1:400 Chi-Glu powders at high pH with the spectra for the 1:400 Chi-Glu crystalline-like materials, there is a noticeable attenuation of the combination band at 2000 cm^{-1} associated with protonated primary ammonium groups. It is concluded that rapid cross-linking with glutaraldehyde occurs as there is no corresponding increase at the $\delta_s(NH_2)$ at 1596 cm^{-1}. For crystalline materials, this is a curious result as a reduction in the amount of ammonium cations would consequently mean a reduction in the strong ion-dipole interactions between ammonium and any of the hydroxyls on another chitosan monomer. This paradox can be rationalized by again considering the environment seen in a pore with an ionic lattice. With an abundance of ammonium cation, both sides of the pores would be positively charged and electrostatically repulsed to each other; thus, the ion-dipole interaction causes repulsion. By reducing the amount of ammonium this repulsion is overcome and the remaining free amine and hydroxyls can undergo intermolecular hydrogen bonding. Hydrogen bonding is considered the primary contributor to crystalline polymer domains, as reported by Crini and Badot (*59*).

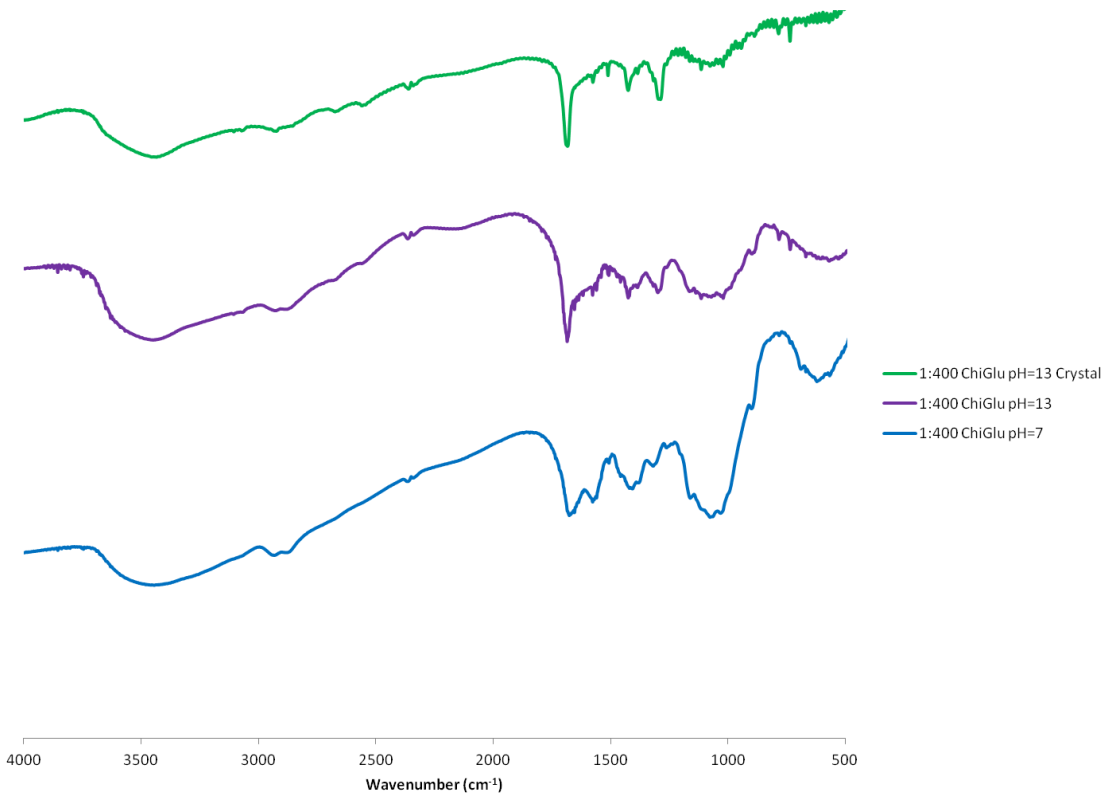

Figure 4.13 FT-IR spectra obtained for 1:400 Chi-Glu copolymers precipitated at neutral pH and pH 12.8; crystalline and powder based materials that were obtained are also analysed for the 1:400 Chi-Glu copolymer at pH 12.8

4.4 TGA

4.4.1 Chitosan

Characterization of the polymers by TGA reveals less about the functional groups and composition of the copolymers as it does the overall structure and relative thermal stability of the copolymer and cross-linkers. When comparing the thermal profile of pristine chitosan with polysaccharides such as guar gum (*116*), and cellulose (*117*), the differential thermogravimetry (DTG) appears to be quite similar as they all possess the band at 300^{o}C. From similar studies done by Basch and Lewin (*117*) on cellulose, this band is likely due to the scission of glycosidic bonds between each glucopyranose monomer followed by pyrolysis which will cause weight loss. Another band at 600^{o}C has been observed for chitosan (*111*). This doubling of thermal stability is likely due to the inherent semi-crystalline nature of the polymer. Through the study of

a similar polysaccharide, Basch and Lewin (*117*) determined a proportional relation between the activation energy for pyrolysis and the degree of crystallinity seen for cellulose. They found that the activation energy for pyrolysis effectively doubles from 30 kcal/mol for amorphous cellulose with no crystalline properties to 60 kcal/mol for fully crystalline cellulose. This stabilizing effect can account for the high temperature needed to decompose 35% of chitosan at a temperature higher than 500^{o}C (*cf.* Figure 4.14). Secondly, Trung et al. (*83*) and Piron et al. (*118*) determined that the percent crystallinity of chitosan can range from 32% to 35-40%, respectively. The crystalline percentage agrees with the thermogram in Figure 4.14 for chitosan where ~ 37% of the total mass remains at 500^{o}C. The difference in value may be due to different degrees of deacetylation and the polydisperse molecular weight distribution of chitosan (*83, 118*).

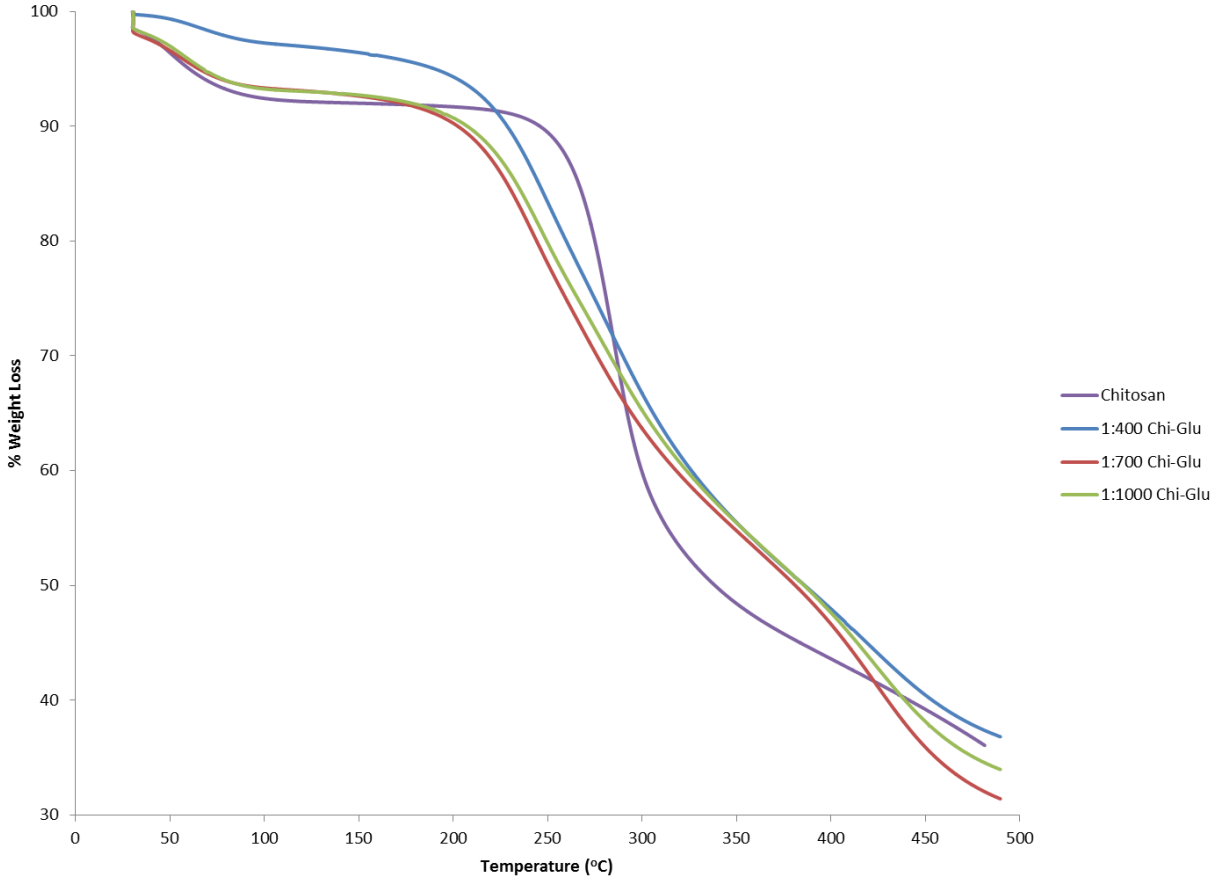

Figure 4.14 The thermogram of chitosan and Chi-Glu copolymers as a function of temperature and % weight loss is shown above. All copolymers were precipitated at pH 7.0 and 298 K.

4.4.2 Chi-Glu copolymers: water absorption band

All the copolymers exhibit four distinct bands in the thermogram. The first band ~ 45-100^{o}C is likely absorbed water from both the pores and surfaces of the copolymers. The shape of this peak can reveal morphological properties of the copolymers. Secondly, the size of the band can elucidate the water sorption capacity of the copolymers. When comparing the copolymers synthesized at neutral pH and at 298 K (*cf.* Figure 4.13) with chitosan it appears that chitosan is able to retain more water. Water comprises ~ 5.78% of the total mass in the chitosan sample while the copolymers were slightly lower, ranging from 2.6-4.8% by mass. This is likely due to the presence of more hydrophilic monomers containing free amines or ammonium cation. A second property is the peak decomposition temperature for absorbed water in chitosan is lower than the copolymers. This suggests that chitosan, while able to retain more water, is not as porous as the copolymers, and much of the water is adsorbed on the surface which agrees with literature (*59*). As more cross-linking occurs, the ability to retain water in the copolymers is enhanced. This can be observed by the increase in the decomposition temperature on the DTG. The amount of absorbed water as a percent of the total mass for 1:700 and 1:1000 Chi-Glu are 4.32% and 4.86%, respectively. These values are larger than the value for 1:400 Chi-Glu at 2.60%. The result, in general, agrees with the swelling ratios.

Table 4.3 TGA results of the copolymer precipitated at pH 7.0 and 298 K unless specified otherwise

Copolymer	Decomposition Temperature (^{o}C)	Percent by mass of each decomposition temperature Band (%)
Low MW Chitosan	45 284	5.78 46.5
1:400 ChiGlu	61 255, 283 428	2.60 46.4* 13.8
1:400 ChiGlu pH 12.8 (Powder)	55-150 (Broad) 255,283 428	5.87 39.1* 8.74
1:400 ChiGlu pH 12.8 (Crystal)	45-150 (Broad) 257,263 (Sharp) 408,444 (Sharp),462 (Sharp)	6.88 40.8* 10.5*
1:700 ChiGlu	51 242,279 423	4.32 38.0* 21.7
1:700 ChiGlu T = 333 K	53 247 418	4.37 38.9 17.9
1:1000 ChiGlu	55-100 240,285 420	4.86 39.3* 18.6

* This percentage contains more than one decomposition temperatures

4.4.3 Chi-Glu copolymers: cross-linker size-dependent bands

The aldol condensation as proposed by Kildeeva et al. (*55*) suggests that glutaraldehyde polymerizes, and this mechanism is supported by the FT-IR spectra (*e.g.*, the broad combination band at 1576 cm^{-1}). Further evidence of self-polymerization of glutaraldehyde is evidenced by the band at 400^{o}C observed for the TGA. From Scheme 4.3, the mechanism revealed that for every two amines used for cross-linking, a self-polymerized glutaraldehyde is likely linked to them. Although two hydrogen bonding sites are lost to cross-linking the cumulative van der Waal (VDW) interactions from polymerized glutaraldehyde can increase the overall thermal stability of the Chi-Glu copolymers. Therefore, the band at 400^{o}C seen in the TGA is a clear indicator of polymerized glutaraldehyde onto the amine units of chitosan. Consequently, if the size of the cross-linker is small (exact number is unknown), the magnitude of the VDW interaction to thermal stability is insufficient to compensate for the loss of cooperative hydrogen bonding along the chitosan backbone. Thus, the copolymer is destabilized, and a reduced decomposition temperature is the result. This can account for the band at ~ 240^{o}C which is lower than the chitosan band at ~ 280^{o}C. Therefore, the stability of the polymer is dependent on the degree of cross-linking and the decrease in H-bonding due to imine formation between chitosan and glutaraldehyde. One factor that can determine the size of the cross-linker formed is the concentration of glutaraldehyde added. As the concentration of glutaraldehyde increases, polymerization of the glutaraldehyde increases, and the result is a more thermally stable polymer, in agreement with the literature (*119*).

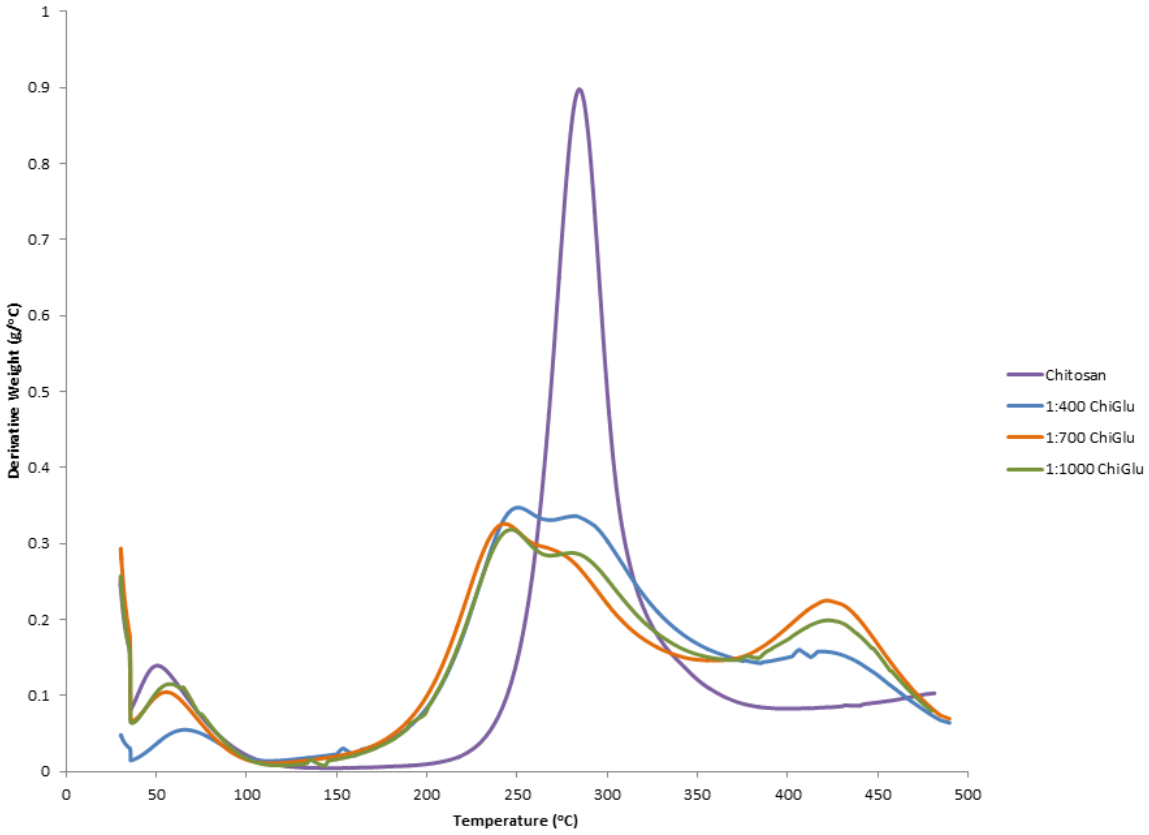

Figure 4.15 The DTG results of Chi-Glu copolymer at pH 7.0, and 298 K with various mole ratios of copolymers are shown in different colors.

In Figure 4.15, the height of the band in the DTG plot for the 1:700 Chi-Glu appears to contain the highest level of cross-linker followed by 1:1000, and lastly, 1:400 Chi-Glu. In Figure 4.16, 1:700 Chi-Glu again has more polymerized glutaraldehyde linkers as compared to 1:700 Chi-Glu at T=333 K. Both of the previous observations are verified by CHN analysis where 1:700 Chi-Glu has the largest total of glutaraldehyde molecules cross-linked to chitosan.

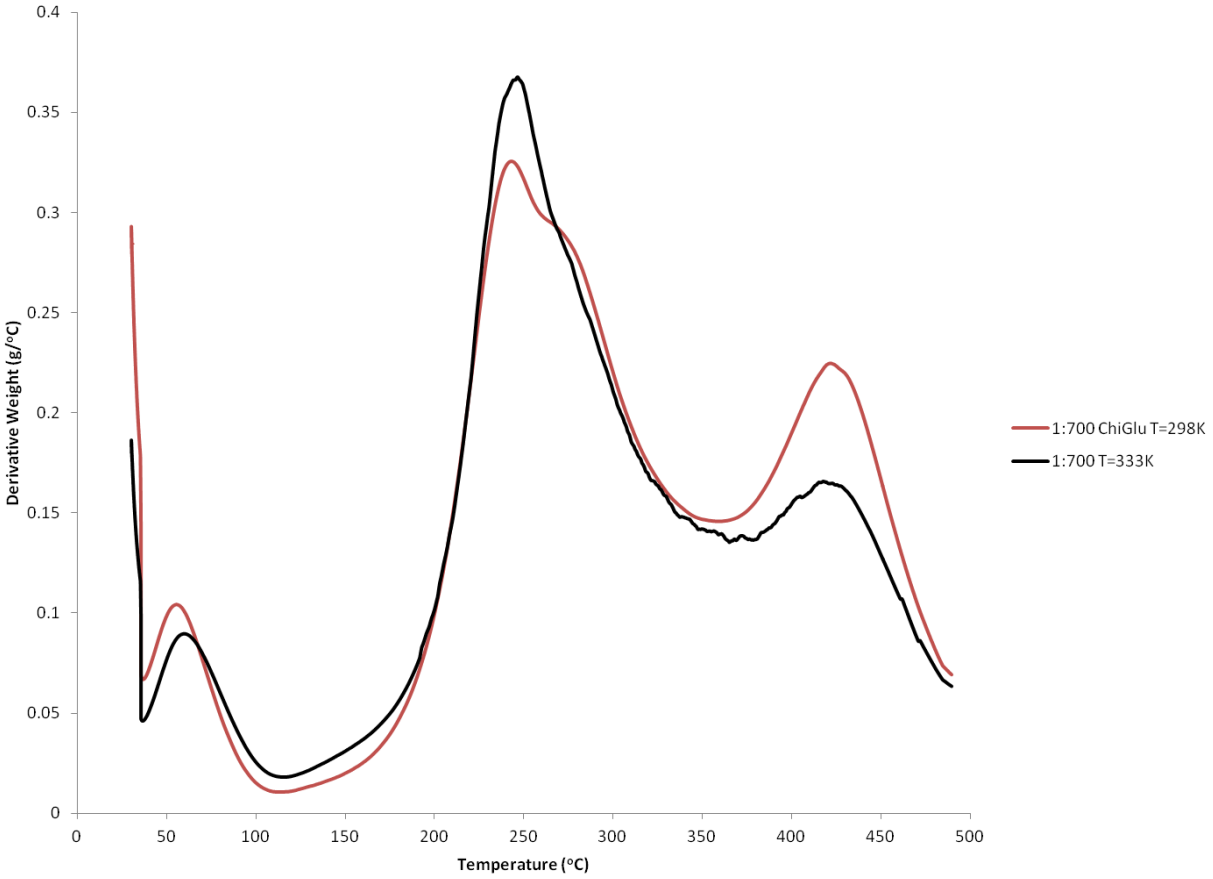

Figure 4.16 DTG of 1:700 Chi-Glu copolymer heated at various temperatures before gelling and undergoing precipitation (or solidification) at pH 7.0.

4.4.4 Chi-Glu Copolymers: Non-cross-linked band

The last band of interest is the decomposition temperature ~ 280^{o}C observed for the copolymers. This band has a similar decomposition temperature to chitosan and therefore, it is likely the pyrolysis of unbound monomers in the Chi-Glu copolymers. Attenuation of the latter band is most apparent for 1:700 Chi-Glu at both temperatures, and 1:400 Chi-Glu at greater pH. It is not surprising that these three bands shows the greatest reduction as they all undergo deacetylation followed by cross-linking as evidenced by their FT-IR spectra. The reduction of the intensity of this band is highest in 1:400 at high pH, followed by 1:700 Chi-Glu at elevated temperature (333 K) and with 1:700 Chi-Glu at 298 K being last (*cf.* Figure 4.16 and 4.17). One conclusion can be drawn by this trend. The magnitude of deacetylation is greatest at high pH as compared to elevated temperature which suggests, again, that pH is a greater factor in promoting deacetylation than temperature.

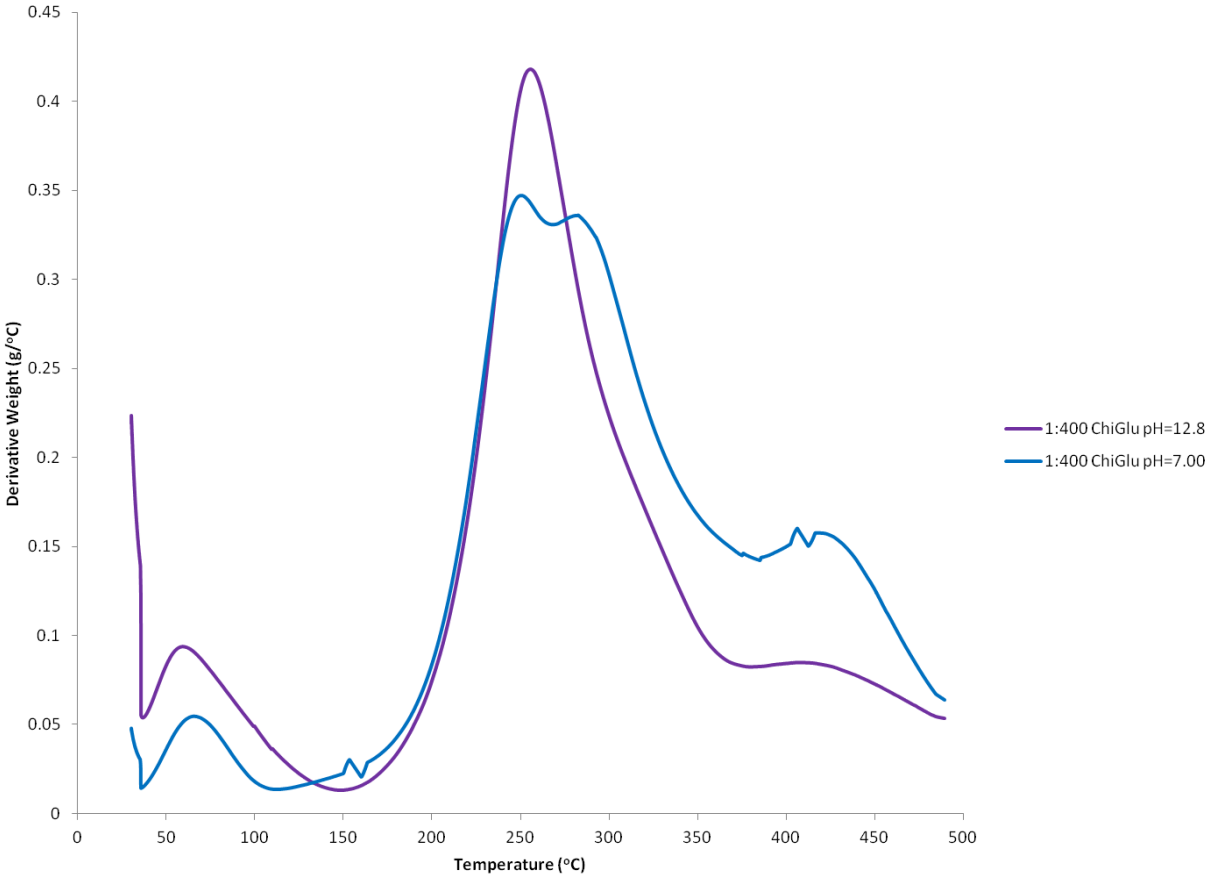

Figure 4.17 DTG of 1:400 Chi-Glu precipitated at pH 7.0 and 12.8

4.4.5 Crystalline Structures

From Figure 4.18, the DTG of both the powder form and the crystalline form share similar profiles which means in terms of the overall composition of the copolymer and cross-linker, they are the same. From the 400^{o}C thermal band the degree of polymerization of glutaraldehyde is identical for both types of material. The difference appears to be the sharp Lorentzian peaks that are exhibited by the crystalline form. The presence of the peaks might be explained by solvent trapped in the crystalline network. As mentioned in Section 4.2.6, the product at high pH polymerized glutaraldehyde quick on the surface than inside the pores. This could lead to relatively non-porous surfaces that can trap water inside the polymeric network. Once pyrolysis occurs for the copolymer at 263^{o}C, 444^{o}C, and 460^{o}C the water is released to temperatures several times higher than the boiling point leading to weight loss events, as observed.

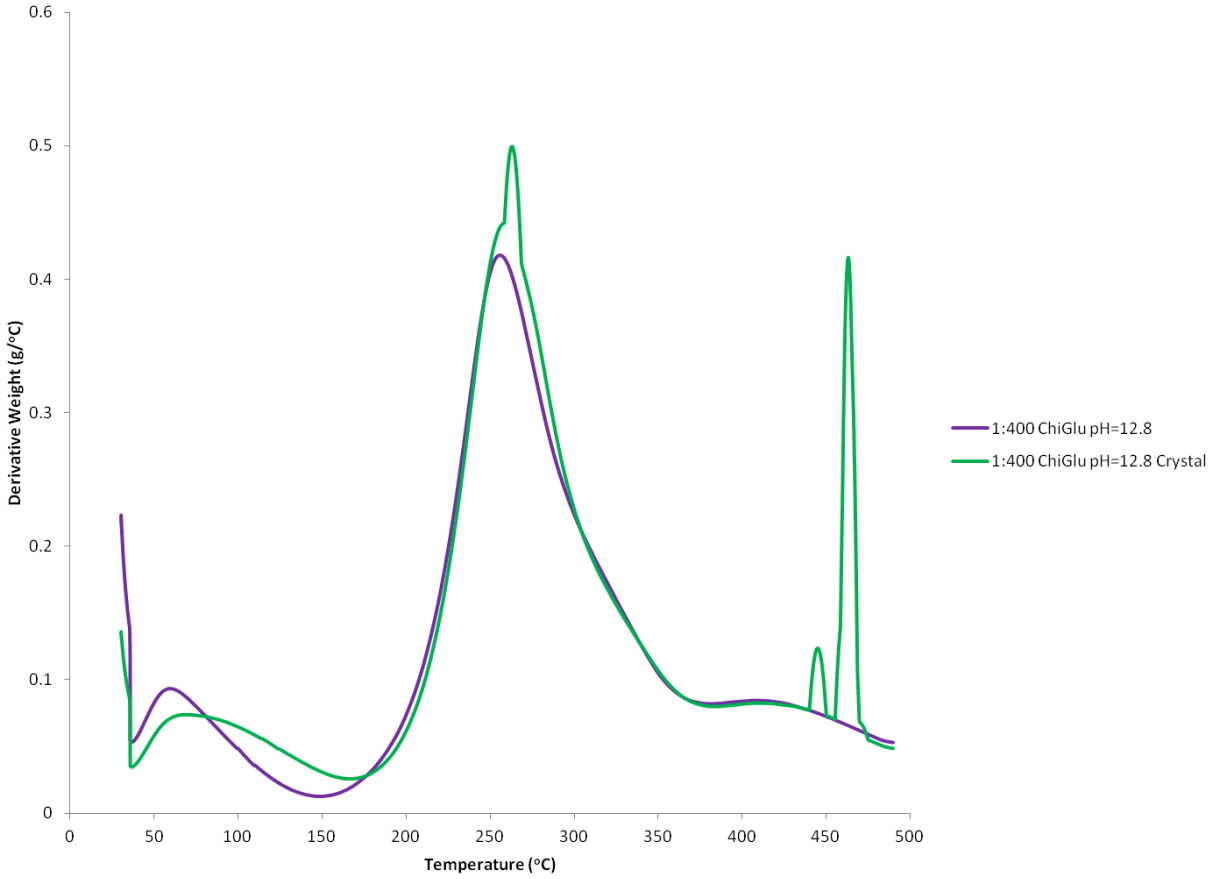

Figure 4.18 DTG of 1:400 Chi-Glu precipitated at pH 12.8 and 298 K with different morphologies: A powder form and a crystalline form.

4.5 CHN Analysis

Similar to TGA, elemental analysis or CHN analysis does not provide information on specific functional groups but rather on the relative composition of the copolymer on the whole. CHN analysis, unlike thermal analysis, provides a simple qualitative measurement of cross-linking content. As more glutaraldehyde cross-links onto chitosan, the percent by mass for carbon would increase. Secondly, since no nitrogen is lost, the percent composition of nitrogen decreases as the cross-linking of glutaraldehyde increases. This can be seen in the copolymers where the percent by mass of carbon increases from 44.4% for 1:400 Chi-Glu to 45.1% for 1:1000 Chi-Glu while nitrogen content decrease from 5.44% to 4.59%.

4.5.1 Theoretical Model

Table 4.4 Experimental Mass percent values obtained from elemental analysis. All mass percent values, except for chitosan, were adjusted for residual water content.

	Chitosan			1:400 Chi-Glu	1:400 Chi-Glu pH 12.8	1:700 Chi-Glu	1:700 Chi-Glu T = 333 K	1:1000 Chi-Glu
	Experimental	Theoretical	Percent Error					
%C	41.6	42.6	2.4	44.4	39.2	46.9	45.8	45.1
%H	7.46	7.05	5.5	6.97	6.58	6.71	6.70	6.68
%N	7.67	7.85	2.4	5.44	5.66	4.20	4.57	4.59
%O*	43.3	42.5	1.8	40.6	42.7	37.9	38.6	38.8

*Calculated by summing the percentages for C, H, and N and subtracting by 100%.

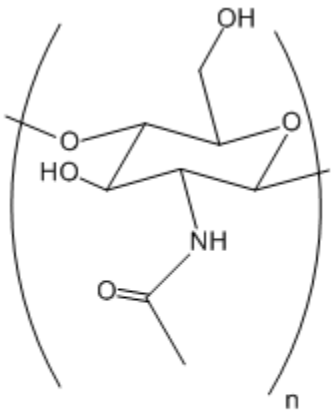

2-acetamido-2-deoxy-b-D-glucopyranose
(Amide)
$C_8H_{13}O_5N$

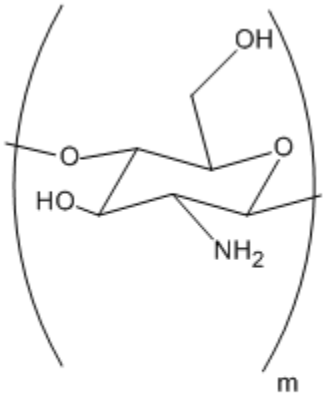

2-amino-2-deoxy-b-D-glucopyranose
(Amine)
$C_6H_{11}O_4N$

Scheme 4.6 The molecular structure of chitosan where all the monomers are assumed to have formed a glycosidic bond and terminal monomers are not included in the calculations

A theoretical calculation for the elemental composition of the copolymers requires several assumptions: known average molar mass (120,000 g/mol), known percent deacetylation (80%), residual water is solely from chitosan, and few terminal monomers. Without size exclusion chromatography data, the first assumption cannot be verified. Residual water

assumption is verified using the TGA. By integrating the thermal events around 100^{o}C, the water content of the polymer can be estimated. The last assumption is based on two physical properties of chitosan: Chitosan is a linear copolymer with many monomers units depending on the degree of polymerization. Each chain can contain n number of monomers that link together but only two of them will be terminal. If n is large then the two terminal monomers become negligible and the chitosan amine and amide monomers can be assumed to have the chemical formula shown in Scheme 4.6 adjusted for glycoside bonds.

From the results seen in Table 4.4, the assumptions appear to be valid with the largest percent error seen for hydrogen at 5.5%. If water content is increased to be closer to 8% (5.78% from TGA) this value will generate a percent composition of 41.6%, 7.15%, and 7.67% for C, H, and N, respectively (See appendix for full calculation). These values are accurate and close to the experimental value where the percent error between them decrease to 0.01%, 4.2%, and 0.02% for %C, %H, and %N, respectively. As only the %H has the largest error, instrumental error involving the measurement of water vapor and the polydisperse nature of the molecular weight for chitosan are contributing factors. Trace amounts of water vapor from the air could have been introduced to the instrument and measured by the thermal conductivity detector. This could account for the increased water content. Even after considering elevated water content, the hydrogen content is underestimated. This is expected because the model neglects terminal monomers. Terminal monomers only form one glycoside bond while the other forms two resulting in an underestimation of the amount of hydrogen and oxygen content. Therefore, the terminal hydrogen and oxygen atoms have not been considered. This is a significant problem if the molecular weight of chitosan is widely dispersed. But since the percent error is less than 5%, the model can still be used to give a good agreement with the experimental determined composition.

4.5.2 Estimation on the number of monomers in chitosan

The CHN mass or composition percentages listed in Table 4.6 can be used to derive an empirical formula. As the number of nitrogen remains constant throughout the reaction, it is possible to derive a molecular formula of the Chi-Glu copolymer. This, of course, assumes that the number of nitrogen is known beforehand. The sole source of nitrogen is the chitosan molecule and there is always one nitrogen atom per monomer. Therefore, if the total number of

chitosan monomers is found then the total nitrogen content can be calculated. Using the same assumptions from the model, the total number of monomers is 714 where 596 are the amine monomer and 118 are amide monomers. Therefore, there are 714 nitrogen atoms in chitosan and all the Chi-Glu molecular formula will contain that amount of nitrogen.

4.5.3 Experimental mole ratio estimation

The key to calculating mole ratio for Chi-Glu copolymers is that the total number of nitrogen remains constant throughout the reaction. Therefore, if chitosan has 714 nitrogen atoms, then the Chi-Glu copolymer should also have 714 nitrogen atoms. Using this fact, it allows for the derivation of the monomeric atomic composition from the empirical formula (*cf.* Table 4.5). By simply multiplying the empirical formula with the number of nitrogen atoms in chitosan the total atomic composition contributed by all the glutaraldehyde molecules bound to one chitosan can be found; Hence, monomeric atomic composition.

Table 4.5 Calculated empirical formulas (EF) and monomeric atomic composition (MAC) are listed below.

	Chitosan	1:400 Chi-Glu		1:400 Chi-Glu pH12.8		1:700 Chi-Glu		1:700 Chi-Glu T=333 K		1:1000 Chi-Glu	
	MAC.	EF.	MAC.	EF	MAC	EF.	MAC.	EF.	MAC	EF	MAC
C	4520	9.51	6787	8.07	5763	13.0	9290	11.7	8335	11.5	8181
H	8089	17.8	12711	16.2	11542	22.2	15846	20.4	14553	20.2	14453
N	**714**	**1**	**714**	**1**	**714**	**1**	**714**	**1**	**714**	**1**	**714**
O	2974	6.53	4664	6.62	4725	7.91	5645	7.40	5282	7.42	5295

Calculating the experiment mole ratio now is a simple matter of eliminating the quantity of atoms contributed by chitosan. Any remainder must belong solely to glutaraldehyde and by applying Equation 4.2; the number of glutaraldehyde can be elucidated. This equation is a variation on a similar one proposed by Ma et al. (*120*) where n_{Glu} is the number of glutaraldehyde molecules cross-linked. C_{CG} is the total number of carbon atoms in the Chi-Glu copolymer. C_{Chi} is the total number of carbon atoms in chitosan. Both C_{Chi} and C_{CG} can be found in the molecular

atomic composition of the copolymers in Table 4.6. The last term, C_G, is the number of carbon atoms in a single glutaraldehyde.

$$n_{Glu} = C_{CG} - C_{Chi}/C_G \quad (4.2)$$

$$\delta n_{Glu} = |\delta C_{CG}/C_G| + |\delta C_{Chi}/C_G| \quad (4.3)$$

$$\delta C_{CG} = \delta n_N C_{EM} + \delta C_{EM} n_N \approx \delta n_N C_{EM} \quad (4.4)$$

Eqn. 4.2 requires only the knowledge of the quantity of nitrogen and one other atom. Because there is no carbon bond cleavage during the reaction, the number of carbon atoms added by one molecule of glutaraldehyde is always five. Note that both hydrogen and oxygen could be used but are more imprecise because of two competing factors: dehydration of alcohols causes water loss while hydrolysis of the imine increases the water content. Both these factors will affect the hydrogen and oxygen atom equivalent of C_G and C_{CG}. The error is calculated assuming maximum possible uncertainty (*cf.* Eqn 4.3) as all the results are from the same instrument and contains the same error (the uncertainty for nitrogen atoms). δC_{CG} was calculated by considering errors in determining the number of nitrogen atoms in chitosan and the error in determining the empirical formula (*cf.* Eqn 4.4). The latter had a very small error (±0.0003) and was discarded. Error for the number of nitrogen atoms was determined through the deacetylation range that the manufacturer provided for chitosan (75-85%). What was found was that at 75% deacetylation the total number of nitrogen was 706 while at 85% it was 722. The average number of nitrogen at 714 (80% deacetylation) is used and a discrepancy of 8 nitrogen atoms occurs from this value. There is a maximum discrepancy of 8 nitrogen atoms (δn_N) from the average, and when multiplied by the number of carbons in the empirical formula, δC_{CG} is obtained. The error for chitosan (δC_{Chi}) was determined the same way and the result was a discrepancy of 14 carbon atoms. Number of carbons in a single glutaraldehyde remains constant so there is no error included for it ($\delta C_G = 0$).

Table 4.6 Calculated number of glutaraldehyde molecules bound to one chitosan molecule.

Copolymer	Experimental	Theoretical	Percent Error
1:400 Chi-Glu	454 ± 79	400	14
1:400 Chi-Glu pH 12.8	249 ± 67	400	38
1:700 Chi-Glu	954 ± 107	700	36
1:700 Chi-Glu T = 333 K	763 ± 96	700	9
1:1000 Chi-Glu	732 ± 95	1000	27

The estimation showed good agreement in two out of the five copolymers (percent error: 9-14%) but unfortunately only those same 2 out of the 5 experimental values agree within the theoretical value within the error range. One major and likeliest source of error is inaccurate measurement of the glutaraldehyde solution. The syringe used can only measure volume to an accuracy of ±0.1ml. This translates into an extra ±30 glutaraldehyde molecules. For both 1:700 and 1:1000 Chi-Glu, the error range is still not large enough to overlap with the theoretical value.

One interesting result is the confirmation of the lack of cross-linking seen for 1:400 Chi-Glu at high pH. The sample submitted for CHN analysis was the light orange powder and contained minimal amounts of the crystalline sample. This ratio is similar to the Chi-Glu copolymers obtained by Wilson and Xue (*68*). The color and texture of the copolymer also resembles their final product. Secondly, CHN analysis also offers evidence of polymerization of glutaraldehyde. As calculated in section 4.4.2, the total number of chitosan monomers with a free amine is 596. If two amines are consumed for every one glutaraldehyde cross-linked then the total number of glutaraldehyde that can be cross-linked to the amine is 298. Therefore, the CHN results should resemble 1:400 Chi-Glu at pH 12.8. Assuming the experimental mole ratio is correct, 4 out of 5 copolymers contain double to triple that number. And from the FT-IR results,

there is still a small absorption band at 2259cm^{-1} for the copolymers suggesting that there are free unbound ammonium ions. Only polymerization of the glutaraldehyde molecules can explain the large number of glutaraldehyde in the copolymers. According to the CHN analysis, 1:700 Chi-Glu has the most glutaraldehyde and should also have the most glutaraldehyde polymerized. This is followed by 1:1000 Chi-Glu, and 1:400 Chi-Glu with the least. This trend agrees with the thermal event at 400^{o}C seen on the TGA (*cf.* Figure 4.14).

4.6 Water swelling properties

Trung et al. (*83*) noted in their article that the removal of water using an oven partially restores the degree of crystallinity in chitosan which is an important factor in the diffusion of Millipore water into the pores. This means that swelling properties should either be measured in copolymers that never went through oven drying or if dried, left in solutions for a long time. Both procedures were done with Table 4.7 containing results from copolymers that were purified with water via Soxhlet extraction but were never oven dried and Table 4.8 contains results from copolymers that were dried for 48h in a vacuum oven. Both sets of samples were submerged in water for 48h and air dried. Masses were recorded when droplets of water were no longer in the pre-weighed filter papers and vials.

Table 4.7 Swelling data from copolymers before drying *in vacuo* were obtained. Polymers were precipitated at pH 7.0 and 298 K unless specified

Copolymer	**Mass of Dried Copolymer**	**Mass of Swelled Copolymer**	**% Swelling (x 10^{3})**
1:400 ChiGlu	0.0225	0.1985	7.70
1:400 ChiGlu at pH 12.8	0.0152	0.1522	9.01
1:700 ChiGlu	0.0097	0.3118	31.1
1:700 ChiGlu at T =	0.0178	0.3383	18.0
1:1000 ChiGlu	0.0188	0.3512	17.7

The swelling data verifies the results from Trung et al. (*83*) in that the oven drying contributes to crystallinity in the polymer. The 1:700 copolymers have the highest sorption capacity and the greatest degree of swelling but when oven dried, had the largest drop in

swelling percentage. The 1:700 Chi-Glu decreased by a factor of ten while 1:700 Chi-Glu at T=333 K decreased by a factor of seven. A comparison of the decrease in swelling and the trends in thermal events, according to TGA, and the CHN analysis reveals a correlation. Decreased swelling is observed for copolymers with greater content of glutaraldehyde. This is likely caused by measuring the swelling percentage when equilibrium had not been reached. Intra-particle diffusion of water is controlled by the degree of crystallinity (*59, 118*). When the polymer was fully hydrated, the crystallinity was kept at a minimum due competition for hydrogen bonding amine sites with solvent. Therefore, the value that is recorded in Table 4.7 should reflect the swelling of the copolymers with minimal crystallinity. Once the copolymers were oven dried, crystalline character of the copolymers is restored as evidenced by the TGA results. Therefore, the equilibrium time for the oven dried is much longer than the fully hydrated samples. This has consequences for sorption because if Chi-Glu copolymer is to be applied for adsorption of pollutants then the dried powder should be submerged for at least 48h in the aqueous solution.

Table 4.8 Swelling Data from Copolymers after drying in a vacuum oven were obtained. Polymers were precipitated at pH 7.0 and 298 K unless specified

Copolymer	**Mass of Dried Copolymer (g)**	**Mass of Swelled Copolymer (g)**	**% Swelling (x 10^3)**	**Factor of decrease in swelling due to drying***
Chitosan	0.05036	0.17036	0.238	NA
1:400 ChiGlu	0.05063	0.23485	0.364	2.1
1:400 ChiGlu at pH 12.8	0.05007	0.34337	0.586	1.5
1:700 ChiGlu	0.04928	0.20117	0.308	10.1
1:700 ChiGlu at T = 333 K	0.04934	0.18190	0.269	6.7
1:1000 ChiGlu	0.04974	0.28639	0.476	3.8

*Calculated by taking the % swelling in Table 4.7 and dividing it by the above % Swelling for their respective copolymers

Another correlation that is of note is that the experimental mole ratio appears to agree with the swelling ratios with the exception of the 1:400 Chi-Glu at high pH. From the data in Table 4.7, increased cross-linking does not decrease the swelling ratio as Ngah and Fatinathan (*53*) have reported. Crini and Badot (*59*) have suggested that low levels of cross-linking with glutaraldehyde disrupt hydrogen bonding between chitosan molecules such that an increase in swelling has been observed (*59*).

CHAPTER 5

RESULTS AND DISCUSSION: β-CD – PNP SORPTION STUDY

5.1 Nitrogen Sorption: Porosimetry

Sorption studies of granular activated carbon (GAC) and its analogues such as carbon black (*41, 81,114,121-125*) with various sorbates are well documented. de Boer et al. (*126*) theorized that sorption occurs inside the pore before saturating the external surface, which allows for characterization of the pore structure. One method is to use the BET equation combined with the sorption and desorption isotherms of nitrogen. Using this data, it is possible to estimate the pore width (*121*), pore volume distribution (*121*), micropore specific surface area (*126*), and external surface area (*126*).

5.1.1 N_2 Sorption isotherms for GAC and β-CD based copolymers

As seen in Figure 5.1, the adsorption isotherm for GAC is a high-affinity isotherm in agreement with literature (*81,121,122*). The relatively high affinity is due to the nature of the pores in GAC. In Table 5.1, much of the specific surface area (SSA) in GAC is due to the micropores (S_{Mic} = 641 m^2/g), and narrow pores provide strong sorbent-sorbate interactions (*82*). Another property of interest is the gradual increase of the adsorption isotherm from a relative pressure of 0.2 (Point B) where a monolayer of N_2 gas is formed to 0.8 where the exponential increase occurs. According to Brunauer (*127*), this gradual increase is due capillary condensation and the rate of the condensation is dependent on the shape of the pore. From the shape of the hysteresis loop, an H4 type plot is observed and attributed to narrow slit-like pores (*34*).

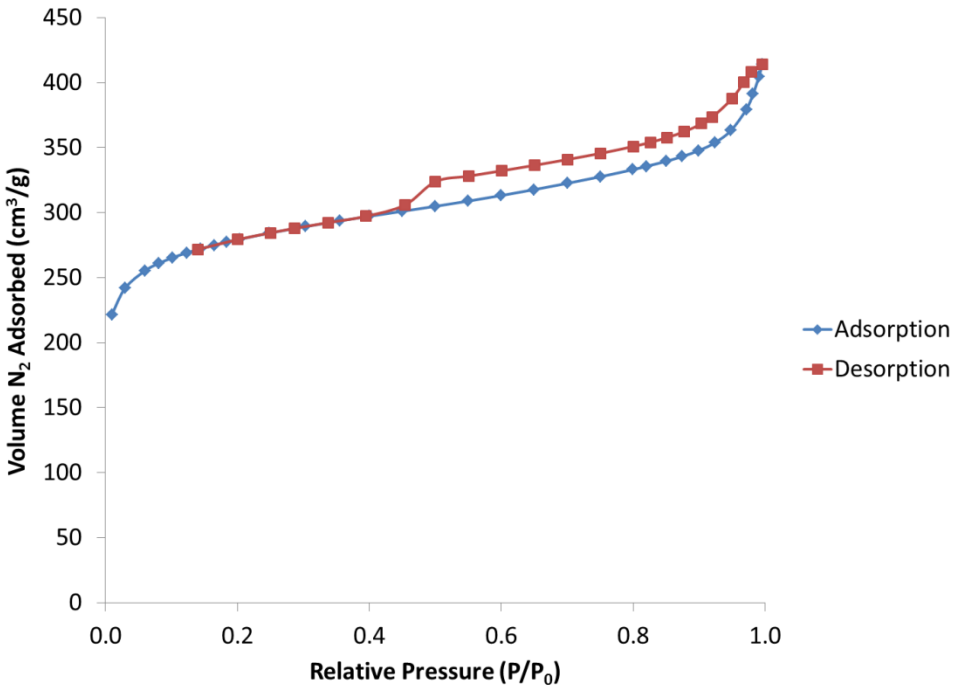

Figure 5.1 N_2 Sorption/Desorption Isotherm with GAC is shown (*35*). Data is with permission from reference (*35*).

A comparison of the GAC sorption isotherm with the cyclodextrin copolymers (*cf.* Figure 5.2 and 5.3) reveals several differences: the relatively low sorption capacity of the cyclodextrin copolymers, and the abrupt increase to saturation from a relative pressure of 0.9. The shape of the adsorption isotherm and the appearance of a hysteresis loop is likely a type I isotherm and indicates minimal micropore contributions. It should be noted that at a relative pressure of 0.2, a local maxima can be detected in the sorption isotherms for 1:9 SCl and 1:9 TCl copolymers. This is due to a significant presence of water. As noted in literature (*33*), solution-based adsorption is governed by the activity of the solvent and solute. In this case, since there is a large amount of water even after purging, water concentration is likely large enough that it competes with nitrogen gas and the sorption isotherm is distorted accordingly (*33*).

Table 5.1 Sorption isotherm data and extrapolation of pore properties at 77 K.

Adsorbent	Specific Surface Area (S_{BET}, m^2/g)	External Specific Surface Area* (S_{EXT}, m^2/g)	Micropore Specific Surface Area* (S_{Mic}, m^2/g)
GAC†	951	310	641
1:9 SCl[1]	0.925	0.759	0.166
1:9 TCl[1]	0.496	0.398	0.098

*These values were calculated using the t-curve as described by Lippens et al. (*126*)

† Results are used with permission from reference (*35*)

[1] "1:X cross-linker" refers to the copolymer where 1 mole of β-CD reacted with X moles of the specified cross-linker (see Materials and Methods chapter)

From the sorption isotherm, there is a lack of an initial slope which suggests minimal micropore contribution to sorption. In the BJH pore volume distribution reported in Figure 5.4, a majority of the micropore volume contains a pore width of 9.5Å which is close to the internal diameter of the cyclodextrin cavity of ~ 8 Å (*44*). Secondly, this is followed up by minimal sorption between relative pressures of 0.2 to 0.8. This result suggests minimal sorption even in the mesopore range and the overlap of the desorption isotherm with the sorption isotherm at most relative pressures except near unity. Cyclodextrin copolymers are concluded to be non-porous except for some slit-shaped pores responsible for the hysteresis (*cf.* Figure 5.4). This can be observed in the results listed in Table 5.1 when comparing the specific surface area of cyclodextrin copolymers with GAC. The total specific surface area (S_{BET}) for the β-CD copolymers are several magnitudes lower and therefore, the resulting micropore and external surface SSA were decreased as well. This result agrees with a study by Mohamed et al. (*90*) on polyurethane cyclodextrin copolymers. Mohamed et al. (*90*) reported that the low sorption capacity is due to shrinkage of the polymeric network, an effect similar to gels after the solvent is removed. This can be rationalized when considering the structure of β-CD copolymers seen in Scheme 3.1. Much of the exterior β-CD cavity contains potential hydrogen bonding sites or polar groups from the ester linkages. Therefore, the polar functional groups are unlikely to provide favourable sorption sites for the non-polar nitrogen gas. Which means the nitrogen gas cannot

swell the copolymer like water and accessibility to the interior of the copolymer is restricted. The occurrence of swellability limits the accuracy of adsorption data obtained from nitrogen porosimetry as one requirement for pore analysis is that the pore structure must be rigid (*34*). Therefore, a dye-based method involving the sorption isotherms was used in place of nitrogen porosimetry to estimate the specific surface area.

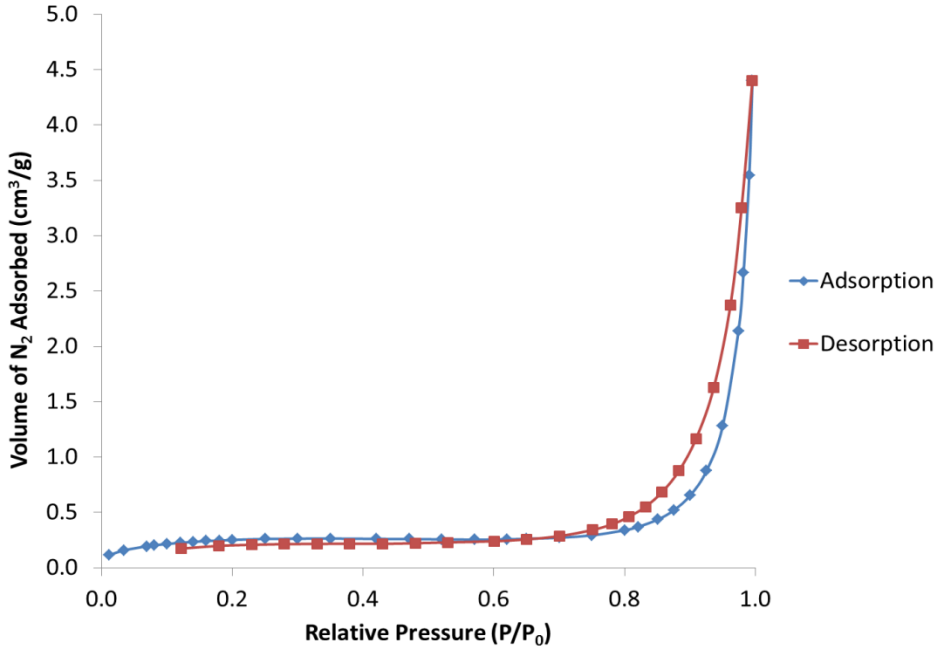

Figure 5.2 N_2 Sorption/Desorption Isotherm with 1:9 SCl is shown.

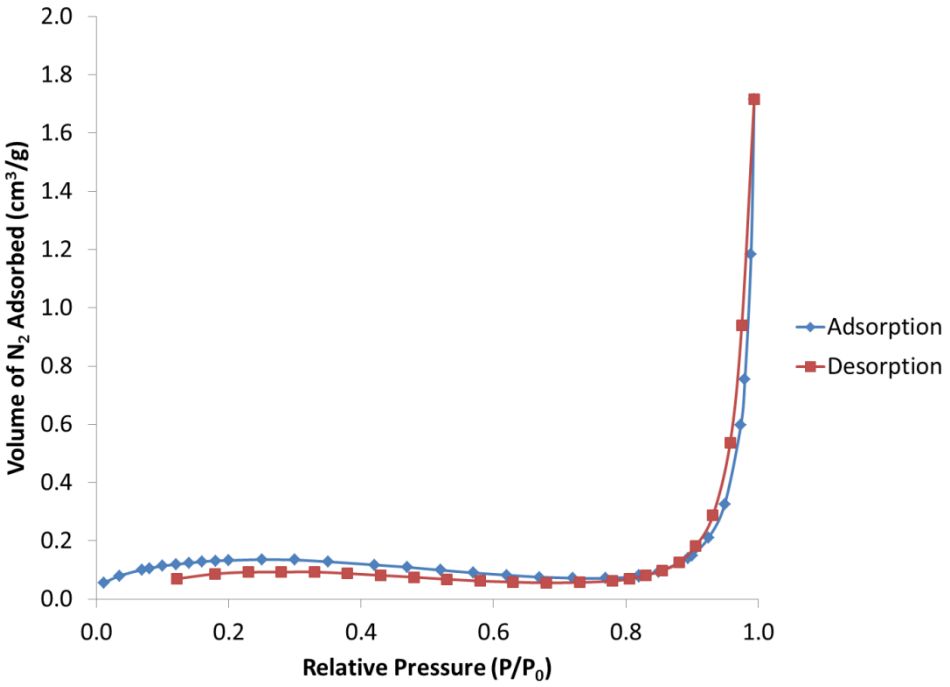

Figure 5.3 N_2 Sorption/Desorption Isotherm with 1:9 TCl is shown.

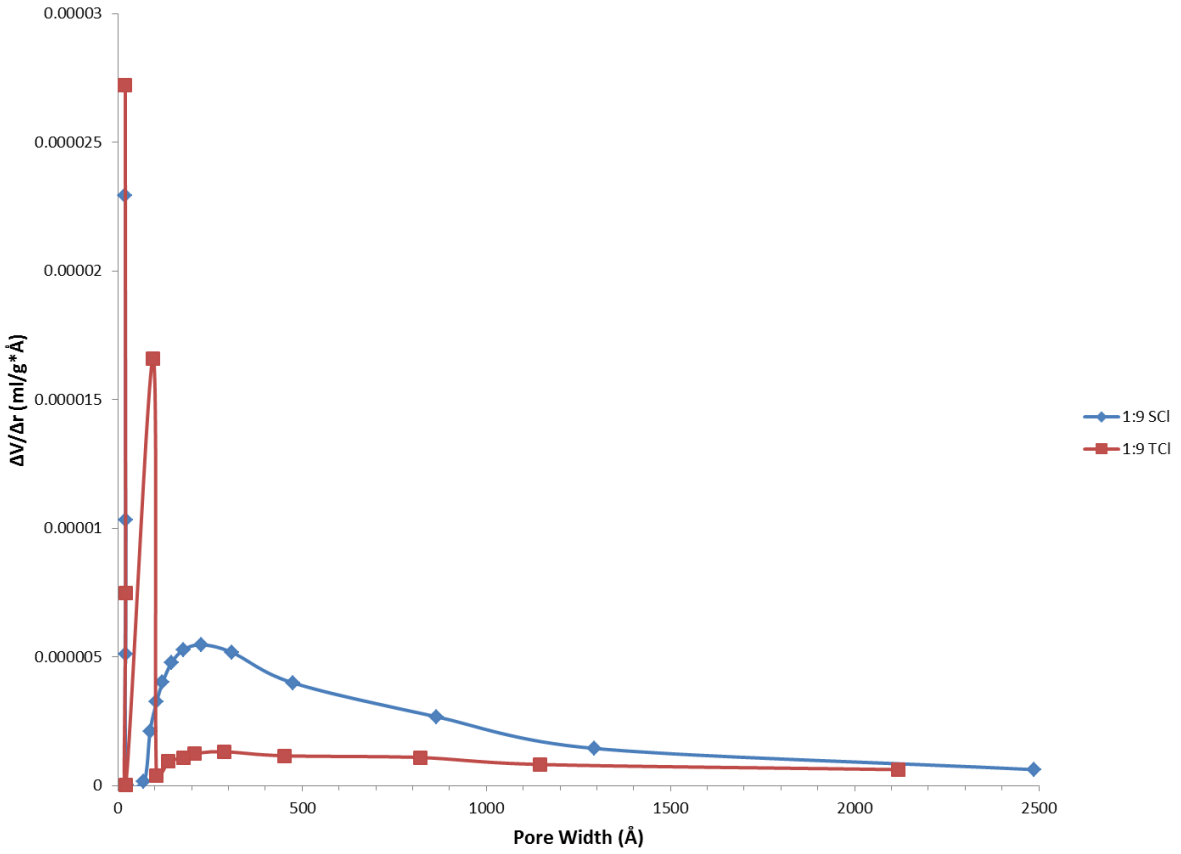

Figure 5.4 BJH Pore volume distribution of the cyclodextrin copolymers is shown.

5.2 Sorption of *p*-Nitrophenol (PNP)

Solubility was measured at pH 9.0 and pH 4.6, respectively. Each sorption isotherm for the copolymers was duplicated and every point on the graph was duplicated 2-4 times to precisions within 5% by difference. GAC was not duplicated but the sorption isotherm was comparable to literature (*87*). The copolymers that did not hydrolyze at pH 4.6 were the 1:6 TCl, 1:9 SCl, and 1:9 TCl materials. All copolymers undergo hydrolysis at pH 9.0; whereas, the hydrolysis of 1:9 TCl and 1:9 SCl copolymers was attenuated. 1:6 SCl copolymers undergoes partial hydrolysis at pH 4.6 since most of the copolymer remains after several days of mixing enabling evaluation of the sorption properties with PNP in aqueous solution at pH 4.6. Unfortunately, the large quantity of copolymer undergoing hydrolysis of the ester linkages renders the sorption isotherm for 1:6 SCl unreliable. Figure 5.5 illustrates the sorption isotherms of various copolymers with PNP at 295 K. According to Figure 5.5, the equilibrium dye concentration (C_e) increases until saturation of the sorption sites is reached. As the mole content

of the linker increases, the sorption capacity of the copolymer increases, as noted with other copolymer materials containing β-CD (*41*).

5.2.1 Sorption Capacity of SCl- and TCl-based Copolymers

A comparison of the sorption capacity of the three polymers with GAC (Q_m = 2.70 mmol/g) illustrates important differences in their sorption properties (*cf.* Table 7). The 1:9 SCl copolymers has a sorption capacity (11.1 mmol/g) that exceeds activated carbon. The 1:6 TCl (2.23 mmol/g) and 1:9 TCl (3.06 mmol/g) copolymer shows comparable sorption relative to GAC. The average monolayer sorption capacity (Q_m) of polyurethane/β-CD copolymers (1.0 mmol/g) (*86*) and epichlorohydrin/β-CD copolymers (0.5mmol/g) (*70*) are lower than the reported Q_m values for the polyesters reported herein.

The sorption isotherms for GAC, 1:6 TCl, and 1:9 TCl are considered more reliable than the results for the 1:9 SCl copolymer due to their relative insolubility and resistance to hydrolysis. A type IV isotherm is seen for 1:9 SCl (*cf.* Figure 8) where a plateau occurs ~ C_e = 5-10mM. For the 1:6 and 1:9 TCl copolymers, the isotherm follows a type I adsorption profile characteristic of microporous materials. The difference between the two types of sorption may be due to the relative size effects and conformational behaviour of the SCl and TCl linker units. The cross-linker chain of SCl may undergo variable conformations from a *coiled*- to an *all-trans* form, affecting the relative accessibility of the β-CD sorption sites (*90, 128*). Variable conformation effects are reduced for the rigid aromatic TCl linker and are anticipated to affect accessibility of the β-CD inclusion sites to a lesser degree. The potential coiling of the SCl linkers is anticipated to reduce the framework access of SCl relative to TCl copolymers. Lastly, the sigmoidal character of the isotherms for the 1:6 SCl and TCl are due to attenuated hydrolysis, as previously reported in literature (*128*).

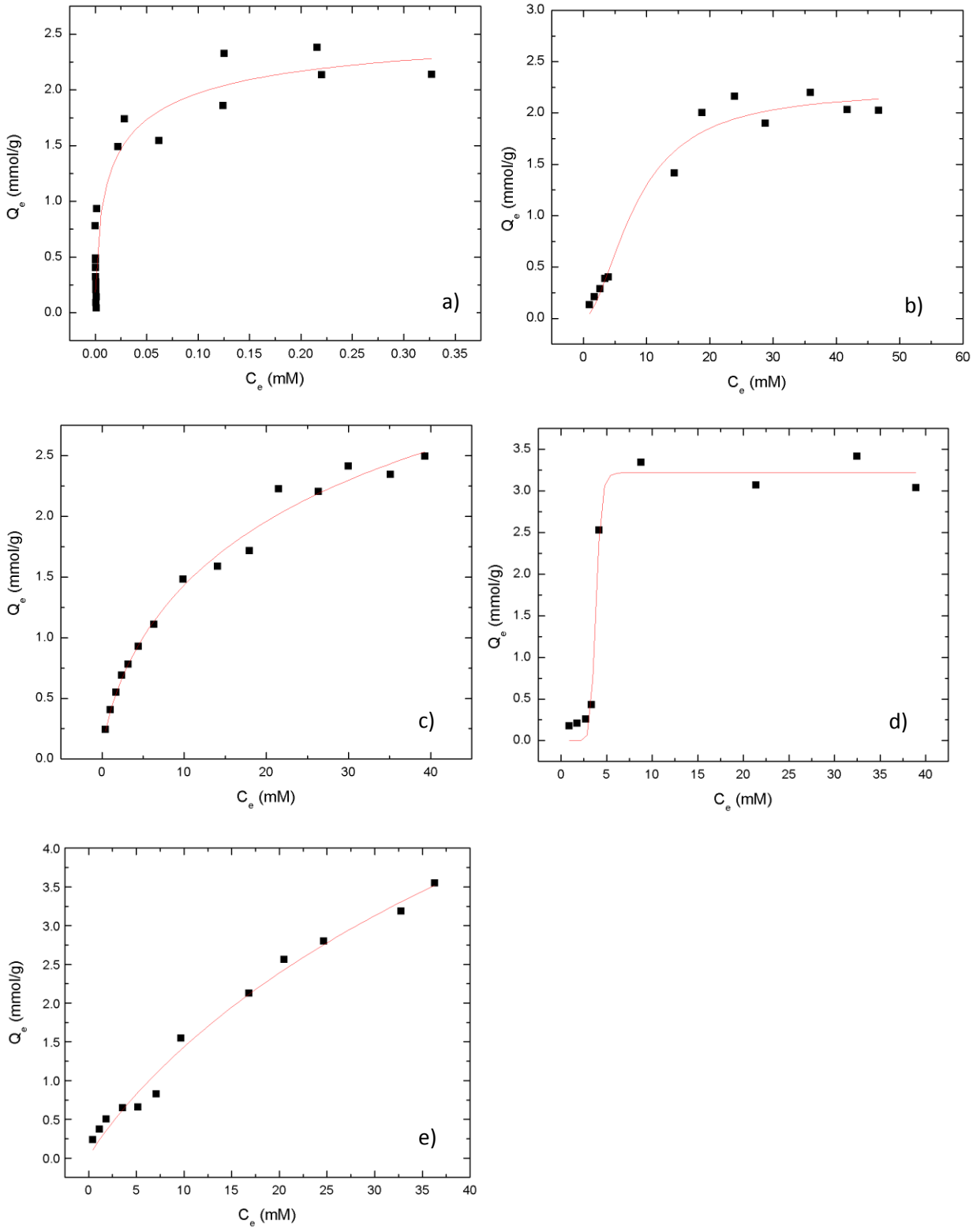

Figure 5.5 PNP sorption isotherms at 298 K and pH 4.6 with: a) GAC; b) 1:6 TCl; c) 1:9 TCl; d) 1:6 SCl; and e) 1:9 SCl.

Table 5.2 Sorption Isotherm results calculated from the Sips' isotherm model. Isotherms were obtained at ambient temperature (295 K) and pH 4.6.

Adsorbent	Q_m (mmol/g)	K_s	n	R^2	RMSE
GAC	2.70	10.6	0.592	0.901	0.472
1:6 SCl	3.22	2.19×10^{-8}	13.2	0.987	0.163
1:9 SCl	11.1	0.0195	0.885	0.986	1.11
1:6 TCl	2.23	0.0146	1.78	0.977	0.871
1:9 TCl	5.16	0.0821	0.671	0.988	0.763

Wilson and Guo (*128*) recently published a novel synthesis and characterization of β-CD microspheres using SCl and TCl as linkers at similar ratios. They determined the sorption capacity for the SCl copolymers ranges from 0.221-0.352 mmol/g where the lowest sorption capacity was associated with the lower linker ratio of SCl-1 and the highest sorption capacity with a greater linker ratio such as SCl-10. For the TCl copolymers, the sorption capacity appears to be independent of the linker ratio. Sorption isotherms obtained for TCl-1, TCl-5, and TCl-10 resulted in variable sorption capacity: 0.245 mmol/g, 0.263 mmol/g, and 0.248 mmol/g, respectively. These values are smaller by several magnitudes when compared with the SCl and TCl copolymers reported here even though the SCl and TCl copolymers both contain relatively similar mole ratios. One explanation involves the morphology of the copolymers. Wilson and Guo (*128*) synthesized the SCl and TCl copolymers through an emulsion-based technique and generated microspheres while the current batch of SCl and TCl copolymers are synthesized using a conventional organic solvent a gelation technique. As the current batch of SCl and TCl copolymers undergoes gelation before precipitation it is highly likely that the cyclodextrin polymers prepared are collapsed xerogels and this has consequences to the swellability of the copolymer and ultimately, the accessibility to sorption sites. For example: the SCl and TCl copolymers of Wilson and Guo (*128*) are microspheres while the current batch of SCl and TCl copolymers are collapsed xerogels. When solvent is introduced to the collapsed xerogels the copolymer swells and for microspheres the same occurs but at a lower rates. Therefore,

mechanical rigidity of the microsphere framework is predicted and supported by literature (*53*). The swelling behaviour for Chi-Glu beads (33%) reported by Ngah and Fatinathan (*53*) is lower compared with swollen Chi-Glu powders (700-3100%, see Table 4.10) obtained from gelation. Mechanical rigidity of microspheres and can account for the lower sorption capacity as accessibility to sorption sites is attenuated compared to the 1:9 TCl copolymers.

5.2.2 Degree of Heterogeneity

The Sips model parameters (*cf*. Table 5.2) provide estimates of the relative distribution of heterogeneous sorption sites as a function of adsorption energies through the n-values. As the value of n approaches unity, the distribution of the sorption sites is narrowed and the energy of all the adsorption sites become more uniform, and relate to the maximum adsorption which represent the fully accessible β-CD sites. Therefore, the accessibility to the β-CD sites decreases as the n-parameter decreases. 1:9 SCl has a value of n=0.885 that is greater relative to 1:9 TCl (n=0.671). The propensity of 1:9 SCl to undergo substantive conformational change and solvent-mediated swelling may contribute to variable accessibility of the sorption sites of the copolymer framework upon hydration. A comparison of the Sips isotherm parameter (n) for the 1:9 SCl and 1:9 TCl copolymers with GAC indicates that the pores of the latter sorbent are not readily accessible (*122*), and display unfavorable energy of adsorption relative to the copolymer. This may be related to inaccessible micropores (*122*), the non-swelling characteristics, and apolar nature of the carbonaceous framework of GAC.

A second factor that affects the n-parameter is surface functional groups. As Kwon (*35*) has noted, GAC has multiple surface functional groups that can range from alcohols to ketenes to carboxylic acids. Each functional group will have a different heat of adsorption, and therefore, a wide distribution of sorption sites will be obtained as n approaches 0 (*125*). This is also true for the TCl copolymers where the n-parameter is generally lower for TCl when compared with the SCl copolymers. For SCl-based copolymers the main sorption site is for the PNP to be adsorbed into the β-CD cavity through a host-guest sorption process. From NOESY studies by Wilson and Guo (*128*), there was no perceptible nuclear Overhauser effect (NOE) correlation seen between the methylene groups on the SCl linker. However, NOE correlation has been observed between PNP and TCl linkers. Wilson and Guo (*128*) hypothesized that π-π interactions between the aromatic rings on the PNP and TCl linkers were responsible for the adsorption in the interstitial

domains (i.e. non-inclusion sites). Therefore, adsorption at the interstitial domains between the TCl linker and PNP can also account for the lowering of the n-parameter.

The Sips isotherm assumes monolayer sorption where only a finite number of sorption sites are available (*39*). If multilayer sorption occurs (*i.e*. n>1), similar to a BET model, the number of sorption sites are not finite since every adsorbed molecule forms a potentially new sorption site. Overall, it appears that monolayer sorption occurs for 1:9 TCl and 1:9 SCl within the limits of experimental error. The observed deviations between the Sips model and experimental Q_m value for the 1:6 TCl copolymer may arise from errors in C_e due to hydrolysis of the ester linkages. The occurrence of hydrolysis of the copolymer will contribute to negative errors in Q_e (*128*). However, the sorption properties of copolymers with greater linker content have lower solubility and attenuated hydrolysis as described previously (*90, 128*).

5.2.3 Equilibrium Constant

K_s is the equilibrium constant for heterogeneous adsorption process (*cf*. Scheme 1.3) where a large K_s value means adsorption is favored. From Table 5.2, GAC has the largest K_s value while the values for the copolymers are highest for the TCl-copolymers. This is not surprising as high-affinity adsorption with PNP has also been shown in literature with GAC (*129*). As noted before the high affinity nature of the sorption isotherm is due to the large contribution of the micropores of GAC in the sorption of PNP. The interesting result is the comparison between the 1:9 CD copolymers containing TCl and SCl. The magnitude of K_s is larger for 1:9 TCl but the n-value is higher for 1:9 SCl. K_s is related to the Gibbs free energy and a larger K_s value suggests a more favourable Gibbs energy of adsorption. Therefore, the 1:9 TCl copolymer appears to have reduced inclusion site accessibility relative to the 1:9 SCl copolymer with PNP. This has consequence when designing a sorbent material as the choice of linker becomes important. Aromatic linkers attached to β-CD enhance the Gibbs' energy of adsorption and consequently the heat of adsorption as well (*24b*). Aliphatic linkers will increase the accessibility of the copolymers and enhance the overall sorption capacity as noted by the high n-values and Q_m, respectively. This is in agreement with literature (*41, 80*). Lastly, a low K_s value can be beneficial for water remediation. One disadvantage of GAC is the energy intensive approach needed to regenerate the adsorbent. This is reflected in the high K_s value where the dyes are bound tightly in the micropores. Therefore, a copolymer with a high sorption capacity but a K_s of several magnitudes lower is an ideal candidate for desorption.

5.2.4 Dye-based surface area calculations

5.2.4.1 Specific surface area results for GAC

Comparing the specific surface area results in Table 5.3 for GAC with the results obtained with nitrogen porosimetry then it appears that PNP likely lies in a planar orientation on GAC (*cf*. Figure 5.6). On the PNP molecule in Figure 5.7, the axes are defined such that the x-axis intersects the electron donor hydroxyl and the acceptor nitro substituent. The y-axis is defined as orthogonal to the x-axis but still bisects the aromatic ring of PNP. The z-axis is normal to both the x-axis and y-axis.

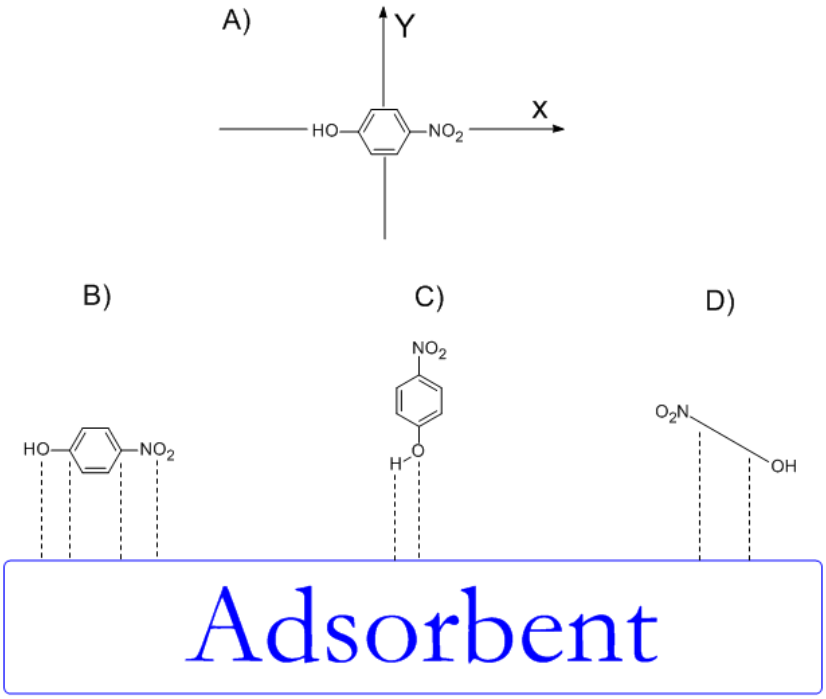

Figure 5.6 Orientation of PNP molecules during sorption is shown above: a) Defined axes on the PNP; b) PNP is co-planar to the adsorbent (XY plane is parallel to sorbent); c) PNP is oriented orthogonally to the sorbent (XY plane intersects the sorbent at a 90^{o} angle); and D) PNP is oriented at an angle (XY plane intersects the sorbent at a 30-60^{o} angle) (*122*).

Therefore, a planar or stacked orientation of PNP means the XY plane is parallel to the surface of activated carbon. At this orientation the main contribution involved with adsorption is the π-π

interaction between the phenyl group of PNP with the graphene structure in GAC (*125, 130*). Hydrogen bonding between the surface oxygen groups in GAC and the hydroxyl groups is another key factor in the adsorption of PNP when it is planar. At low pH, it is likely that the orientation of PNP is in a co-planar orientation.

This result is obtained by comparing the specific surface area calculated at that orientation for PNP (*cf.* Table 5.3) with the specific surface area calculated using nitrogen porosimetry (951 m^2/g). The percent difference between the two values is 10%, which is quite close. Discrepancy between the results is due to the relative availability of micropores for PNP. Haghseresht et al. (*122*) noted the inaccessible fraction of micropores toward larger aromatic sorbates when the total pore volume calculated using a toluene sorption isotherm is smaller than the total pore volume calculated using nitrogen porosimetry. For the orthogonal orientation of PNP, the XY plane of PNP intersects the sorbent surface. In this orientation either the hydroxyl group or the nitro group contributes to adsorption. As noted by Kwon (*35*), it is likely that the nitro group is involved in adsorption to GAC because of favorable ion-dipole interaction between the negatively charged oxygen on PNP with water at higher pH conditions. Secondly, the negatively charged oxygen on PNP would be repulsed through electrostatic interaction by the negatively charged graphene surface of GAC. This is supported by potentiometric titration data obtained by Müller et al. (*131*). Müller et al. (*131*) measured the surface charge of activated carbon at various pH values using potentiometric titration. The point of zero charge was determined to be close to pH 6.5 and the surface potential above that pH were negative in magnitude. Therefore, at pH > 6.5 the overall potential on the surface of activated carbon is negative and would interact unfavourably due to electrostatic repulsion between the oxygen on PNP.

Table 5.3 Specific surface area values obtained using equation 2.8.

Adsorbent	**Q_m (mmol/g)**	**Specific surface area assuming PNP is planar (m^2/g) (x 10^3)**	**Specific surface area assuming PNP is orthogonal (m^2/g) (x 10^3)**
GAC	2.70	0.863	0.411
1:6 SCl	3.22	1.02	0.485
1:9 SCl	11.1	3.51	1.67
1:6 TCl	2.23	0.705	0.336
1:9 TCl	5.16	1.63	0.777

5.2.4.2 Specific surface area results for the SCl and TCl copolymers

The sorption of dyes into cyclodextrins occurs through well-defined host-guest interactions (*114, 128, 132*) therefore the quantitative application of the calculated dye-based specific surface area listed in Table 5.3 should be treated accordingly. Qualitatively, the specific surface area values obtained further support that the copolymers being collapsed xerogels. This can be done by comparing the specific surface area results via dye-based and nitrogen porosimetry from Wilson and Guo with the values obtained herein. For simplicity, comparisons will be done using only 1:9 TCl and TCl-10 (1:9 SCl and SCl-10 can also be used). The specific surface area calculated from nitrogen porosimetry for the TCl-10 copolymers is 20.7 m^2/g while the specific surface area calculated using the dye-based methodology is 37.3 m^2/g (PNP is assumed planar, see Section 5.2.4). For 1:9 TCl copolymers, the specific surface area obtained from nitrogen porosimetry is 0.496 m^2/g and 1631 m^2/g from the dye-based method. When comparing the nitrogen porosimetry results for TCl-10 microspheres from Wilson and Guo (*128*) and 1:9 TCl copolymers from this project, the former has a larger surface area without solvent while the latter has a much higher specific area when solvent is introduced into the network. When solvent is removed the specific surface area of TCl-10 microspheres is reduced by a factor of 3 while the specific surface area for 1:9 TCl copolymers is reduced by a factor of 1500 to 3000 depending on PNP orientation (777-1631 m^2/g from PNP to 0.496 m^2/g from N_2 porosimetry). This demonstrates mechanical rigidity in the framework for TCl-10 microspheres (*128*). Secondly, the range of specific surface area values obtained is consistent with the specific

surface area obtained for xerogels. For example: silicate xerogels have a specific surface area of 515-910 m^2/g (*58e*).

CHAPTER 6

RESULTS AND DISCUSSION: CHITOSAN – PNP SORPTION

6.1 Introduction

As noted in the previous section, cyclodextrin copolymers may hydrolyze at higher pH. Therefore, a more stable material was needed for naphthenic acid (NAs) adsorption. The design of chitosan copolymers cross-linked to glutaraldehyde (Chi-Glu) is a well-known material and has been applied to the adsorption of dyes of various species (*53, 76, 112*). Unlike cyclodextrin copolymers, Chiou et al. (*112*) noted Chi-Glu copolymers sorption occurs mainly through the deacetylated primary amines and ammonium. Ion-dipole and hydrogen bonding interactions are therefore, the primary contributions to the sorption of dyes. This is verified by multiple studies published (*53, 76, 112*). More importantly, Chi-Glu copolymers are resistant to hydrolysis at pH 9.0 which is an ideal pH to simulate OSPW conditions for the sorption of NAs in aquatic environments.

Lastly, as noted in chapter 4 Chi-Glu copolymers were synthesized under various conditions therefore, a review of the names used for the copolymers will be done for clarity. *1:400, 1:700 and 1:1000 Chi-Glu* all followed the synthesis procedure outlined in chapter 2. *1:400 Chi-Glu at pH 12.8* refers to a 1:400 Chi-Glu copolymer that followed the experimental in chapter 2 until precipitation where the supernatant solution of the suspension was at pH 12.8 (*cf.* Section 4.2.5). *1:700 Chi-Glu at T = 333 K* is a 1:700 Chi-Glu copolymer where the solution temperature before gelation was increased to 333 K until 400 ml of water has been driven off and the solution was cooled to allow gelation to occur.

6.2 Nitrogen Sorption: Porosimetry

Nitrogen sorption isotherms recorded in Figure 6.1-6.3 are similar to the soft materials of cyclodextrin copolymers. Both contain total specific surface area many magnitudes lower than the dye-based method of calculating SSA. As shown by Chang et al. (133), unless the Chi-Glu copolymers are kept in the swelled state the values obtained from porosimetry are unreliable and data for S_{Mic} and S_{Ext} are not included for these copolymers. Pristine chitosan and Chi-Glu copolymers sorption isotherms that were obtained are indicative of a non-porous material (*cf.* Table 6.1). This is of course contradicted with surface area calculations in Section 6.5 which supports the conclusion that Chi-Glu copolymers undergo swelling. Because of this collapse of gel structure, the pore volume distributions do not reflect the pore structures in Chi-Glu copolymers during sorption of PNP and NAs. Two plausible methods have been proposed by Brinker and Scherer (*58e*) to remove the solvent without destroying the gel network: freeze drying and supercritical fluids. Freeze drying was attempted by Wilson and Guo (*128*) but the nitrogen adsorption results were consistent with a non-porous gel material similar to that shown by Figures 6.1-6.3. This is not unusual as the process of freeze drying is known to crystallize the dispersed phase that proceeds to grow until it stretches the gel network to the breaking point (*58e*). Only the removal of the solvent using supercritical fluids has been shown to preserve the gel structure (*58e*). This is supported by Chang et al. (*133*) who has synthesized Chi-Glu aerogels. Using supercritical CO_2 to remove solvents from swelled Chi-Glu gels, Chang et al. (*133*) obtained a nitrogen sorption and desorption isotherms and their Chi-Glu aerogels had a specific surface area of 504 m^2/g, and is closer to the specific surface area calculated using the dye-based methodology (*cf.* Table 6.5). The BJH pore volume distribution obtained by Chang et al. (*133*) reveals the Chi-Glu framework is of mesoporous nature with an average BJH pore width of 5 nm.

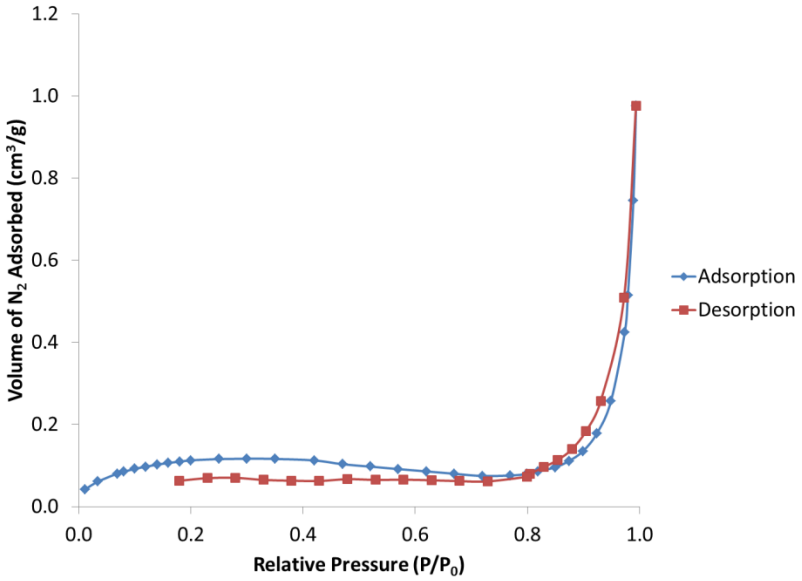

Figure 6.1 Chitosan sorption/desorption profile at 77 K.

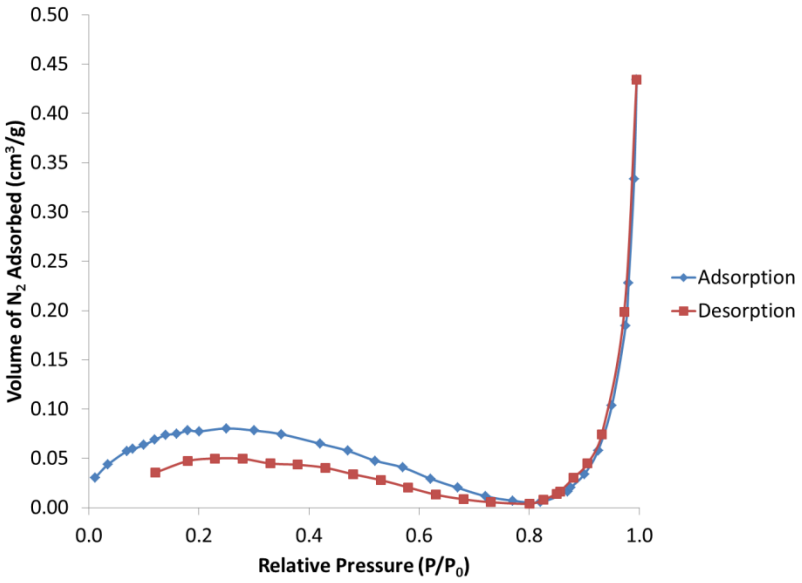

Figure 6.2 1:400 Chi-Glu nitrogen sorption spectra are shown. Nitrogen sorption occurs at 77 K

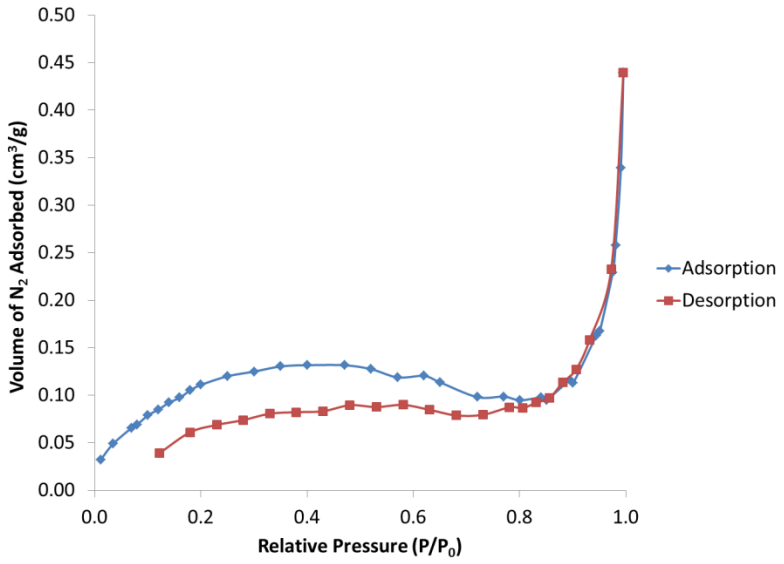

Figure 6.3 1:700 Chi-Glu nitrogen sorption spectra are shown. Nitrogen sorption occurs at 77 K

Table 6.1 Total specific surface area from nitrogen porosimetry data are calculated using the BET equation.

Copolymers	**BET Specific Surface Area (S_{BET}, m^2/g)**
Chitosan	0.433
1:400 Chi-Glu	0.301
1:700 Chi-Glu	0.479

6.3 Sorption of PNP at pH 7.0

6.3.1 Introduction

A recent study on the zeta potential of Chi-Glu aerogels produced using a similar procedure as described herein deduced an isoelectric point at pH 9.0 (*133*). Therefore, at pH 9.0, the Chi-Glu copolymers likely have an overall neutral charge in the diffuse layer at the slip-plane (or shear-plane). As defined by literature (*58f*), the slip-plane is a certain distance in the electric double layer (specifically, inside the diffuse layer) where the fluid can move freely. The rate or

flux of the particles is highly dependent on the zeta-potential of the particle. Secondly, Kyzas et al. (*134*) have determined the primary non-covalent interaction for anionic dyes like PNP at pH 9.0 occur through electrostatic attraction. Unlike the sulfonate dyes (*135*) which have a very low pK_a (<2), the pK_a of PNP is 7.14. This opens up an opportunity to do a sorption study where the copolymer surface contains a positive zeta-potential and a significant quantity of PNP is still in the anionic form. A study of this kind addresses the following hypothesis: Could a more positive adsorbent surface at a lower pH be better for an anion dye sorption than a neutral adsorbent surface? Anionic dye such as PNP at pH values above the pK_a is a probe for NAs and this study enable determination of the ideal pH for the sorption study of naphthenates. The main factor of importance in solving this hypothesis is the pH of the solution. Alkaline pH (pH 8.0) conditions were considered but results obtained by Pratt et al. (*76*) showed a low sorption capacity (Q_m = 0.2-0.8 mmol/g) compared to the SCl- and TCl-based copolymers investigated herein. Thus, a choice of pH 7.0 seems ideal as it is a pH above the pK_a range for NAs (pK_a = 5-6, (*5*)) while close to the pK_a of PNP. The latter ensures a significant quantity (41% by moles) of PNP remains anionic.

6.3.2 Determination of the initial PNP concentration

Since pH 7.0 is close to the pK_a, a significant portion of PNP remained anionic and another portion has been protonated into the neutral form. As a result, the initial concentration of the dye is the sum of the two portions and a method in determining the concentration of the anionic and neutral form of PNP is needed. This can be done using the Henderson-Hasselbalch equation (*cf.* Eqn. 6.1). Assuming constant volume, Equation 6.2 is valid and can be applied. The initial concentration (C_0) measured using the mass of PNP powder and the total volume of water is the sum of the two forms for PNP: The concentrations of anion form (i.e. [PNP^-]) and the non-ionized form (i.e. [PNP]) (*cf.* Scheme 6.1). By substituting equation 6.2 into equation 6.1, and isolating the term [PNP^-], Equation 6.3 is obtained. Both the pK_a and pH are already known so those values can be substituted into Equation 6.3 and the final form is obtained relating [PNP^-] and C_0. Equation 6.3 relates three known terms (pK_a, pH, and C_0) to [PNP^-] and through Equation 6.2, [PNP] can be determined. Therefore, the initial concentration of the anionic and neutral form of PNP can now be calculated. The λ_{max} for the two forms are determined to be 325 nm (PNP^-) and 400 nm (PNP), respectively, and a Beer-Lambert plot can be used.

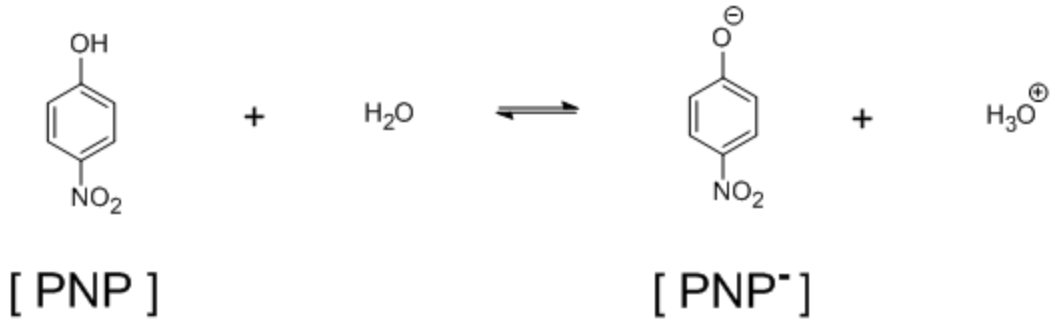

Scheme 6.1 Acid-base neutralization reaction involving PNP is shown. Note that the neutral form of PNP noted in the following sections refers to [PNP] and the anionic form of PNP is referring to [PNP^-] in the above scheme.

$$pK_a = pH + log\left({[PNP]}/{[PNP^-]}\right) \quad (6.1)$$

$$[PNP] + [PNP^-] = C_0 \quad (6.2)$$

$$[PNP^-] = {C_0}/{(10^{(pK_a - pH)} + 1)} = {C_0}/{2.38} \quad (6.3)$$

6.3.3 Sorption capacity of Chi-Glu copolymers

Table 6.2 Results from sorption of anionic PNP (PNP^-) at 22°C and at pH 7.0 using the Sips model. 10mM of potassium monobasic phosphate buffer adjusted to pH 7.0 with 1 M NaOH.

Copolymer	Q_m (mmol/g)	K_s	n	R^2	RMSE
1:400 ChiGlu	0.768	0.0685	1.04	0.982	0.015
1:700 ChiGlu	1.76	0.0614	0.834	0.993	0.014
1:1000 ChiGlu	0.463	0.0763	1.71	0.947	0.027

6.3.3.1 Adsorption of PNP at pH 7.0: anionic form ([PNP^-] in Scheme 6.1)

The highest sorption capacity, Q_m, is the 1:700 Chi-Glu copolymer at 2.17 mmol/g. This is followed by 1:400 Chi-Glu at 0.768 mmol/g and 1:1000 Chi-Glu at 0.463 mmol/g. Using swelling results, the difference in sorption capacity between 1:400 and 1:700 Chi-Glu can be explained by the accessibility of internal sorption sites caused by hydration effects. This is in accordance with results found by Wilson and Guo (*128*) using related copolymer systems. Wilson and Guo (*124*) adsorbed methylene blue with chitosan cross-linked polyacrylic acid copolymers and determined a direct correlation between the swelling ratio and the sorption capacity.

Pratt et al. (*76*) determined the sorption capacities for Chi-Glu copolymers with PNP in its anion form as 0.212-0.822 mmol/g. It should be noted that relatively high levels of loading of glutaraldehyde were used in this study and the decrease in sorption capacity was inversely correlated to the linker density. CPL-3 (*76*) had the highest concentration of glutaraldehyde bound to chitosan and also had the lowest sorption capacity for anionic PNP. This is supported by literature (*53, 59,112,128*) and explained through the cross-linking mechanism. As noted in Section 4.1, glutaraldehyde cross-links with chitosan through the primary amine on chitosan. Chiou et al. (*112*) surmised that at higher concentration of glutaraldehyde the number of unreacted primary amines should be reduced. Since binding of dyes occurs mainly with the primary amine group of chitosan, elevated levels of glutaraldehyde cross-linking will result in a reduced sorption capacity. If this adsorption mode is true then the 1:700 Chi-Glu copolymer should display the lowest sorption capacity because of its high levels of glutaraldehyde cross-linking., From the results tabulated in Table 6.2 and 6.3, this is not observed and may be attributed to the differing levels of glutaraldehyde employed herein. As indicated above, the greater loading of glutaraldehyde employed by Pratt et al. (*76*) should be noted.. For their CPL-3 copolymer, they used 10 times more glutaraldehyde than the 1:1000 Chi-Glu in this project. From their DTG, it is apparent that there is a great degree of cross-linking and as Mohamed et al. (*41*) noted, large quantities of cross-linking can discourage sorption due to inaccessibility to sorption sites. Therefore, the current batch of copolymers contain enough glutaraldehyde to enhance sorption capacity as noted by Kyzas et al. (*134*) but not in such an excessive amount

such that the cross-linker prohibits the dye from accessing sorption sites as reported by Mohamed et al. (*41*).

As well, Pratt et al. (*76*) did not document whether 1h is sufficient for aging to occur (*cf.* Section 1.5.3.1 and (*58*) for more information on aging process). As noted by Brinker and Scherer (*58b*), the aging process may occur over days depending on the type of gel and the overall structure of the gel may drastically change. For example: the initial pore volume distribution of titania gel (*58b*) revealed mainly small mesoporous materials averaging 3.0 nm and after aging for 1 day the average pore width effectively doubled to 7 nm. By affecting the size of the pores, insufficient aging of the gel will affect accessibility to the pores and reduce the overall sorption capacity (*58b, 134*). The equilibrium constant, K_s, appears to be not as affected by cross-linker density as the sorption capacity but a trend is there nonetheless. The equilibrium constant is lowest for 1:700 Chi-Glu and higher for 1:400 Chi-Glu and is inversely correlated to cross-linking ratios. This is in contrast to various reports (*53, 76,112,128,134*) and the reason is not known.

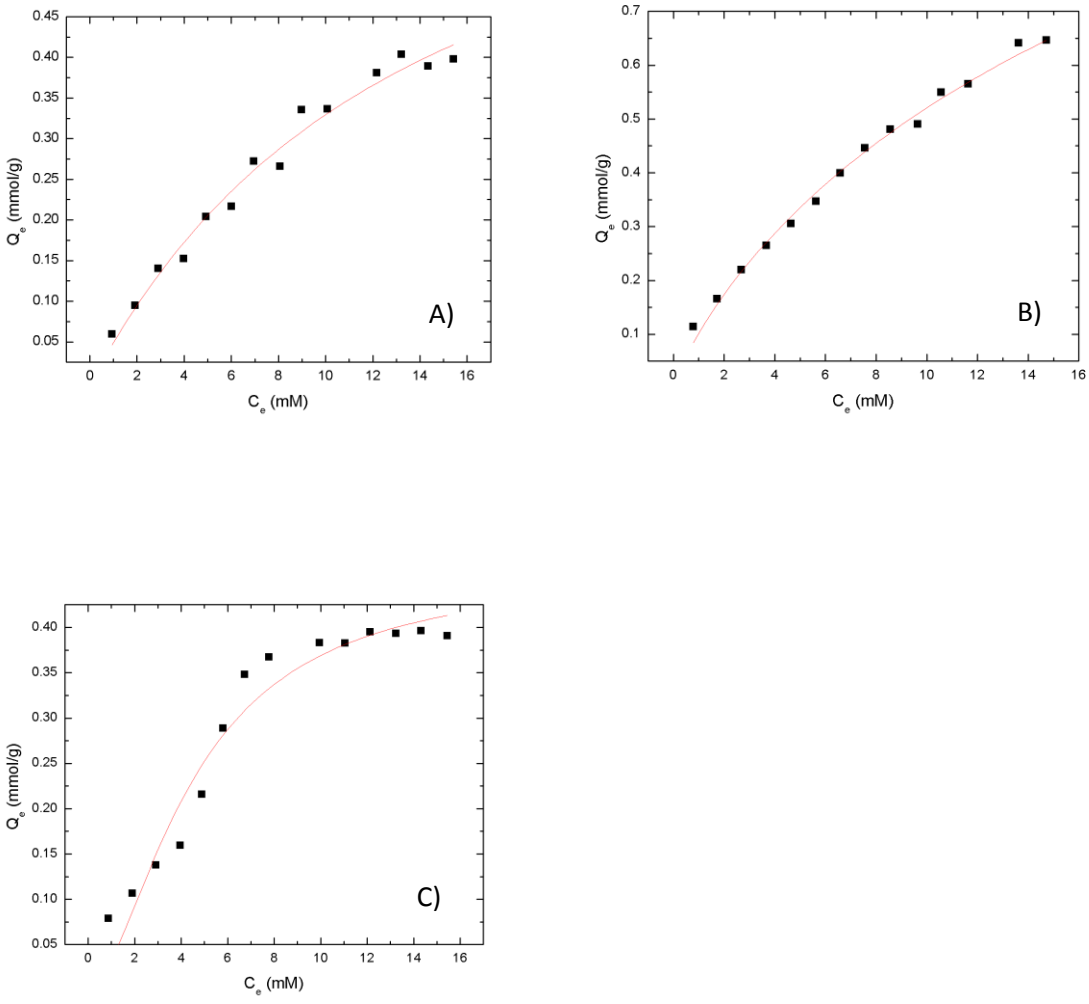

Figure 6.4 The sorption isotherm for anionic PNP (PNP^-) at 22°C and at pH 7.0 is shown. 10mM of potassium monobasic phosphate buffer adjusted to pH 7.0 with 1M NaOH was used. Sips isotherm model is applied and graphed using a red line (λ_{max} = 400 nm). A) 1:400 Chi-Glu; B) 1:700 Chi-Glu; and C) 1:1000 Chi-Glu.

From the values of the heterogeneity factor and the shape of the isotherms 1:400 and 1:700 Chi-Glu copolymers are type I isotherms. 1:400 is closest to the Langmuir model with an n-value of 1.04 (*cf.* Table 6.2) which suggests that the sorption sites are likely the most accessible (*39*). A second possibility for the n-value was suggested by Langmuir (*136*) where the sorption sites are far apart such that lateral interactions between sorbates are minimized. This explanation is supported by Kyzas et al. (*134*) through their diffusion models. 1:700 Chi-Glu has an n-value of 0.840 which suggests a more heterogeneous surface compared to the 1:400 Chi-

Glu. From TGA and CHN, it was noted that the 1:700 contained greater quantities of homo-polymers of glutaraldehyde and overall cross-linking of glutaraldehyde. Therefore, the simplest explanation is steric effects at the amine sites of chitosan arising from the large amount of glutaraldehyde cross-linkers which hinders access to the sorption sites. This is supported by the consistent n-value obtained for both pH 7.0 and 9.0. The trend is also independent of the form PNP as the isotherms for the neutral and anionic forms of PNP have consistent n-values. These results support that the Sips n-value parameter is influenced by changes on the adsorbent surface from homogeneous to heterogeneous. Of interest then is the case of 1:1000 Chi-Glu which breaks (n>1) the Sips isotherm model (*cf.* Figure 6.4C and 6.6C).

Since the n-value is greater than unity the Sips model cannot be used accurately to describe the sorption site distribution. The Sips model mathematically asserts that n cannot be greater than unity but does not outline situations where the n-parameter on the model can exceed unity. The first situation that breaks Sips model is observed for the sorption isotherm for 1:1000 Chi-Glu in Figure 6.4. The sigmoidal curve is a strong sign of lateral interactions between adsorbates and mutually cooperative effects. In this case, the adsorbed anionic PNP binds better to its neighboring PNP on the surface rather than the adsorbent surface. A sigmoidal isotherm is also observed for the neutral form of PNP but the sigmoidal shape disappears at pH 9.0 where only the anionic PNP is present (*cf.* Figure 6.5) and electrostatic repulsion between the anion form of PNP limits lateral interactions. Combining these results suggests a cooperative effect between the neutral and anionic forms of PNP. These effects could be caused by hydrogen-bonding between the hydroxyl and anionic oxygen on PNP^- or π-π interactions. The origins of the cooperative interactions observed for 1:1000 Chi-Glu copolymer system is unknown at the present.

6.3.3.2 Adsorption of PNP at pH 7.0: neutral form ([PNP] in Scheme 6.1)

Similar to the anionic form of PNP the sorption capacity is highest for 1:700 Chi-Glu (2.17 mmol/g) and lowest for 1:400 Chi-Glu (1.07 mmol/g) (*cf.* Table 6.3 and Figure 6.6). In comparison with literature, these values far exceed the sorption capacity reported by Pratt et al. (*76*). Secondly, the comparison between the K_s values from Table 6.2 and 6.3 reveals that sorption of copolymers with the anionic form had larger K_s which suggest a stronger binding compared with the neutral form. A more interesting observation is the sorption capacity of the

neutral form is larger than the anionic form. In one sense, this is a peculiar result because of positive zeta-potentials found for Chi-Glu aerogels at pH 7.0 by Chang et al. (*133*). The positive value for Chi-Glu aerogels suggests that glutaraldehyde renders the adsorbent surface more positively charged. Therefore, diffusion of the anionic form over the neutral form into the pores should be favored. This is verified when comparing the equilibrium constants of adsorption (K_s) for the two forms of PNP; larger values are observed for the anion vs. neutral form of PNP. One explanation is proposed by Kyzas et al. (*134*) through their diffusion model. Kyzas et al. (*134*) concluded through their diffusion study that for neutral dyes it is the pore sites that account for a majority of the adsorption of the neutral dye species. In the case of the anionic form of PNP, the primary sorption mechanism is electrostatic interaction. A positively charged copolymer surface either through grafting or pH modifications becomes the driving factor in enhancing diffusion into pores and increasing the sorption capacity. At pH 7.0, the pH is above the pK_a of chitosan and most of the primary ammonium groups have been deprotonated resulting in a relatively neutral surface. Secondly, equation 6.3, illustrates that the initial concentration of the two dyes is uneven with the anion form in lesser abundance than the neutral form of PNP. Both of these factors discourage intra-particle diffusion and a restriction on the relative accessibility to the sorption sites within the pore is predicted to occur for the anion form; hence, a lower sorption capacity is observed.

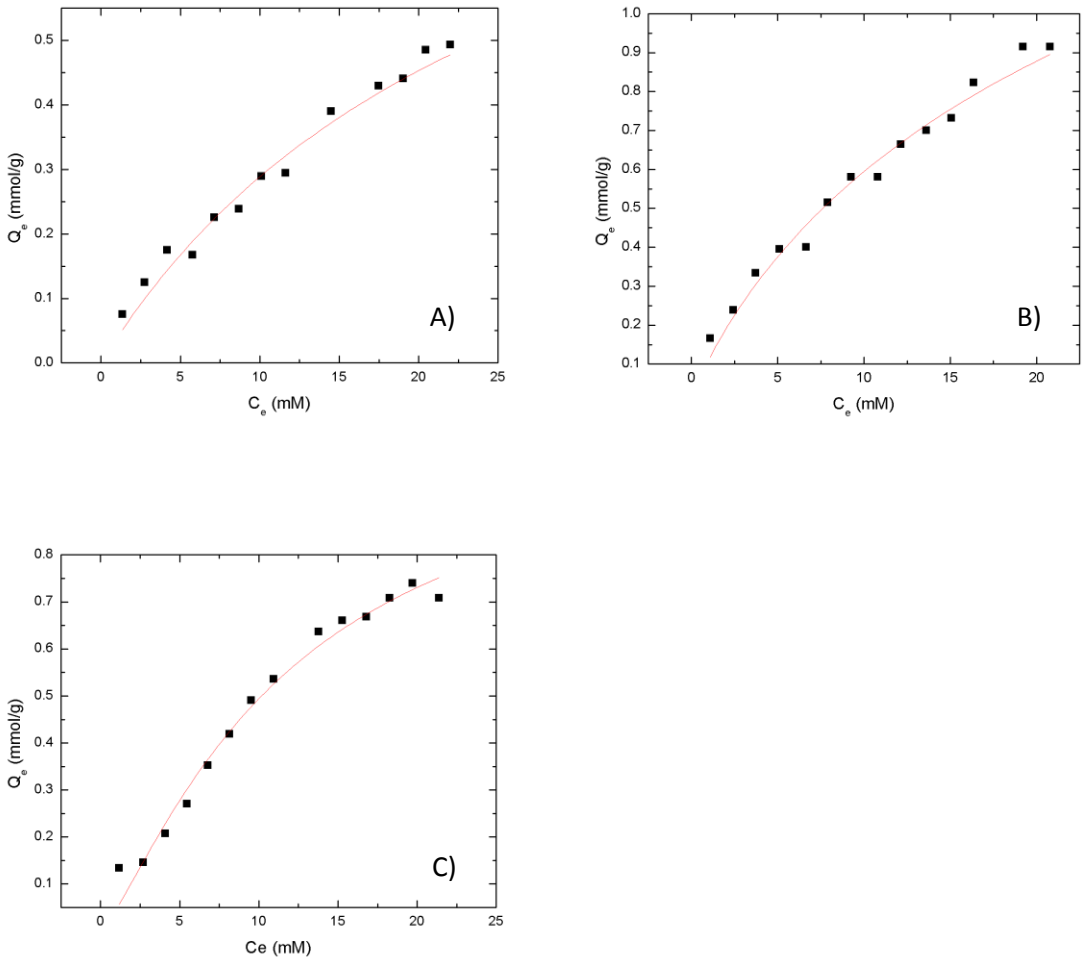

Figure 6.5 The sorption isotherm for neutral PNP at 22^{o}C and pH 7.0 is shown. 10mM of potassium monobasic phosphate buffer adjusted to pH 7.0 with 1M NaOH was used. The solid line represents the best-fit according to the Sips where λ_{max} = 325nm. A) 1:400 ChiGlu; B) 1:700 ChiGlu; and C) 1:1000 ChiGlu

Table 6.3 Isotherm fitting results from sorption of neutral PNP at 22^{o}C and at pH 7.0 according to the Sips model. 10mM of potassium monobasic phosphate buffer adjusted to pH 7.0.

Copolymer	**Q_m (mmol/g)**	**K_s**	**n**	**R^2**	**RMSE**
1:400 Chi-Glu	1.07	0.0377	0.992	0.979	0.020
1:700 Chi-Glu	2.17	0.0535	0.830	0.981	0.040
1:1000 Chi-Glu	1.11	0.0438	1.264	0.982	0.028

Another factor that can reduce the number of ammonium sites is the amount of cross-linking. The effect of cross-linking is illustrated by Figure 6.6 where the equilibrium concentration is held constant at a value where the sorption has reached saturation. From Figure 6.6, it can be observed that at higher cross-linking densities, the neutral form of PNP is favored over the anionic form. Secondly, although the neutral form is favored, the overall sorption capacity for both the neutral and anionic forms increases with greater levels of cross-linking.

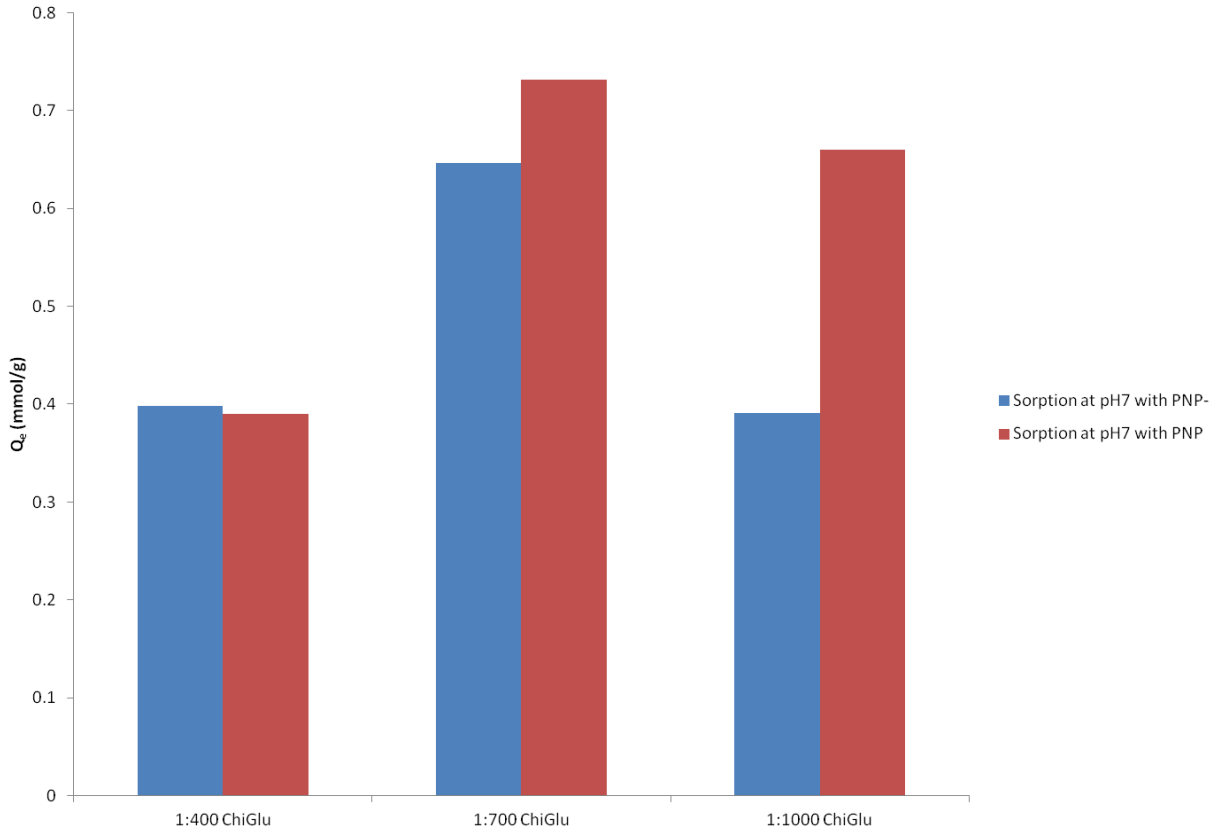

Figure 6.6 Comparison of the sorption capacity of PNP at pH 7.0 for the copolymers with the anionic and neutral forms of PNP at a fixed equilibrium concentration of 15mM. 10mM of potassium monobasic phosphate buffer adjusted to pH 7.0.

6.4 Sorption of PNP at pH 9.0

Sorption isotherms with PNP at pH 9.0 were obtained using five types of Chi-Glu copolymers. Three of the copolymer isotherms were already studied at pH 7.0. The 1:400 Chi-Glu at pH 12.8 and 1:700 Chi-Glu at T = 333 K are also included in this sorption study (*cf.* Section 6.1) to investigate the effects of various synthetic conditions (i.e. temperature and high pH) on the sorption capacity of the Chi-Glu copolymers. High sorption capacities of the Chi-Glu materials were obtained when compared to the starting material. The sorption capacity of pristine chitosan is 0.0255 mmol/g and is comparable to previous literature (*137, 138*) (Q_m = 0.0143-0.0260 mmol/g) results. The sorption capacity of the Chi-Glu copolymers from this study is several magnitudes larger than the literature values, and range from 2.20 mmol/g to 4.77 mmol/g. The Q_m values for the Chi-Glu copolymers exceed those for GAC where the sorption capacity is

determined to be 1.19 mmol/g. A more significant result is the relatively low K_s value for Chi-Glu copolymers when compared to GAC. The relatively high K_s are attributed to the microporous nature of GAC. The GAC micropores are at the molecular length scale relative to PNP. This size-fit matching enhances the van der Waals interactions within the pore sites which can favourably bind PNP. The favourable binding of PNP contributes to the challenges with regeneration of the GAC adsorbent. In contrast to GAC, the lower K_s values for Chi-Glu copolymers are due, in part, to its mesoporous nature. A benefit is that removal efficiencies up to 50% can occur for Chi-Glu copolymers (*76*). Secondly, the widened pores improve the accessibility to the interior adsorption sites. This is verified with the heterogeneity factor for GAC and the Chi-Glu copolymers. All the copolymers except 1:400 Chi-Glu at pH 12.8 exhibits n-parameter values close to unity which suggests a majority of sorption sites obey the Langmuir model. For GAC, the energy distribution of the sorption sites are more dispersed and a more heterogeneous surface (n = 0.461). The foregoing agrees with literature (*125*) where a direct correlation between pore volume of GAC and the heat of adsorption is found to be linear. Secondly, González-Martín et al. (*125*) noted that oxygen functional groups (i.e. carboxylates and hydroxyls) could also contribute to surface heterogeneity.

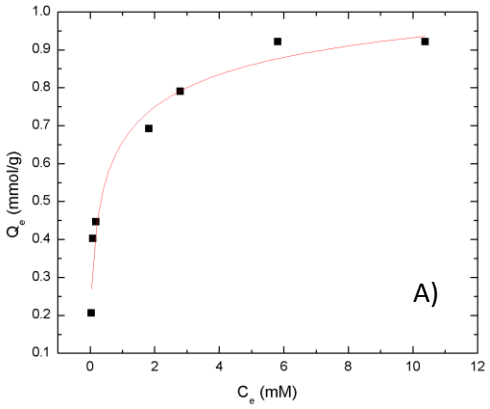
A)
Q_e (mmol/g)
C_e (mM)

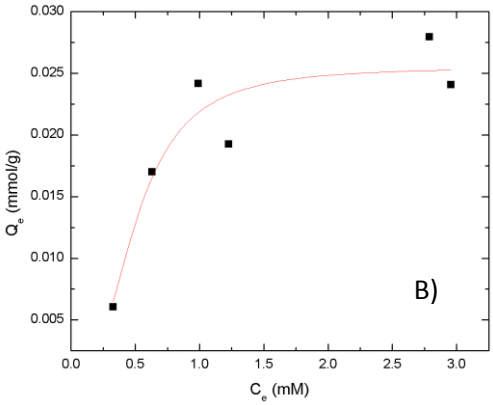
B)
Q_e (mmol/g)
C_e (mM)

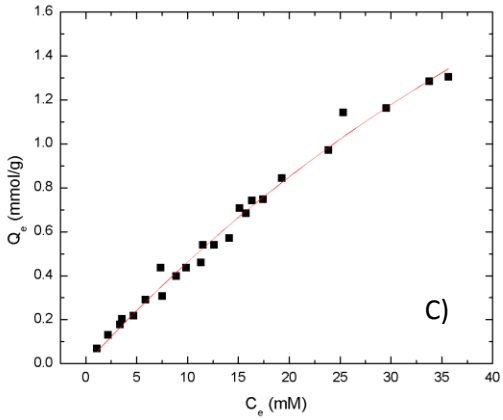
C)
Q_e (mmol/g)
C_e (mM)

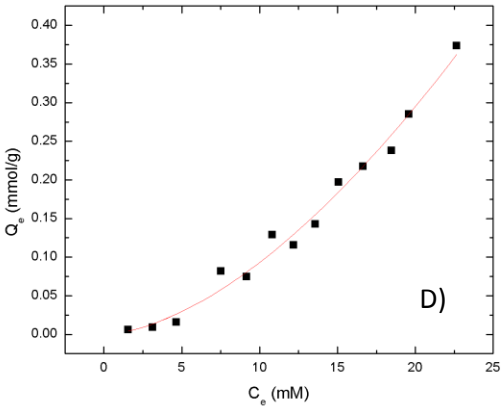
D)
Q_e (mmol/g)
C_e (mM)

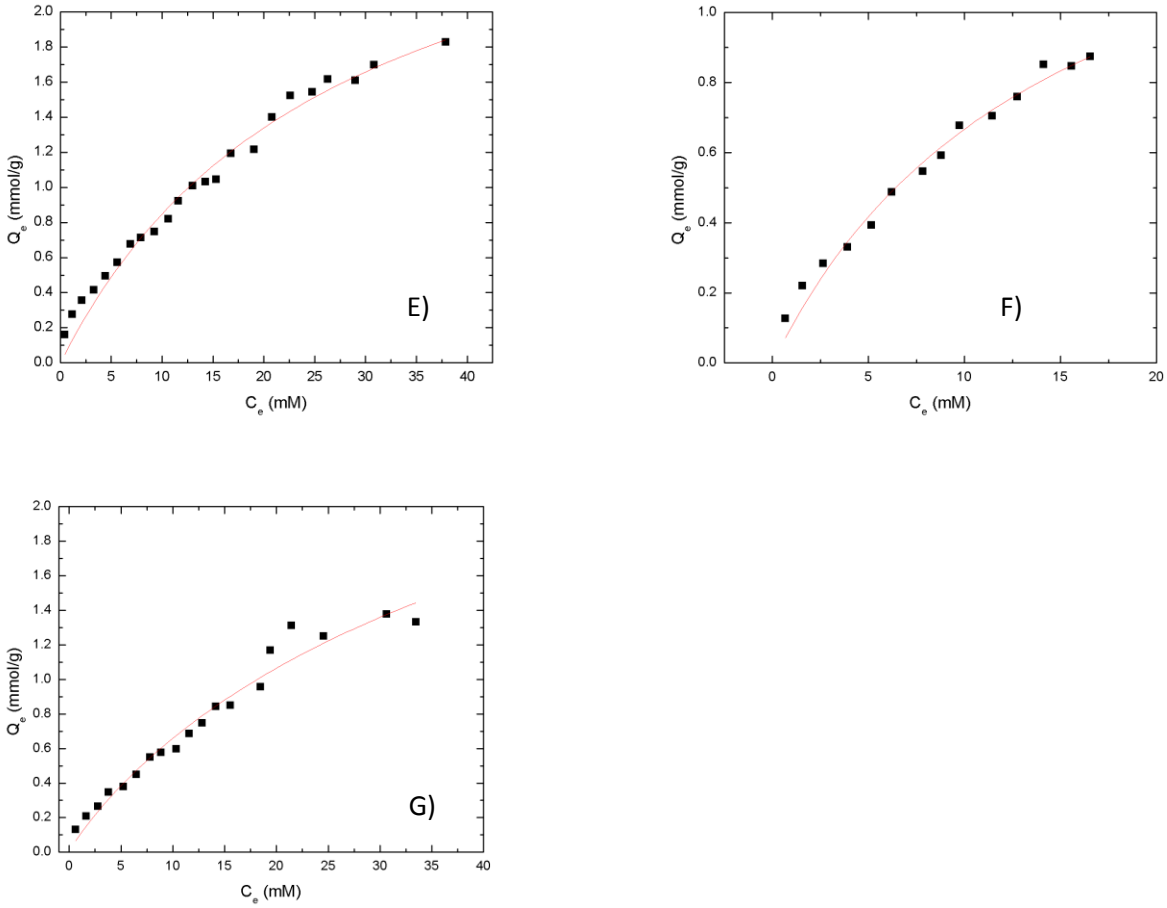

Figure 6.7 Sorption of PNP using Chi-Glu at pH 9.0 and 295 K is shown. 10mM of sodium bicarbonate buffer adjusted to pH 9.0 with 1M NaOH was used. A) GAC; B) Low MW Chitosan; C) 1:400 Chi-Glu; D) 1:400 Chi-Glu precipitated at pH 12.8; E) 1:700 Chi-Glu; F) 1:700 Chi-Glu gelled at 333 K; and G) 1:1000 Chi-Glu

The sorption capacities are inversely correlated to the cross-linking ratio between glutaraldehyde and chitosan which coincides with previous reports (*76, 112,128*). The 1:400 Chi-Glu had the highest sorption capacity (Q_m = 4.77 mmol/g) followed by 1:700 Chi-Glu (4.25 mmol/g) and 1:1000 Chi-Glu (3.58 mmol/g). A more interesting result is in the equilibrium constant. When comparing the magnitude of K_s for the different copolymers and the height of the thermal event at 400^{o}C on the TGA one conclusion can be made: the values for K_s are correlated to the amount of homo-polymers of glutaraldehyde where the largest K_s (0.0364) are with 1:700 Chi-Glu. As a large equilibrium constant suggests, the accessibility to the sorption sites are

highest with 1:700 Chi-Glu even though it does not have the largest sorption capacity. Allowing the homo-polymerization of glutaraldehyde through a base-catalyzed aldol condensation (*cf.* Section 4.2.4**)** to go to completion enhanced the accessibility of the sorption sites to PNP and should be noted for future synthesis.

Table 6.4 Results from sorption of PNP at 295 K and at pH 9.0 using the Sips model are tabulated. 10mM of sodium bicarbonate buffer adjusted to pH 9.0 with 1 M NaOH

Copolymer	**Q_m (mmol/g)**	**K_s**	**n**	**R^2**	**RMSE**
Low MW Chitosan	0.0255	6.05	2.58	0.898	0.008
GAC	1.19	1.22	0.464	0.974	0.086
1:400 ChiGlu	4.77	0.0103	1.02	0.988	0.034
1:400 ChiGlu at pH 12.8	ND*	6.55×10^{-6}	1.66	0.985	ND*
1:700 ChiGlu	4.25	0.0364	0.840	0.986	0.037
1:700 ChiGlu at T = 333 K	2.20	0.0603	0.851	0.988	0.281
1:1000 ChiGlu	3.58	0.0279	0.907	0.967	0.065

* Not Determined

Two batches of 1:700 Chi-Glu were synthesized according to the procedures described in Section 2.10.2 with one type of variable (i.e. temperature). One batch of 1:700 Chi-Glu followed the procedure and was allowed to gel at room temperature while another batch of 1:700 Chi-Glu was heated to 333 K and then cooled. The results are denoted as "1:700 Chi-Glu" for the room temperature and "1:700 Chi-Glu at T = 333 K" for the synthesis at higher temperature, as listed in Table 6.4. By increasing the gelation temperature the resulting copolymer had an attenuated

sorption capacity. Q_m for 1:700 Chi-Glu at T = 333 K is 2.20 mmol/g while 1:700 Chi-Glu has a sorption capacity of 4.25 mmol/g (*cf.* Figure 6.7E) and F)). The energy distribution of the sites on both of the 1:700 Chi-Glu copolymers do not appear to be affected because the n-value remains relatively constant (n = 0.851). The greater K_s value for the 1:700 copolymer prepared at T = 333 K cannot be fully explained and may be an artifact caused by a lack of data points used to fit the sorption isotherm.

The effect of pH on the isolation of products and the relative sorption capacity of the Chi-Glu copolymers is more pronounced than temperature effects. The 1:400 Chi-Glu copolymers were synthesized as described in section 2.10.2 except for the variable pH (see section 4.2.3 for more information) conditions. One batch of 1:400 Chi-Glu followed the procedure and precipitation occurred with the addition of 1M NaOH. The supernatant solution of the precipitate was held at pH 7.0 for 24h. Another batch of 1:400 Chi-Glu followed the procedure but the pH of the supernatant solution was increased to 12.8 and remained so for 24h. The results are listed as "1:400 Chi-Glu" for the neutral pH and "1:400 Chi-Glu at pH 12.8" (pH 13 is sometimes used) in Table 6.4. From Figure 6.7C) and D), the difference is stark as there is a type III isotherm for the 1:400 Chi-Glu at pH 12.8. Type III isotherm is characteristic of an adsorbate weakly bound to the adsorbent. As noted in the synthesis, aldol condensation is regarded to occur rapidly on the surface which poses restrictions on polymerization in the pores. One effect is that the cross-linking ratios on the external surface are much denser as compared to the interior. Combined with the swelling results for 1:400 Chi-Glu, the pores are likely blocked for medium sized molecules such as PNP but highly accessible to water.

6.4.1. Effect of cross-linking density on sorption

Figure 6.8 succinctly describes the effects of the cross-linking density towards the sorption capacity of the materials. Figure 6.8 is a graph of the ratio of moles of glutaraldehyde and primary amines on chitosan as a function of sorption capacity. The red points are the sorption capacity obtained by this project and the blue points are sorption results with PNP obtained by Pratt et al. (*76*). A maximum is obtained near the theoretical 1:1 Glu/NH_2 (1:400 Chi-Glu) which correlates to observations noted by Crini and Badot (*59*). Therefore, there is an optimum cross-linking ratio and should be noted for future studies.

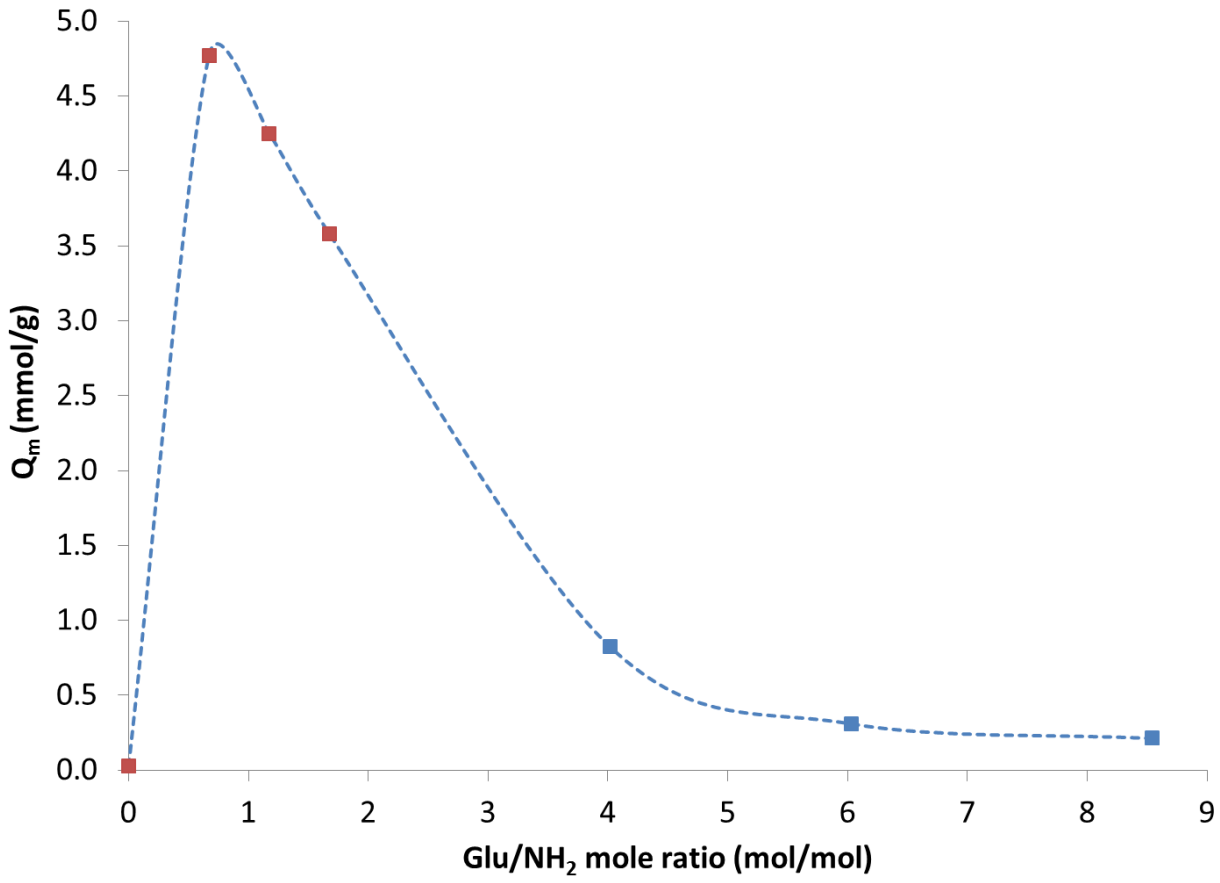

Figure 6.8 Sorption of PNP at pH 9.0 using Chitosan and Chi-Glu copolymers at various theoretical mole ratios. The red points correlate to data obtained in this project while the blue points are data obtained from Pratt et al. (*76*).

6.4.2 Comparison to β-CD copolymers

The objective of cross-linking β-CD and chitosan were to improve sorption. Cyclodextrins are soluble in water and by cross-linking with TCl and SCl the solubility of cross-linked β-CD decreased. For chitosan, the semi-crystalline nature of the copolymer inhibited sorption by restricting access to the sorption sites. By cross-linking with glutaraldehyde the crystallinity of chitosan would be reduced in the process. Both of these objectives have been met. Of interest is the effectiveness of the Chi-Glu copolymers compared to the β-CD copolymers. When comparing tables 6.2-6.4 with Table 6.4, the first trend is the change in sorption capacity as a function of cross-linking. When the cross-linking of TCl increased from 1:6 TCl (Q_m = 2.23 mmol/g) to 1:9 TCl (Q_m = 5.16 mmol/g), the sorption capacity doubled. The same cross-linking

density doubling was observed for the 1:400 Chi-Glu (Q_m =4.77 mmol/g) and 1:700 Chi-Glu (Q_m = 4.25 mmol/g) and the sorption capacity decreased. Therefore, increased cross-linking had a stronger effect for the cyclodextrin copolymers. Another advantage of the cyclodextrin copolymers is the overall sorption capacity of the materials. The Q_m values for 1:9 SCl and 1:9 TCl, were both larger than the Chi-Glu copolymers. Therefore, had the cyclodextrin copolymers not hydrolyze, they would have been ideal for NAs sorption.

6.5 Surface area calculations

Table 6.5 Specific surface area values obtained using equation 5.2 with data from the sorption of PNP at pH 9.0 AND 295 K. 10mM of sodium bicarbonate buffer adjusted to pH 9.0.

Copolymer	**Q_m (mmol/g)**	**Specific surface area assuming PNP is planar (m^2/g)**	**Specific surface area assuming PNP is orthogonal (m^2/g)**
Low MW Chitosan	0.0255	8	4
GAC	1.19	376	179
1:400 ChiGlu	4.77	1508	718
1:700 ChiGlu	4.25	1344	640
1:700 ChiGlu at T = 333 K	2.20	696	331
1:1000 ChiGlu	3.58	1132	539

The specific surface area obtained is similar to the cyclodextrin copolymers and is characteristic of xerogels (Silicate xerogels have a specific surface area of 515-910 m^2/g (*58e*)).

For GAC the reduced specific surface area is supported by literature (*35*) and explained in Section 5.2.4.1.

CHAPTER 7

RESULTS AND DISCUSSION: CHITOSAN – NAs SORPTION STUDY

7.1 Introduction

Through the sorption of PNP, many physicochemical properties of the materials were elucidated using a dye whose share several traits (adsorbs via hydrogen bonding and van der Waal's interaction, and anionic at pH 8.0) with individual components in the OSPW NAs mixtures. The cyclodextrin copolymers had the largest sorption capacity (Q_m = 2.20-11.1 mmol/g) and a weak binding affinity (K_s = 0.0146-0.0821) which is ideal for desorption. Therefore, from studies involving PNP 1:9 SCl should theoretically bind more NAs than GAC and can be regenerated through desorption instead of combustion. Unfortunately, these copolymers hydrolyzed at pH 9.0. At the present time, cyclodextrin polyester-based copolymers are not suitable for NAs adsorption studies. Chi-Glu copolymers also showed elevated sorption capacity when compared to GAC as well as a weak binding affinity in the PNP sorption study. Since the Chi-Glu copolymers did not hydrolyze at high pH, these are good candidates for NAs adsorption.

The adsorption of naphthenic acids (NAs) is not as straightforward as dye sorption because of the potential of competing equilibrium such as micellization of NAs at OSPW concentrations (*10*). NAs are a mixture of carboxylic acids and the micelles formed have been shown to be composed of carboxylic acids of varying molecular weight (*10*).While a sorption isotherm can still be obtained; the sorption capacity of NAs becomes challenging to explain since the unbound fraction of adsorbate is assumed to be available for participation in the adsorption process of NAs.

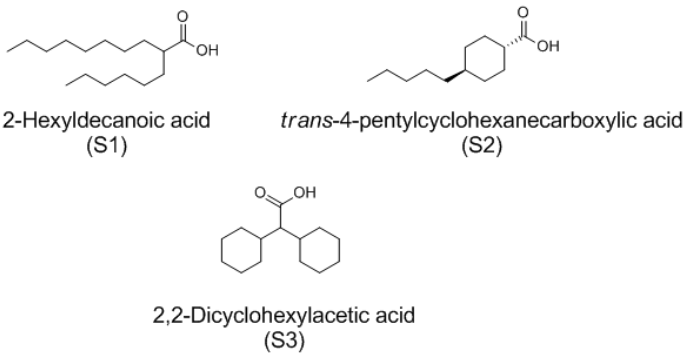

Figure 7.1 The three single component carboxylic acids used in this study: A) 2-Hexyldecanoic acid (Z = 0); B) trans-4-pentylcyclohexylcarboxylic acid (Z = -2); C) 2,2-Dicyclohexylacetic acid (Z = -4)

Therefore, to understand the sorptive properties an adsorbent such as Chi-Glu and GAC towards NAs it becomes necessary to divide the study into three steps. Sorption of individual carboxylates will be done to study any selectivity behavior in the Chi-Glu copolymers and steric factors. As OSPW NAs contain thousands of components, a simpler commercial NAs mixture (Fluka and Acros) containing a dozen components will be used in a sorption study prior to OSPW sorption studies. Should sorption of commercial NAs mixture demonstrate high sorption capacity then sorption capacity of Chi-Glu materials to OSPW refined NAs will be studied.

Through a single carboxylate adsorption study, the behavior of Chi-Glu copolymers towards a variety of carboxylic acids can be elucidated and a qualitative estimation of the effectiveness towards NAs can be made. As NAs are mixtures of acyclic as well as cyclic carboxylic acids, three example carboxylic acids have been chosen to reflect the diverse mixtures in NAs. These single-component acid compounds (*cf.* Figure 7.1) have been used as a model system in previous studies (10, *41,139*) and were chosen to correspond to a different Z number (number of hydrogen atoms lost to cyclization). Secondly, the molecular weight differences between the three carboxylates are minimized. Lastly, sorption isotherms of these three acids were obtained under the critical micelle concentration and ion concentration is kept constant through the usage of Millipore water and an ammonium hydroxide solution.

7.2 Granular activated carbon (GAC) – Single component carboxylate adsorption

The sorption capacity of GAC increases as the z-number increases. GAC has a Q_m of 81 mg/g, 289 mg/g, and 389 mg/g for S1, S2, and S3, respectively. This trend is supported by Freundlich (*32b*) who correlated the size of the hydrophobic fragments to the adsorption capacity of the adsorbent. As the hydrophobic fragment size increases, the adsorption capacity increases as well. Recent literature (*25b*, *122*, *140-142*) indicates that the Freundlich approximation is linked to the orientation of the adsorbate molecule on the surface of the adsorbent as well as the polarity of the adsorbent.

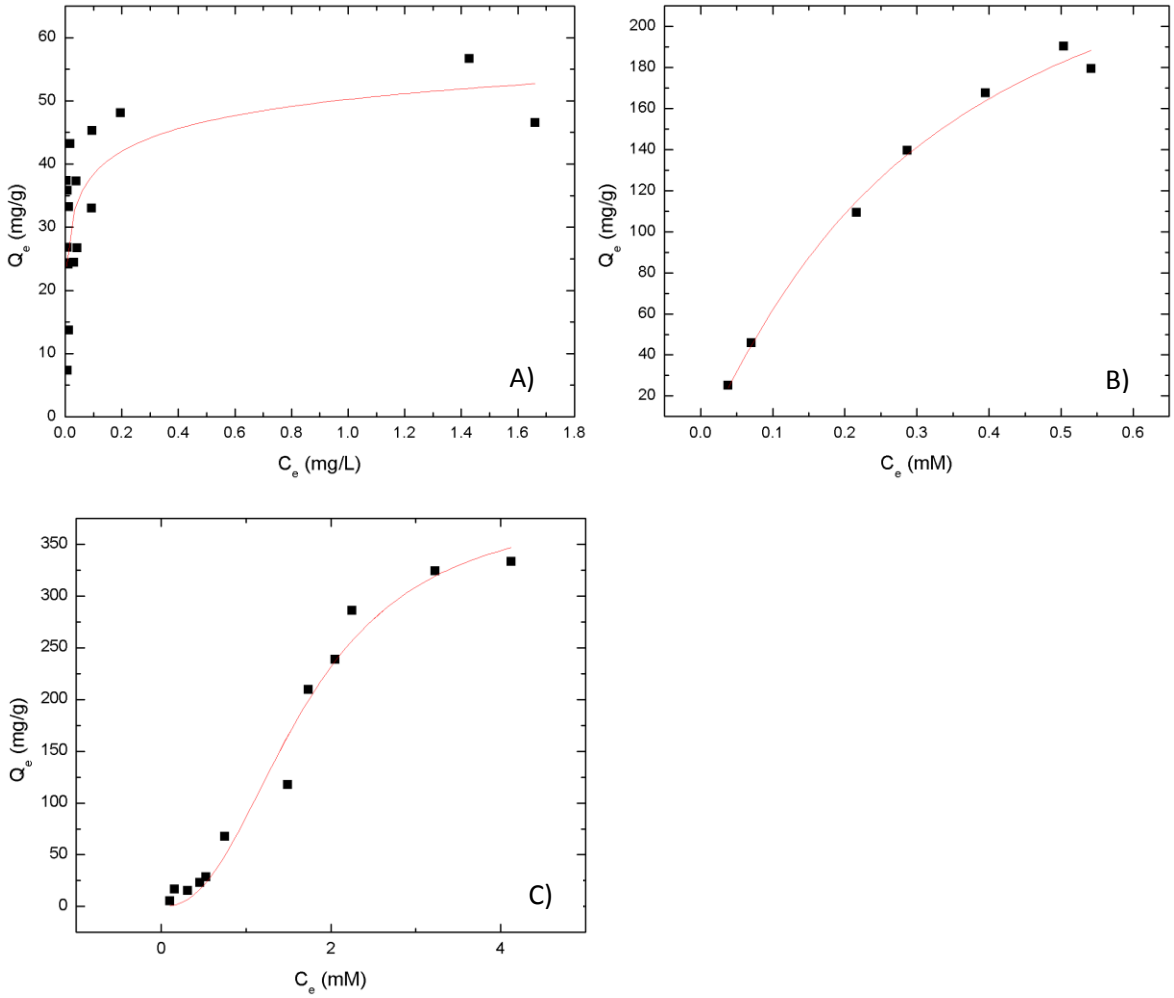

Figure 7.2 Sorption Isotherms of GAC with S1, S2, and S3 at 295 K and pH 9.0 are shown: A) Sorption with S1; B) Sorption with S2; and C) Sorption with S3. No buffers were used.

GAC is a relatively hydrophobic in nature with surfactants adsorbing onto the surface through van der Waal interaction (VDW). At low concentrations, the lipophilic fragment are oriented parallel to the adsorbent surface (*cf*. Figure 7.3). When the equilibrium concentration increases near saturation the surfactant adopts a more orthogonal orientation although an angle could be developed (*cf*. Figure 7.3) (*25b, 142*). If the orientation of the adsorbed surfactant is parallel then the sorption capacity should be inversely proportional to the size of the lipophilic fragment because of the finite surface area of the adsorbent. This is in agreement with the results for S1 because it possesses the largest lipophilic surface area (*10*), and has the lowest sorption capacity.

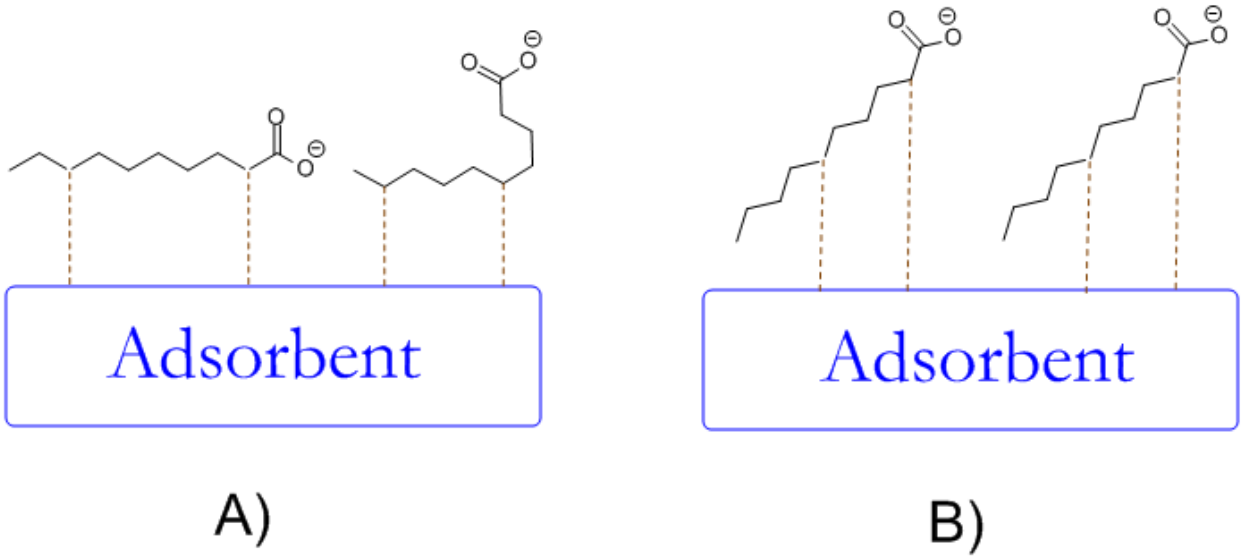

Figure 7.3 Orientation of an adsorbed molecule on GAC: A) parallel to adsorbent; and B) orthogonal to adsorbent

7.2.1) Shape of isotherm and Equilibrium Constant (K_s)

Adsorptions of surfactants to nonpolar surfaces are usually Type I and VI isotherms depending on whether hemi-micelles are formed below the CMC (*142*). For GAC, a high affinity type I isotherm is obtained for S1 which is peculiar as the size of the molecule should exclude it from micropore adsorption sites, therefore; another mechanism is responsible for its relatively high affinity.

Table 7.1 Sips' Isotherm model parameters for S1, S2, and S3 with GAC at 295 K and pH 9.0. No buffers were used.

Surfactant	Q_m (mg/g)	K	n	R^2	RMSE
S1	55.3	7.68	0.258	0.449	13.7
S2	262	4.80	1.18	0.995	7.56
S3	389	0.285	2.36	0.980	17.6

Kern and Findenegg (*143*) studied the adsorption of long *n*-alkanes onto graphite and determined that a parallel orientation of long alkanes coupled to strong lateral interactions is responsible for the high affinity observed in such systems. Rabe and Bucholz (*144*) offers further evidence of lateral interaction through scanning tunneling microscopy (STM) images of heptacosane adsorbed onto graphite in a parallel orientation. Therefore, the high affinity nature of S1 is due to the large lipophilic surface area of S1 (*10*) that allows for favourable VDW interaction with GAC and neighboring S1 molecules. Lateral interactions may decrease as the initial slope decreases from a high affinity isotherm for S1 to a typical Langmuir curve for S2 (*cf.* Figure 7.2). Although not high affinity (K_s for S1 = 7.65) the K_s value for S2 at 3.78 is still large suggesting adsorption is still highly favored. The sigmoidal nature of the sorption isotherm for S3 further demonstrates the primary importance of VDW interaction in the adsorption of alkyl carboxylates to GAC. S3 has the smallest K_s at 0.285 reflecting the small lipophilic surface area and the weakened VDW interaction between adsorbates (*10, 142*).

Through adsorption studies of PNP, lateral interactions have been shown to skew the heterogeneity factor. Langmuir, Freundlich, and Sips isotherms all assumes ideal solution where

interactions between molecules are assumed to be the negligible whether adsorbed or in the bulk solution (*28*). Large heterogeneity factors were noted to occur in the PNP sorption isotherms where PNP was weakly bound as in the type III isotherm obtained with 1:400 Chi-Glu at pH 12.8. In contrast, the high affinity sorption isotherm with GAC/PNP at pH 4.6 results in a low n-value. This is verified by the large n-value for S3 bound to GAC and the low n-value for S1. Therefore, the n-value in this case only, correlates inversely to the magnitude of the lateral interaction.

7.3) Chitosan and Chi-Glu copolymers – Single component carboxylate adsorption

Adsorption of surfactants with chitosan and Chi-Glu copolymer is quite different from GAC. The adsorbent itself is a hydrophilic surface as evidenced by the swellability with water while GAC is hydrophobic. Evidence of hydrophilic properties is the large swelling percentage with water while a type III isotherm with water is well known for GAC (*122*). This is crucial because solution-based adsorption requires the displacement of solvent molecules from the adsorption site by the solute. If the solvent is bound strongly to the adsorbent, limited adsorption will occur but also negative adsorption caused by solvent adsorption (*25b, 32*). Negative adsorption in this case is likely the result of the swelling character of the polymer. Since sorption of solute is discouraged, the hydrated pores of the Chi-Glu copolymers will contain mainly solvent. This can decrease the apparent volume in the vials and arbitrarily increase the solute concentration causing $C_e > C_0$ and Q_e to be negative. Another factor which promotes adsorption is the hydrophobic effect. When the ordered domain of water is disrupted with a surfactant, a hydration shell is generated by water and surrounds the surfactant. As the shell decreases the entropy of the solution, surfactants are often aggregated to minimize surface area of the shell. This aggregation will occur on the surface of a relatively hydrophobic adsorbent instead of in the bulk solution. At pH 9.0, the zeta-potential of chitosan and Chi-Glu copolymers have been shown to be anionic and neutrally charged (*63, 133*). The adsorption process will primarily involve hydrogen bonding, VDW interactions, and hydrophobic effect between the adsorbate and the copolymers (*63, 133,138,142*).

Table 7.2 Results from sorption isotherms are listed below. All data was obtained using the Sips isotherm model. Sorption isotherms were obtained at pH 9.0 and 295 K. No buffers were used.

	Copolymers	Chitosan	1:400 Chi-Glu	1:700 Chi-Glu	1:1000 Chi-Glu
S1	**Q_m (mg/g)**	0.303	0.089	0.077	0.073
	K_s	0.193	1.73	1.92	10.5
	n	1.20	2.22	1.75	3.04
	R^2	0.979	0.963	0.900	0.937
	RMSE	0.081	0.055	0.044	0.030
S2	**Q_m (mg/g)**				
	K_s	0.0385	0.0410	0.0373	0.0302
	n	1.19	2.39	2.26	1.67
	R^2	0.981	0.992	0.994	0.967
	RMSE				
S3	**Q_m (mg/g)**				
	K_s	0.00462	0.00601	0.00203	0.01069
	n	2.51	2.84	3.72	2.94
	R^2	0.988	0.951	0.958	0.981
	RMSE				

7.3.1 Chitosan and Chi-Glu – Single carboxylate adsorption

From the results obtained in Table 7.2 the first result is the low sorption capacity obtained for chitosan and Chi-Glu when compared to GAC. Of the three carboxylates studied, the polar head group remains highly hydrated due to the carboxylate anion at alkaline pH conditions. Hydrogen bonding may occur via water mediated H-bonds but does not play a major role in binding carboxylates at pH 9.0. This is supported by literature (*134*). What remains is adsorption

through VDW interactions and the hydrophobic effect. Effects of VDW interactions are observed according to the shape of the sorption isotherm.

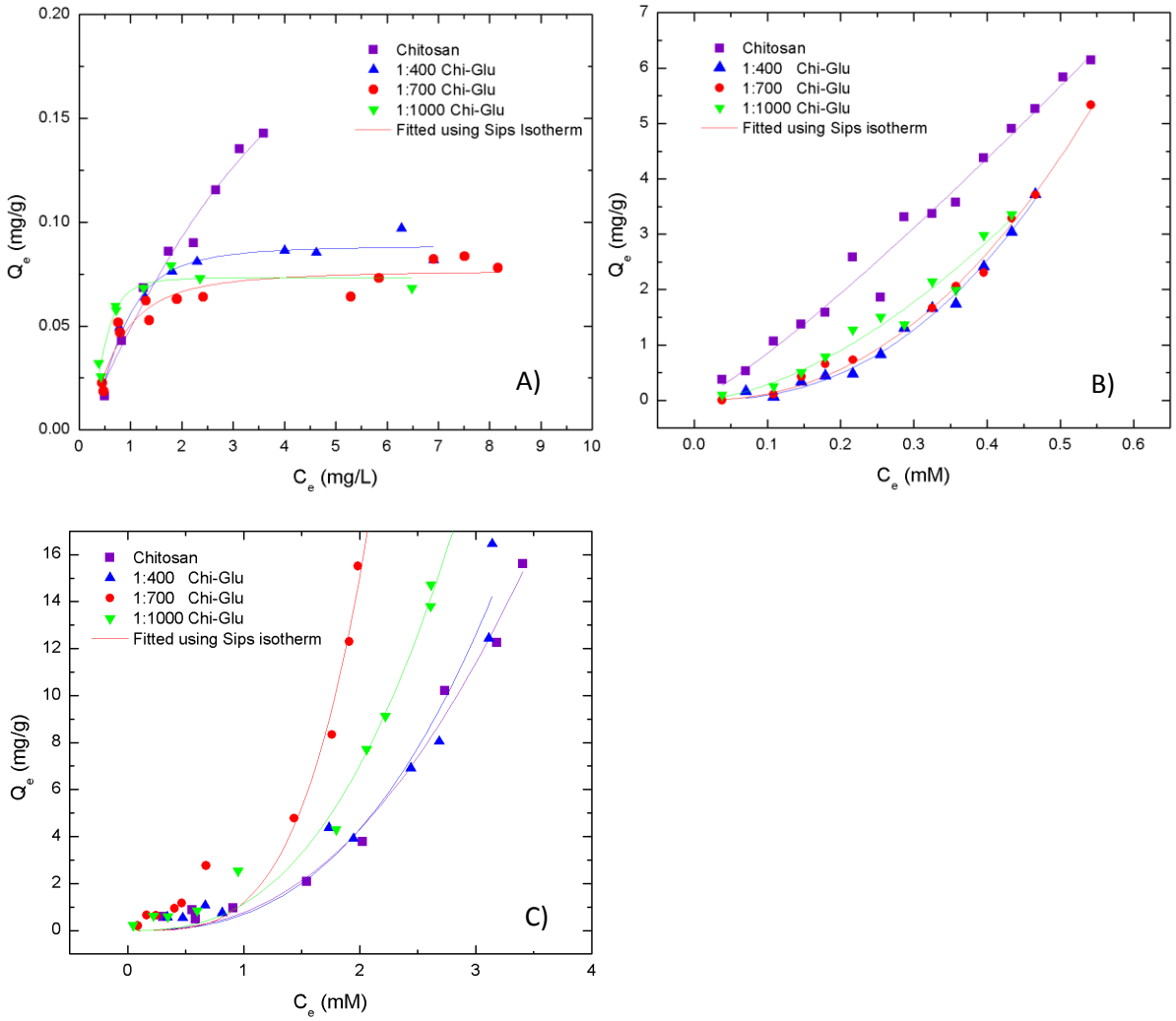

Figure 7.4 Sorption isotherms for Chitosan and Chi-Glu copolymers with single component carboxylates at pH 9.0 and 298 K: a) S1; b) S2; and c) S3

As S1 has the greatest lipophilic surface area (*10*), it also will have the largest lateral VDW interaction between adsorbates. This is reflected in the type I isotherm obtained for S1 with the Chi-Glu copolymers which suggests adsorption is favored. As the lipophilic fragment decreases in size, the strength of the lateral VDW interaction also decreases. As a result, a change of the sorption isotherm from a type I to a type III system for S2 and S3 can be observed (*cf.* Figure 7.4). Numerically, the decrease in the equilibrium constant from S1 to S3 is also correlated to the decrease in VDW interaction. Type III isotherms indicate weakly bound

adsorbates with relatively strong lateral interactions which have been known to lead to surface aggregation; hence the resulting exponential slope (*24b, 33*).

7.4 Naphthenate adsorption

Adsorption of naphthenic acids (NAs) was done in a concentration range that reflects the conditions found in OSPW. Sorption trials were done from a concentration range of 8 to 110 ppm for both Fluka and Acros NAs and the procedures were based off of a previous study done by Mohamed et al. (*41*). As Mohamed et al. (*10*) noted the onset of micellization occurs for Fluka and Acros at 5 and 12 ppm, respectively. Therefore, sorption of naphthenic acids occurs in a concentration range where a majority of the naphthenic acids are above the CMC. Secondly, the pK_a range of NAs is 5-6 and at pH 9.0, the naphthenic acids are deprotonated to the naphthenate anion form. Therefore, NAs will hereafter be referred to as naphthenates and not naphthenic acids.

Micellization is the aggregation of surfactant molecules to reduce interfacial energy and many of the forces that govern it also affect adsorption onto an uncharged surface. This relationship between micellization and adsorption is summarized most succinctly by Freundlich who extended Traube's rule in correlating surface activity to the length of the surfactant chain (*37b*). Freundlich noted that adsorption of surfactants increase on a hydrophobic uncharged surface as the length of the surfactant increases. This is verified by the studies outlined in the previous section for GAC. One important assumption to Freundlich's extension of Traube's rule is that adsorption should be favored over micellization. This allows the adsorbent to compete with the micelle-monomer equilibrium and causes the micelles to dissociate to allow the monomer surfactants to undergo adsorption onto the adsorbent (*145*). This is observed for GAC sorption isotherms where a type I curves are shown for both Fluka and Acros NAs. The sorption capacity of GAC to Acros is 170 mg/g while Fluka is 92.4 mg/g. The plateau observed for a Type I isotherm is not due to monolayer formation but rather equilibrium occurs between an adsorbed phase and the formation of micelles (*142*). Another result is the sorption capacity of GAC with Acros NAs is double in comparison with Fluka NAs (*cf.* Table 7.3).

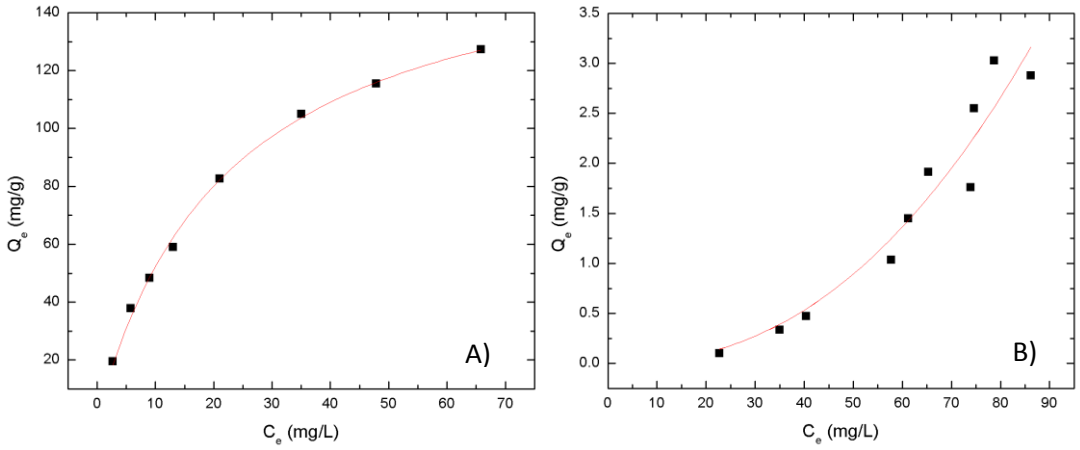

Figure 7.5 Sorption of Acros NAs using GAC and 1:1000 Chi-Glu copolymers is shown. The isotherms are fitted using the Sips model (solid red line). A) GAC; and B) 1:1000 Chi-Glu.

The results obtained with Chi-Glu copolymers are discouraging where only one copolymer shows any sorption. From Figure 7.5 and 7.6, only the 1:1000 Chi-Glu shows any sorption and the isotherm is a type III which denotes relatively weak adsorbent-adsorbate interactions. Due to the shape of the isotherm no reasonable Q_m could be obtained using the Sips model. The weak interaction between adsorbent and adsorbate is also verified by the small equilibrium constants in Table 7.3 where adsorption is not favored.

A consequence of the micellization process being favored over the adsorption process is observed with the Chi-Glu copolymers. With the exception of 1:1000 Chi-Glu, most copolymers do not adsorb NAs to any appreciable extent. In fact, negative adsorption occurs and the addition of the copolymers appears to promote micellization as all Q_e values for 1:400 and 1:700 Chi-Glu with NAs are negative. The role of micellization can be observed in the sorption isotherm for chitosan with Fluka NAs where a maximum is observed at 10 ppm where micellization is occurring for Fluka NAs (*10*) (*cf*. Figure 7.7). Afterwards, only negative adsorption is recorded. This is also noted in literature (*25b*) where the more surface active components in mixtures of surfactants are initially adsorbed but afterwards will desorb to form micelles or molecular aggregates once CMC has been reached. Further evidence is from the Chi-Glu copolymer sorption isotherms with S2 and S3 where the Chi-Glu copolymers exhibit a type III isotherm that indicates weakly adsorbed surfactants.

Table 7.3 Results from sorption isotherms with Fluka and Acros NAs are listed below. All data were fit with the Sips isotherm model. Sorption isotherms were obtained at pH 9.0 and 298 K.

Copolymers		**GAC**	**1:1000 Chi-Glu**
Acros	**Q_m (mg/g)**	182	
	K_s	0.0470	1.30×10^{-7}
	n	0.935	2.33
	R^2	0.998	0.930
	RMSE	1.61	
Fluka	**Q_m (mg/g)**	92.4	
	K_s	0.0290	6.19×10^{-7}
	n	1.28	2.30
	R^2	0.939	0.966
	RMSE	5.61	

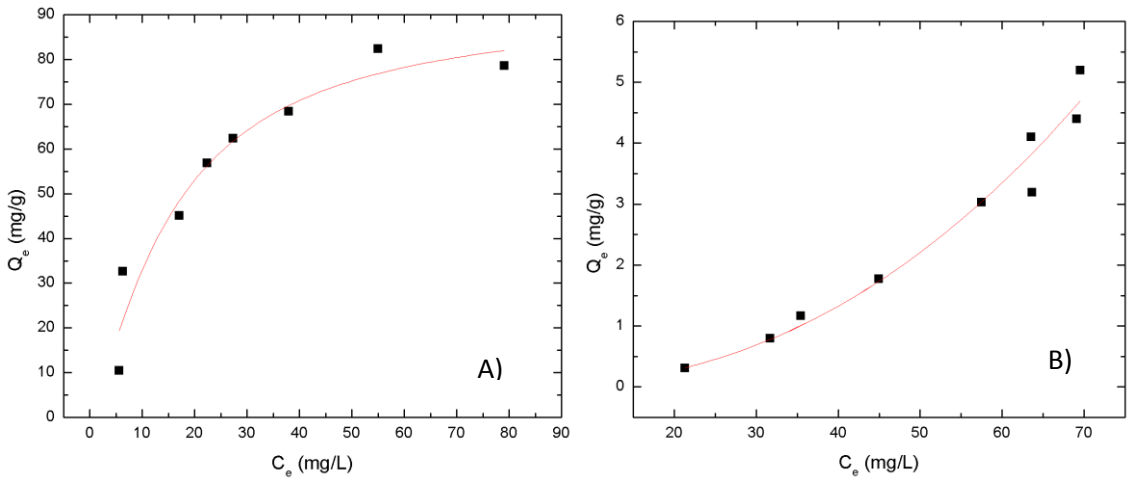

Figure 7.6 Sorption of Fluka NAs using GAC, Chitosan, and 1:1000 Chi-Glu copolymers is shown. The isotherms are fitted using the Sips model (solid red line). A) GAC; and B) 1:1000 Chi-Glu.

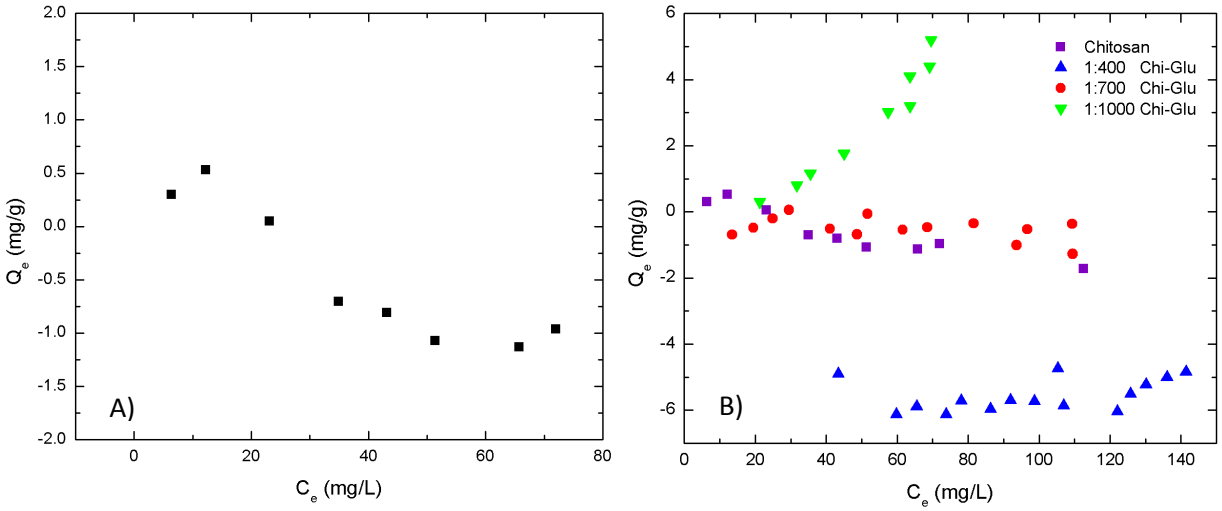

Figure 7.7 Sorption Isotherms of Chi-Glu Copolymers with Fluka NAs is shown: A) Chitosan only; and B) all Chi-Glu copolymers. All sorption isotherms are obtained at pH 9.0 and at 298 K.

An interesting result is that the "*apparent*" magnitude of the sorption is negative and greatest for the 1:400 and lowest for 1:1000 Chi-Glu. This is rationalized through zeta-potential studies done by Jin and Bai (*64*) and Chang et al. (*133*). Jin and Bai (*63*) determined the isoelectric point for chitosan to be pH 6.6 which is close to the known pK_a for chitosan (*59*). When glutaraldehyde cross-links with chitosan, the isoelectric point of the resulting aerogel is increased to a pH 9.0 (*133*). The presence of glutaraldehyde causes the chitosan backbone to

become more positively charged and attracted towards anionic surfactants. Therefore, one possible explanation for the reduced negative sorption in 1:700 and 1:1000 Chi-Glu is that the large quantity of glutaraldehyde attached may have rendered the copolymer surface to be more positive as compared to 1:400 Chi-Glu.

CHAPTER 8

CONCLUSION AND FUTURE WORK

8.1 Introduction

To remove naphthenates in the OSPW three questions were posed at the beginning of the project: Can the mole ratios of linkers affect the sorption capacity of the copolymers? Can the mechanism and sorption capacity of NAs be elucidated through the adsorption of PNP and carboxylates with varying z-components? Are chitosan and β-cyclodextrin copolymers applicable to the removal of NAs in OSPW environments?

8.2 Can the mole ratios of linkers affect the sorption capacity of the copolymers?

Goals that were set to evaluate the question involved the following criteria

1. Increased surface area
2. Increased sorption capacity due to cross-linking
3. Increased sorption capacity compared to other materials

The answer is yes and is proven through the synthesis of chitosan and β-cyclodextrin based copolymers. Chitosan-glutaraldehyde copolymers were synthesized using a gelation based method. Products were characterized using FT-IR, TGA, and CHN analysis. Polymerization of glutaraldehyde was determined through the thermal event at 400^{o}C via the TGA. Calculations in determining the number of glutaraldehyde molecules attached to one chitosan molecule through the CHN analysis also supported the presence of polymerized glutaraldehyde. Through the reduction of the amide I-III bands and the deformation of the methyl group band in the FT-IR, evidence of deacetylation of the amide on chitosan were detected. Ultimately, through this process Chi-Glu materials were synthesized with swelling percentages with water that ranged from 770-3111%. Sorption studies done with PNP and compared with GAC and chitosan at pH 9.0. With the exception of one copolymer, all Chi-Glu copolymers had a sorption capacity greater than GAC and chitosan. The trend in sorption capacity is: 1:400 Chi-Glu > 1:700 Chi-Glu> 1:1000 Chi-Glu> 1:700 Chi-Glu at 333 K> GAC> Chitosan> 1:400 at pH 12.8.

β-CD based copolymers were synthesized at varying mole ratios with sebacoyl and terephthaloyl chloride. The copolymers were characterized using ^{1}H NMR, FT-IR, CHN, and TGA. Through a hydrolysis test at pH 4.6, only 1:6 and 1:9 SCl and TCl were deemed to be suitable candidates for PNP sorption at pH 4.6. All copolymers hydrolyzed at pH 9.0 and were concluded to not be suitable for naphthenate sorption. At pH 4.6, most copolymers had a greater sorption capacity (Q_m) compared to GAC: 1:9 SCl> 1:9 TCl> 1:6 SCl> GAC> 1:6 TCl.

Therefore all copolymers that were considered suitable for sorption studies with PNP had a higher sorption capacity when compared with GAC. Secondly, for the Chi-Glu materials, the introduction of glutaraldehyde cross-linkers significantly improved the sorption capacity of chitosan from 0.025mmol/g to 2.20-4.77 mmol/g (a 200-fold increase).

Comparisons between the nitrogen porosimetry data and the dye-based methodology for calculating surface area demonstrated the materials undergo swelling. Swelling percentage of chitosan in water is 238% while the Chi-Glu copolymers ranged from 770-3111%.

8.3 Can the mechanism and sorption capacity of NAs be elucidated through the adsorption of PNP and carboxylates with varying z-components?

Since the SCl and TCl copolymers hydrolyzed at basic pH this question remains open for these copolymers. For chitosan based copolymers the sorption mechanisms are not the same for dyes and surfactants. Strong adsorptions of dyes have been attributed to electrostatic interactions at low pH and hydrogen bonding at high pH (*134*) for chitosan copolymers. From the single carboxylate adsorption isotherm results, it is the VDW interaction that dominates. Therefore, the incompatibility of the intermolecular forces governing sorption for PNP at pH 9.0 and the surfactants ensures that PNP is not a valid probe for sorption capacity of surfactants.

8.4 Are chitosan and β-cyclodextrin copolymers applicable to the removal of NAs in OSPW environments?

Since SCl and TCl copolymers hydrolyze at pH 9.0 and most Chi-Glu copolymers show negative adsorption with NAs at pH 9.0 the answer in this case is no. Incompatibility between the adsorbate and the adsorbent is the main reason. Assuming identical polar head groups, surfactants such as NAs are adsorbed onto the adsorbent through VDW interactions. The larger

the lipophilic surface area, and the more hydrophobic the adsorbent is, the better the NAs adsorption. This has been proven through the single component carboxylate adsorption with GAC. Chi-Glu copolymers have been shown to be relatively hydrophilic through the large swelling percentages with water and adsorbs mainly through hydrogen bonding at pH 9.0 (*134*). Therefore, adsorption of surfactants is unlikely to occur at current conditions.

8.5 Future research involving NAs

Unfortunately, NAs adsorption cannot be done with the current set of materials that were synthesized: What can be done to solve this problem?

8.5.1 Improving the β-CD Polyester Compounds

The β-CD cavities are similar in size to micropores and the host-guest interaction is complementary to dyes and NAs. SCl- and TCl-based copolymers have demonstrated to have sorption capacities of PNP greater than β-CD poly urethane copolymers. Therefore, SCl and TCl copolymers have a real potential in NAs sorption and the hydrolysis problem needs to be solved. One method is to increase the cross-linker ratio. 1:9 SCl have shown resilience to hydrolysis at pH 4.6 and attenuated hydrolysis at pH 9.0. Therefore, higher ratios such as 1:12, 1:24, etc. should be synthesized and checked for hydrolysis at pH 4.6 and 9.0.

8.5.2 Improving Chi-Glu Copolymers

For Chi-Glu copolymers, the problem lies in incompatible interactions between the surfactant and the adsorbent. When the forces are compatible, Chi-Glu copolymers demonstrate a high sorption capacity for surfactants. One example is the adsorption of dodecyl sulfate onto Chi-Glu aerogels at pH 3.0 (*133*). Due to the strong electrostatic interaction, sorption capacity of the Chi-Glu aerogel towards the anionic surfactant is ~ 900 mg/g. Therefore, one possibility is to study adsorption of NAs at a lower pH such as 7.0 to protonate more of the amines into ammoniums.

Another route that can be taken is to use more hydrophobic linkers. One such linker is β-CD. Pratt et al. (*146*) has devised a synthesis route to attach β-CD to chitosan and the presence of the host-guest macrocycle should enhance NAs sorption.

In the literature (*64, 133*), the addition of glutaraldehyde shifted the isoelectric point from pH 6.6 for pristine chitosan to pH 9.0 for Chi-Glu aerogels. Unfortunately, a quantitative relationship between glutaraldehyde concentration and the isoelectric point of the Chi-Glu copolymers have not been determined. Therefore, a zeta-potential study on the current Chi-Glu materials would be done to determine the isoelectric point of each of the materials. The objective of this study is to determine whether there is an optimal cross-linking density that affords the largest isoelectric point; preferably, pI > 9.0 where chitosan remains cationic at OSPW conditions. Another possible alternative is determination of the point of zero charge for the polymers developed herein.

REFERENCES

1. Alberta Energy. Facts and Statistics. http://www.energy.alberta.ca/oilsands/791.asp (Accessed April 12, 2013)
2. Masliyah, J.; Zhou, Z.; Xu, Z.; Czarnecki, J.; Hamza, H., *Can. J. Chem. Eng.*, **2004**, *84*, 628-654
3. Clark, K.A., *Trans. Can. Inst. Min. Metall.*, **1944**, *47*, 257-274
4. Headley, J.; McMartin, D., *J. Environ. Sci. and Health Part A*, **2004**, *39*, 1989-2010
5. Bota, G.; Qu, D.; Nesic, S.; Wolf, H.A. Proceedings of NACE International: Corrosion Conference and Expo, San Antonio, United States of America, March 14-18, 2010. www.onepetro.org/mslib/servlet/onepetropreview?id=NACE-10353 (Accessed April 25, 2013)
6. Mamer, M. Oil Sands Tailings Technology: Understanding the Impact to Reclamation. Suncor Energy Inc. https://circle.ubc.ca/bitstream/handle/2429/30342/13%20Mamer.pdf?sequence=1 (Accessed April 25, 2013)
7. Seifert, W.; Howells, W., *Anal. Chem.*, **1969**, *41*, 554-562
8. Clemente, J.S.; Prasad, N.G.N.; MacKinnon, M.D.; Fedorak, P.M. *Chemosphere*, **2003**, *50*, 1264-1274
9. Golder Associates. Summary of Naphthenic Acids Predictions for the Oil Sands Region. Golder Associates Ltd. http://www.ceaa.gc.ca/050/documents_staticpost/59540/52090/summary.pdf (Accessed February 23, 2013).
10. Mohamed, M.H.; Wilson, L.D.; Peru, K.M.; Headley, J.V.; *J. Colloid. Interface Sci.*, **2013** (*In Press*)
11. Rogers, V.V.; Wickstrom, M.; Liber, L.; MacKinnon, M.D., *Chemosphere*, **2002**, *48*, 519-527
12. Rogers, V.V.; Wickstrom, M.; Liber, L.; MacKinnon, M.D., *Toxicol. Sci.*, **2002**, *66*, 347-355
13. Mackinnon, M.D.; Boerger, H., *Water Poll. Res. J. Can.*, **1986**, *21*, 496-512
14. Rockhold, W. *AMA Arch. Ind. Health*, **1955**, *12*, 477-482
15. Landis, W.; Yu, M., "*Introduction to Environmental Toxicology*", Boca Raton, CRC Press, **2003**, p. 34-35
16. Clemente, J.; Fedorak, P., *Chemosphere*, **2005**, *60*, 585-600
17. Jones, D.; Scarlett, A.; West, C., Rowland, S., *Environ. Sci. Technol.*, **2011**, *45*, 9776-9782
18. Holowenko F.; MacKinnon, M.; Fedorak, P., *Water Res.*, **2002**, *36*, 2843-2855
19. Clemente, J., 2004. Characterization, Analyses, and Biodegradation of Naphthenic Acids. MSc Thesis. University of Alberta

20. Mackinnon, M.; Boerger, H., *Water Pollut. Res. J. Can.*, **1986**, *21*, 496-512
21. Toor, N., 2011. Degradation and Aquatic Toxicity of Oil Sands Naphthenic Acids using Simulated Wetlands. PhD Thesis. University of Saskatchewan
22. Nero, V.; Farwell, A.; Lee, L.; Van Meer, T.; Mackinnon, M.; Dixon, D.; *Ecotox. Environ. Safe.*, **2006**, *65*, 252-264
23. Kamaluddin, M., Zwiazek, J.; *Tree Physiol.*, **2002**, *22*, 1265-1270
24. a) Butt, H.; Graf, K.; Kappl, M., "Physics and Chemistry of Interfaces", Darmstadt, Wiley-VCH Verlag GmbH, 2006, p. 267-273 b) Ibid p. 187-216
25. a) Myers, D., "Surfactant Science and Technology", Hoboken, Wiley-Interscience, 2006, p. 150-152; b) Ibid, p. 329-348
26. Frank, R.; Fischer, K.; Kavanagh, R.; Burnison, B.; Arsenault, G.; Headley, J.; Peru, K.; Van Der Kraak, G.; Solomon, K., *Environ. Sci. Technol*., **2009**, *43*, 266-271
27. Martin, J.; Barri, T.; Han, X.; Fedorak, P.; Gamal El-Din, M.; Perez, L.; Scott, A.; Jiang, T., *Environ. Sci. Technol*., **2010**, *44*, 8350-8356
28. McMartin, D.; Headley, J.V.; Friesen, D.; Peru, K.; Gillies, J., *J. Environ. Sci. Health Part A*, **2004**, *A39*, 1361-1383
29. Smith, B.; Lewis, A.; Belt, S.; Whitby, C.; Rowland, S., *Environ, Sci. Technol*., **2008**, *42*, 9323-9328
30. Huang J., Nemati, M.; Hill, G.; Headley, J.V., *J. Hazardous Materials*, **2012**, *201-202*, 132-140
31. Quagraine, E.K.; Peterson, H.G., Headley, J.V, *J. Environ. Sci. Health Part A*, **2005**, *A40*, 685-722
32. IUPAC Goldbook. http://goldbook.iupac.org/A00036.html. (accessed 05/07/2012), part of IUPAC goldbook. iupac.goldbook.org/ (accessed 05/07/2012)
33. Adamson, A., Gast, A., Physical Chemistry of Surfaces. Wiley-Interscience, New York; 1997, p. 390-420
34. Sing, K.S.W.; Everett, D.H.; Haul, R.A.W.; Moscou, L.; Pierotti, R.A.; Rouquérol, J.; Siemeniewska, T., *Pure & Appl. Chem.*, **1985**, *57*, 603-619
35. a) Kwon, J. H.; Wilson, L. D., *J. Env. Sci. & Health Part A*, **2010**, *45*, 1775-1792. b) Kwon, J. H.; Wilson, L. D. *J. Env. Sci. & Health Part A*, **2010**, *45*, 1793-1803.
36. Langmuir, I., *J. Am. Chem. Soc*., **1918**, *40*, 1393

37. a) Freundlich. H, Colloid and Capillary Chemistry. Methuen & Co. LTD., London, H. Stafford Hatfield; 1926, p. 111,153,172; b) Ibid, p. 61-69,195
38. Skopp, J., *J. Chem. Ed.*, **2009**, *86*, 1341-1343
39. Sips, R., *J. Chem. Phys.*,**1948**, *16*,490-495
40. Brunauer, S.; Emmett, P.H.; Teller, E., *J. Am. Chem. Soc.*, **1938**, *60*, 309-319
41. Mohamed, M.; Wilson, L.; Headley, J.V.; Peru, K., *Phys. Chem. Chem. Phys*., **2011**, *13*, 1112-1122
42. Rezaei Gomari, K.A.; Denoyel, R.; Hamouda, A.A., *J. Colloid Interface Sci.,* **2006**, *297*, 470-479
43. Zou, L.; Han, B.; Yan, H.; Kasperski, K.L.; Xu, Y.; Hepler, L.G., *J. Colloid Interface Sci.*, **1997**, *190*, 472-475
44. Szejtli, J., *Chem. Rev.*, **1998**, *98*, 1743-1754
45. Gaml El-Din, M.; Fu, H.; Wang, N.; Chelme-Ayala, P.; Pérez-Estrada, L.; Drzewicz, P.; Martin, J.; Zubot, W.; Smith, D., *Science of the Total Environment*, **2011**, *409*, 5119-5125
46. Norit® Rox 0.8. http://www.norit-americas.com/product/norit-rox-0.8 (accessed 05/07/2012)
47. van De Manakker, F.; Vermonden, T.; van Nostrum, C.; Hennink, W., *Biomacromolecules*, **2009**, *10*, 3157-3175
48. Chan, W.; Yu, W.;Che, C.; Wong, M., *J. Org. Chem.*, **2003**, *68*, 6576-6582
49. Hirayama, F.; Yamanaka, M.; Horikawa, T.; Uekama, K., *Chem. Pharm. Bull.*, **1995**, *43*, 130-136
50. a) Muzzarelli, R.A.A., Chitin. 1977, Pergamon Press: Toronto, pg. 53-54. b) Ibid. pg. 62
51. Ravi Kumar, M.N.V., *React. Funct. Polym.*, **2000**, *46*, p. 1-27
52. a) Muzzarelli, R.A.A., Natural Chelating Polymers. 1973, Toronto, Pergamon Press, pg. 164. b) Ibid. p.146-176
53. Ngah, W.S.W.; Fatinathan, S., *Chem. Eng. J.*, **2008**, *143*, 62-72
54. Draget, K., *Polym Gels Networks*, **1996**, *4*, 143-151
55. Kildeeva, N.; Perminov, P.; Vladimirov, L.; Novikov, V., Mikhailov, S., *Rus. J. Bioorganic Chem.*, **2009**, *35*, 360-369
56. Ritthidej, G.C.; Chomto, P.; Pummangura, S.; Menasveta, P., *Drug. Dev. Ind. Pharm.*, **1994**, 2109-2134
57. Piepenbrock, M.M., Lloyd, G.; Clarke, N.; Steed, J., *Chem. Rev*., **2010**, *110*, 1960-2004

58. a) Brinker, C.J.; Scherer, G., Sol-Gel Science: The Physics and Chemistry of Sol-Gel Processing. 1990, Academic Press, London, p. 1-17; b) Ibid, p. 358-405; c) Ibid, p. 309; d) Ibid, p. 411-412; e) Ibid, p. 501-523; f) Ibid, p. 242-243
59. Crini, G. Badot, P.M., *Prog. Polym. Sci*., **2008**, *33*, 399-447
60. Bruck, W.; Slater, J.; Carney, B., Chitin, Chitosan, Oligosaccharides, and Their derivatives: Biological Activities and Applications. Se Hwon, K., Ed.; 1990, Taylor & Francis, Boca Raton, 2010, pg. 11-24.
61. Ghosh, B.; Urban, M., *Science*, **2009**, *323*, 1458-1460
62. Chen, X.; Zheng, L.; Wang, Z.; Lee, C.; Park, H., *J. Agric. Food Chem.,* **2002**, *50*, 5915-5918
63. Chiou, M.; Chuang, G., *Chemosphere*, **2006**, *62*, 731-740
64. Jin, L.; Bai, R., *Langmuir*, **2002**, *18*, 9765-9770
65. Xu, D.; Hein, S.; Loo, S.; Wang, K., *Ind. Eng. Chem. Res*., **2008**, *47*, 8796-8800
66. Jafarinejad, S.; Gilani, K.; Moazeni, E.; Ghazi-Khansari, M.; Najafabadi, A.; Mohajel, N., *Powder Technology*, **2012**, *222*, 65-70
67. Shu, X.Z.; Zhu, K.J., *Eur. J. Pharm. Biopharm.,* **2002**, *54*, 235-243
68. Lu, P.; Ma, Y.; Yu, R.; Yue, H.; Dezhi, N.; Wei, W.; Ma, G., *Mol. Pharmaceutics*, **2012**, (Just Accepted) **doi:** 10.1021/mp300051h
69. Bodnar, M.; Hartmann, J.; Borbely, J., *Biomacromolecules*, **2006**, *7*, 3030-3036
70. Pratt, D.; Wilson, L.D.; Kozinski, J.; Mohart, A., *J. Appl. Polym. Sci.,* **2009**, *116*, 2982-2989
71. Breslow, R.; Yang, Z.; Ching, R.; Trojandt, G.; Odobel, F., *J. Am. Chem. Soc.*, **1998**, *120*, 3536-3537
72. Mohamed, M.H.; Wilson, L.D.; Headley, J.V., *Carbohydr. Polym.,* **2010**, *80*, 186-196
73. Wilson, L.D., Xue, C. *J. Appl. Polym. Sci.*, **2013**, *128*, 667-675
74. Chiou, M.; Ho, P.; Li, H., *Dyes and Pigments*, **2004**, *60*, 69-84
75. Kyzas, G.; Bikiaris, D.; Lazaridis, N., *Langmuir*, **2008**, *24*, 4791-4799
76. Pratt, D.Y.; Wilson, L.D.; Kozinski, J.A., *J. Colloid Interface Sci.*, **2013**, *395*, 205-211
77. Einbu, A., Varum, K.M. Structure-Property Relationships in Chitosan. In *Chemical and Functional Properties of Food Saccharides*; Tomasik, P., Ed.; CRC Press: New York, 2004; p. 217-230
78. a) Silverstein, R.; Webster, F.; Kiemle, D., "Spectroscopic Identification of Organic Compounds". 7th ed., John Wiley & Sons. Hoboken. Pg. 96-98 b) Ibid. p. 1-17

79. Günzler, H., Gremlich, H.U., IR Spectroscopy; Wiley-VCH: Weinheim, 2002, p. 171-274
80. Edlund, U.; Albertsson, A.-C., *Adv. Drug Delivery Rev.*, **2003**, *55*, 585-609
81. De Boer, J.H.; Linsen, B.G.; Osinga, T.J., *J. Catalysis*, **1965**, *4*, 643-648
82. Allen, T., Particle Size Distribution Measurement Volume 2: Surface Area and Pore Structure Determination. 5th Ed., Chapman & Hall, New York, 1997. p. 104-122
83. Trung, T.; Ng, C.H.; Stevens, W., *Biotechnol. Lett.*, **2003**, *25*, 1185-1190
84. Atkins, P., de Paula, J., Physical Chemistry. Oxford University Press, 2002, New York. p. 515-529
85. Keeler, J., Understanding NMR Spectroscopy. John Wiley & Sons, 2010, Chichester. p. 1-20
86. Hurtta, M.; Pitkänen, I.; Knuutinen, J., *Carbohydr. Res.*, **2004**, *339*, 2267-2273
87. Mohamed, M.H.; Wilson, L. D.; Headley, J. V., *Carbohydr. Res.*, **2011**, *346*, 219-229**.**
88. a) Gross, J., "Mass Spectrometry". 2nd Ed., Springer-Verlag, Berlin, 2011. p. 561-619 b) Ibid. p. 117-221
89. Kirsten, W., "Organic Elemental Analysis". 1st ed., 1983, Academic Press, Toronto. p. 43-60
90. Mohamed, M.H.; Wilson, L.D.; Headley, J.V.; Peru, K.M., *J. Colloid Interface Sci.*, **2011**, *356*, 217-226
91. a) Clayden, J.; Greeves, N.; Wothers, P.; and Warren, S. Organic Chemistry; Oxford University Press: New York, 2001, p. 279-281; b) Ibid, p. 199; c) Ibid, p. 689-695; d) Ibid, p. 292-293
92. March, J., Advanced Organic Chemistry: Reactions, Mechanisms, and Structure; Wiley-Interscience: Toronto, 1992, p. 392-393
93. Bambo, M., 2007. Synthesis, Characterization, and Application of Nanoporous Cyclodextrin Polymers. Master of Technology in Chemistry, University of Johannesburg
94. Knaul, J.; Hudson, S.; Creber, K., *J. Polym. Sci. Part B*, **1999**, *37*, 1079-1094
95. Cordes, E.; Jencks, W., *J. Org. Chem.*, **1961**, *84*, 832-837
96. Amedjkouh, M., *Tetrahedron Assym.*, **2005**, *16*, 1411-1414
97. Rohr, K.; Mahrwald, R., *Org. Lett.*, **2012**, 14, 2180-2183
98. Houlhan, W.; Nielson, A., Organic Reactions; John Wiley & Sons: New York, 1968, pp. 2-10
99. Stork, G.; Brizzolara, A.; Landesman, H.; Szmuszkovicz, J.; Terrell, R., *J. Org. Chem.*, **1962**, *85*, 207-222
100. a) List, B.; Hoang, L.; Martin, H., *Proc. Natl. Acad. Sci.*, **2004**, *101*, 5839-5842; b) List, B., *Synlett.*, **2001**, *11*, 1675-1686

101. Torii, H.; Nakadai, M.; Ishihara, K.; Saito, S.; Yamamoto, H., *Angew. Chem. Int. Ed.*, **2004**, *43*, 1983-1986
102. Monteiro Jr., O.; Airoldi, C., *Int. J. Biol. Macromol.*, **1999**, *26*, 119-126
103. Reddy, K.; Rajgopal, K.; Maheswari, U.; Lakshmi Kantam, M., *New J. Chem.*, **2006**, *30*, 1549-1552
104. Henderson, A.P.; Bleasdale, C.; Clegg, W.; Golding, B., *Chem. Res. Toxicol.*, **2004**, *17*, 378-382
105. Olsen, R.; Backman, J.; Molander, P.; Øvrebø, S.; Thorud, S.; Lundanes, E.; Greibrokk, T; Kronberg, L., *Chem. Res. Toxicol.*, **2007**, *20*, 965-974
106. a) Maury, C.; Wang, Q.; Gharbaoui, T.; Chiadmi, M.; Tomas, A.; Royer, J.; Husson, H.P., *Tetrahedron*, **1997**, *53*, 3627-3636; b) Takahata, H.; Ouchi, H.; Ichinose, M.; Nemoto, H., *Org. Lett.*, **2002**, *4*, 3459-3462; c) Liu, L.X., Xiao, K.J.; Huang, P.Q., *Tetrahedron*, **2009**, *65*, 3834-3841
107. Russo, A.; Chandramouli, N.; Zhang, L.; Deng, H., *J. Proteome Res.*, **2008**, *7*, 4178-4182
108. Kovaříček, P.; Lehn, J.M., *J. Am. Chem. Soc.*, **2012**, *134*, 9446-9455
109. Youn, D.; No, H.; Prinyawiwatkul, W., *Carbohydr. Polym.*, **2007**, *69*, 707-712
110. Henry, L.; Puspitasari-Nienaber, N.; Jarén-Galán, M.; van Breeman, R.; Catignani, G.; Schwartz, S., *J. Agric. Food. Chem.*, **2000**, *48*, 5008-5013
111. Desai, K.; Kit, K.; Li, J.; Zivanovic, S., *Biomacromolecules*, **2008**, *9*, 1000-1006
112. Chiou, M.S.; Li, H.Y., *Chemosphere*, **2003**, *50*, 1095-1105
113. Lazaridis, N.; Kyzas, G.; Vassiliou, A.; Bikiaris, D., *Langmuir*, **2007**, *23*, 7634-7643
114. Poon, L.; Wilson, L.D.; Headley, J.V., *J. Appl. Polym. Sci.*, **2012**, 1-9
115. Mohamed, M.H.; Wilson, L.D.; Headley, J.V.; Peru, K.M., *IChemE: Process Saf. Environ. Protect.*, **2008**, *86*, 237-243
116. Gliko-Kabir, I.; Penhasi, A.; Rubinstein, A., *Carbohydr. Res.*, **1999**, *316*, 6-13
117. Basch, A.; Lewin, M., *J. Polym. Sci. Part A*, **1973**, *11*, 3071-3093
118. Piron, E.; Accominotti, M.; Domard, A., *Langmuir*, **1997**, *13*, 1653-1658
119. Neto, C.G.T.; Giacometti, J.A.; Ferreira, F.C.; Fonseca, J.L.C.; Pereira, M.R., *Carbohydr. Polym.*, **2005**, *62*, 97-103
120. Ma, G.; Qian, B.; Yang, J.; Hu, C.; Nie, J., *Int. J. Biol. Macromol.*, **2010**, *46*, 558-561
121. Barrett, E.; Joyner, L.G.; Halenda, P.P., *J. Am Chem. Soc.*, **1951**, *73*, 373-380
122. Haghseresht, F.; Finnerty, J.J.; Nouri, S.; Lu, G.Q., *Langmuir*, **2002**, *18*, 6193-6200

123. Meshko, V., Markovska, L., Mincheva, M., Rodrigues, A.E., *Water Res.*, **2001**, *35*, 3357-3366
124. González-Martín, M.L.; Valenzuela-Calahorro, C.; Gómez-Serrano, V., *Langmuir*, **1991**, 7, 1296-1298
125. González-Martín, M.L.; Valenzuela-Calahorro, C.; Gómez-Serrano, V., *Langmuir*, **1994**, 10, 844-854
126. Lippens, B.C., Linsen, B.G., de Boer, J.H., *J. Catalysis*, **1965**, *4*, 319-323
127. Brunauer, S., *Pure & Appl. Chem.*, **1976**, *48*, 401-405
128. Wilson, L.D.; Guo, R., *J. Colloid Interface Sci.*, **2012**, *387*, 250-261
129. Kwon, J.; Wilson, L.D., *J. Environ. Sci. Health Part A*, **2010**, *10*, 1793
130. Coughlin, R.W.; Ezra, F.S., *Environ. Sci. Technol.*, **1968**, *2*, 291
131. Müller, G., Radke, C.J.; Prausnitz, J.M., *J. Phys. Chem.*, **1980**, *84*, 369-376
132. Connors, K.A., *Chem. Rev.*, **1997**, *97*, 1325-1357
133. Chang, X.; Chen, D.; Jiao, X., *J. Phys. Chem. B.*, **2008**, *112*, 7721-7725
134. Kyzas, G.Z.; Kostoglou, M.; Lazaridis, N.K., *Langmuir*, **2010**, *26*, 9617-9626
135. Momenzadeh, H.; Tehrani-Bagha, A.R.; Khosravi, A.; Gharanjig, K.; Holmberg, K., *Desalination*, **2011**, *271*, 225-230
136. Langmuir, I., *Chem. Rev.*, **1933**, *13*, 147-191
137. Li, J.M.; Meng, X.G.; Hu, C.W.; Du.J, *Bioresource Technol.*, **2009**, *100*, 1168-1173
138. Ngah, W.S.W., Fatinathan, S., *Colloids Surf. A: Physicochem. Eng. Aspects*, **2006**, *277*, 214-222
139. Wang, X.; Kasperski, K.L., *Anal. Methods*, **2010**, *2*, 1715-1722
140. Atkin, R.; Craig, V.S.J.; Wanless, E.J.; Biggs, S., *Adv. Colloid Interface Sci.*, **2003**, *103*, 219-304
141. Somasundaran, P.; Huang, L., *Adv. Colloid Interface Sci.*, **2000**, *88*, 179-200
142. Rosen, M.J., Surfactants and Interfacial Phenomena. Wiley-Interscience, Hoboken; 2004, p. 34-59
143. Kern, H.E.; Findenegg, G.H., *J. Colloid Interface Sci.*, **1980**, *75*, 3463
144. Rabe, J.P.; Bucholz, S., *Science*, **1991**, *253*, 424
145. Song, Q.; Yuan, M., *J. Colloid. Interface Sci.*, **2011**, *357*, 179-188
146. Pratt, D.Y.; Wilson, L.D.; Kozinski, J.A., *J. Colloid Interface Sci.*, **2013**, *393*, 271-277